Electronic Supporting Information (ESI)

Heterobimetallic Pd/Mn and Pd/Co Complexes as Efficient and Stereoselective Catalysts for the Sequential Cu-free Sonogashira Coupling–Alkyne Semi-Hydrogenation Reactions

Reike Clauss[a†], Saral Baweja[a†], Dmitri Gelman[b] and Evamarie Hey-Hawkins[a]*

[a] Faculty of Chemistry and Mineralogy, Institute of Inorganic Chemistry, Leipzig University, Johannisallee 29, D-04103 Leipzig, Germany.
Phone: (+49)341 97 36151. E-mail: hey@uni-leipzig.de

[b] Institute of Chemistry, The Hebrew University of Jerusalem, Jerusalem, 91904 Israel.

Table of Content

1. Ligands

1.1 L2 (Molecular Structure in the Solid State; NMR Spectra (^{1}H, $^{13}C\{^{1}H\}$, $^{31}P\{^{1}H\}$, ^{1}H-^{1}H COSY, ^{1}H-^{13}C HMBC, ^{1}H-^{13}C HSQC, ^{1}H-^{1}H NOESY))

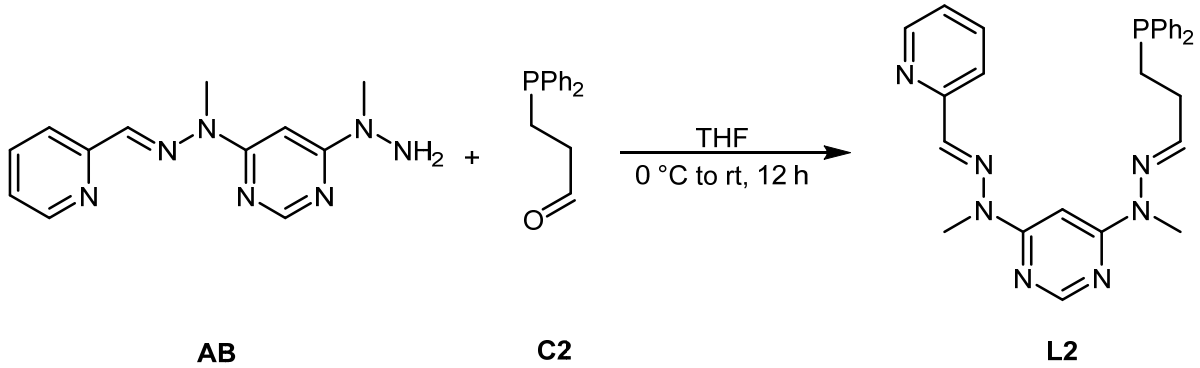

Scheme S1. Synthesis of ligand **L2**.

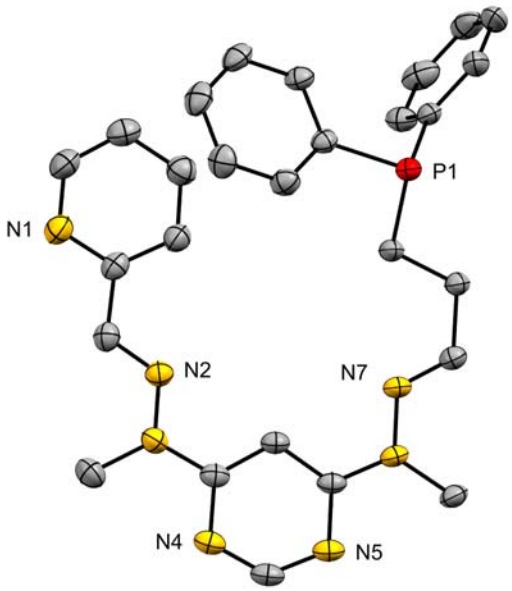

Figure S1. Molecular structure of ligand **L2** (hydrogen atoms are omitted for clarity; thermal ellipsoids are set at the 50% probability level).

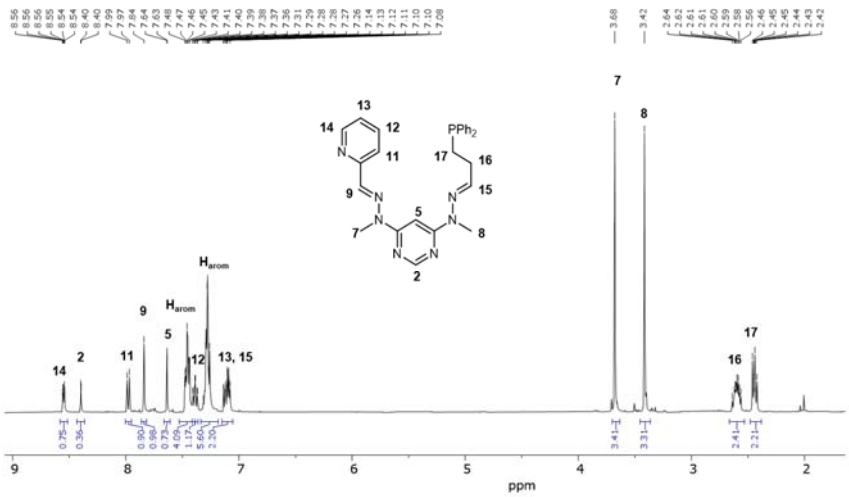

Figure S2. ^{1}H NMR spectrum of ligand **L2** in CD_3CN at 25 °C.

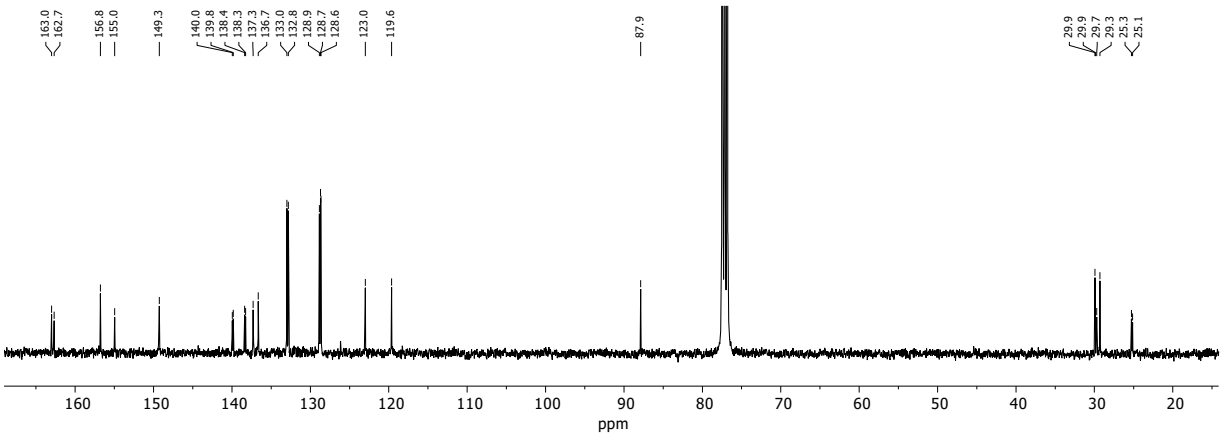

Figure S3. ^{13}C{^{1}H} NMR spectrum of ligand **L2** in CD_3CN at 25 °C.

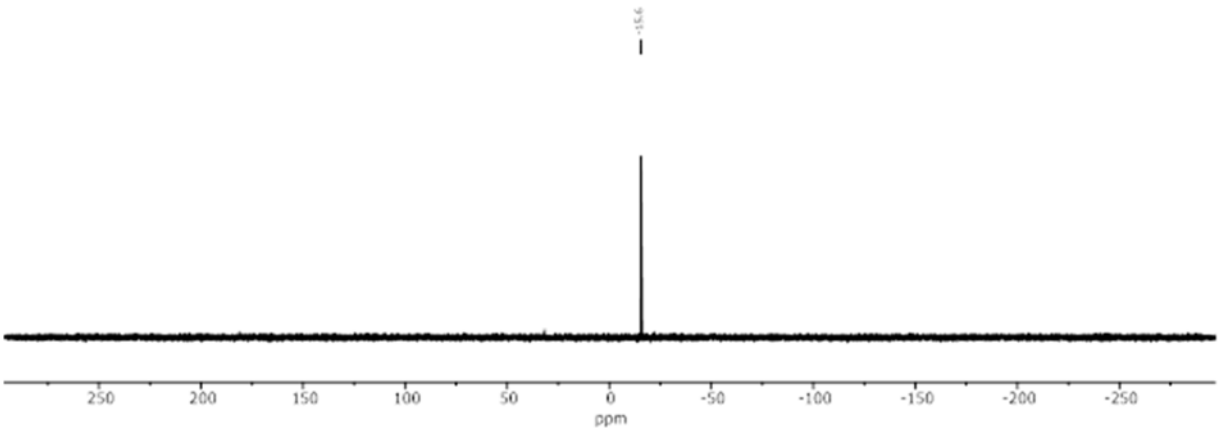

Figure S4. ^{31}P{^{1}H} NMR spectrum of ligand **L2** in CD_3CN at 25 °C.

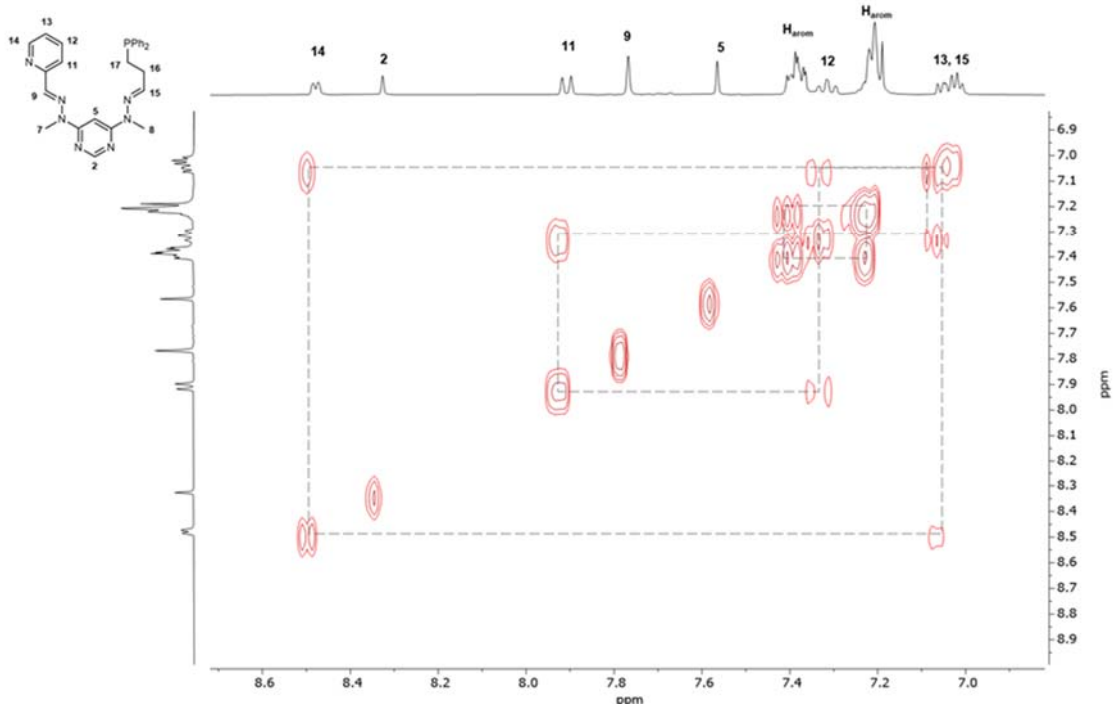

Figure S5. ^{1}H-^{1}H COSY spectrum of ligand **L2** in CD_3CN at 25 °C.

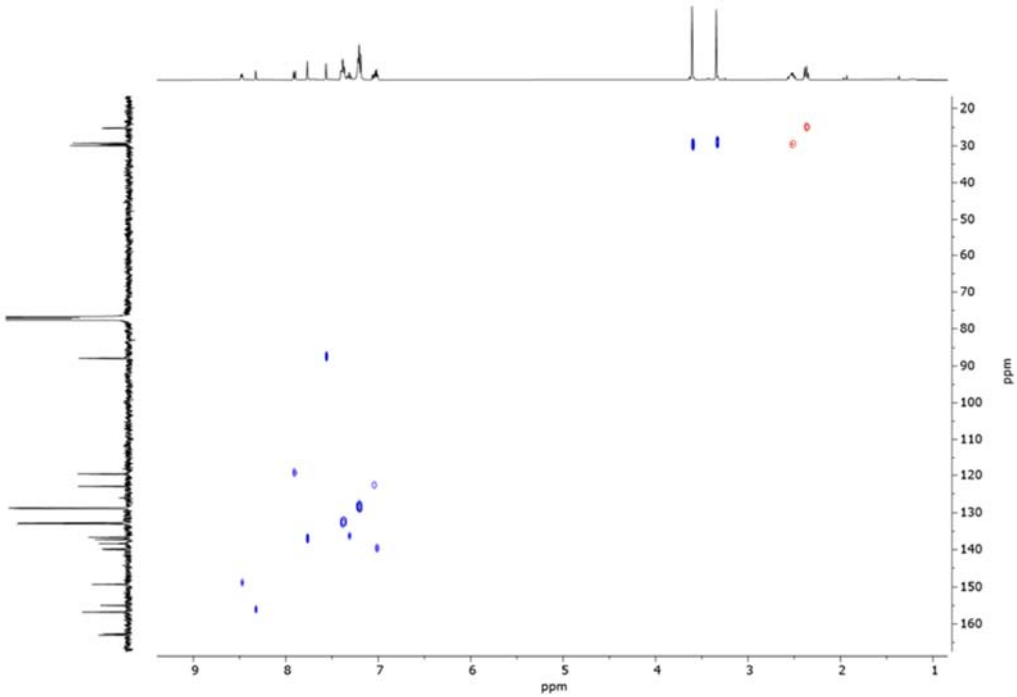

Figure S6. ^{1}H-^{13}C HSQC spectrum of ligand **L2** in CD_3CN at 25 °C.

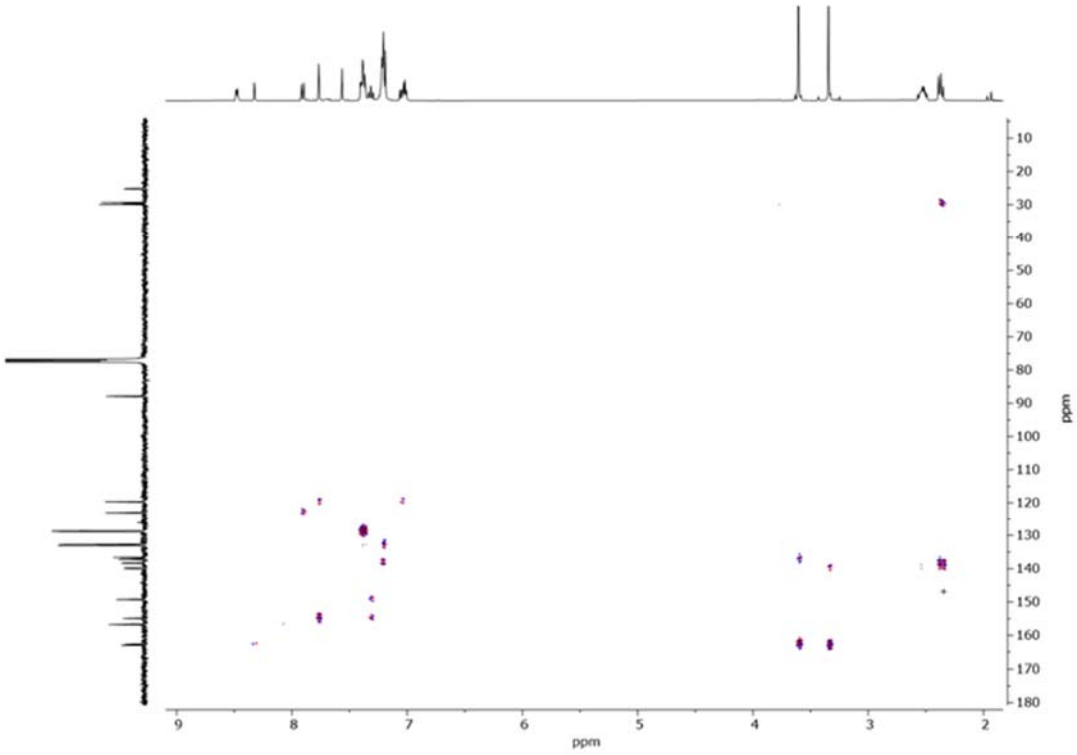

Figure S7. ^{1}H-^{13}C HMBC spectrum of ligand **L2** in CD_3CN at 25 °C.

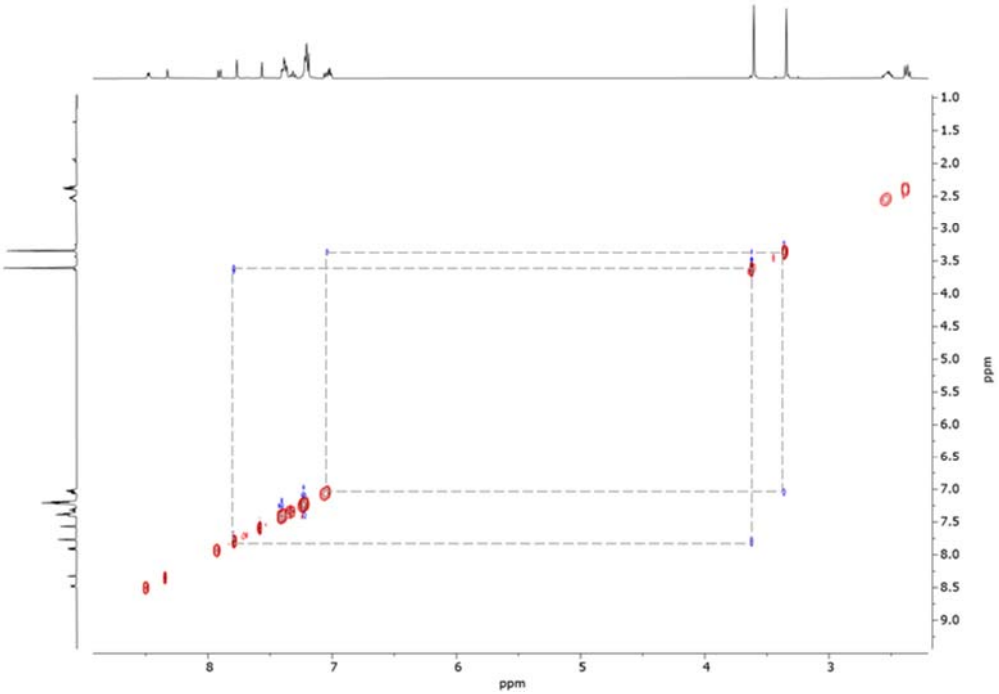

Figure S8. ^{1}H-^{1}H NOESY spectrum of ligand **L2** in CD_3CN at 25 °C.

1.2 **L3** (NMR Spectra (^{1}H, ^{13}C{^{1}H}, ^{31}P{^{1}H}, ^{1}H-^{1}H COSY, ^{1}H-^{13}C HMBC, ^{1}H-^{13}C HSQC, ^{1}H-^{1}H NOESY))

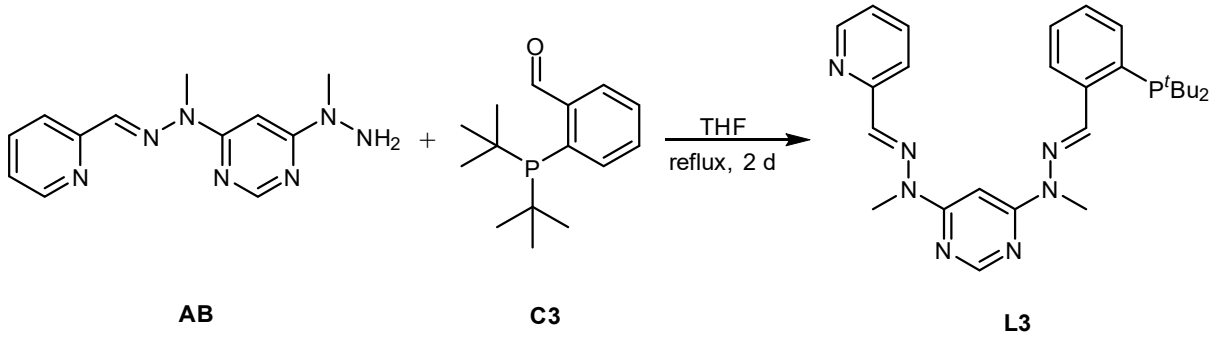

Scheme S2. Synthesis of ligand **L3**.

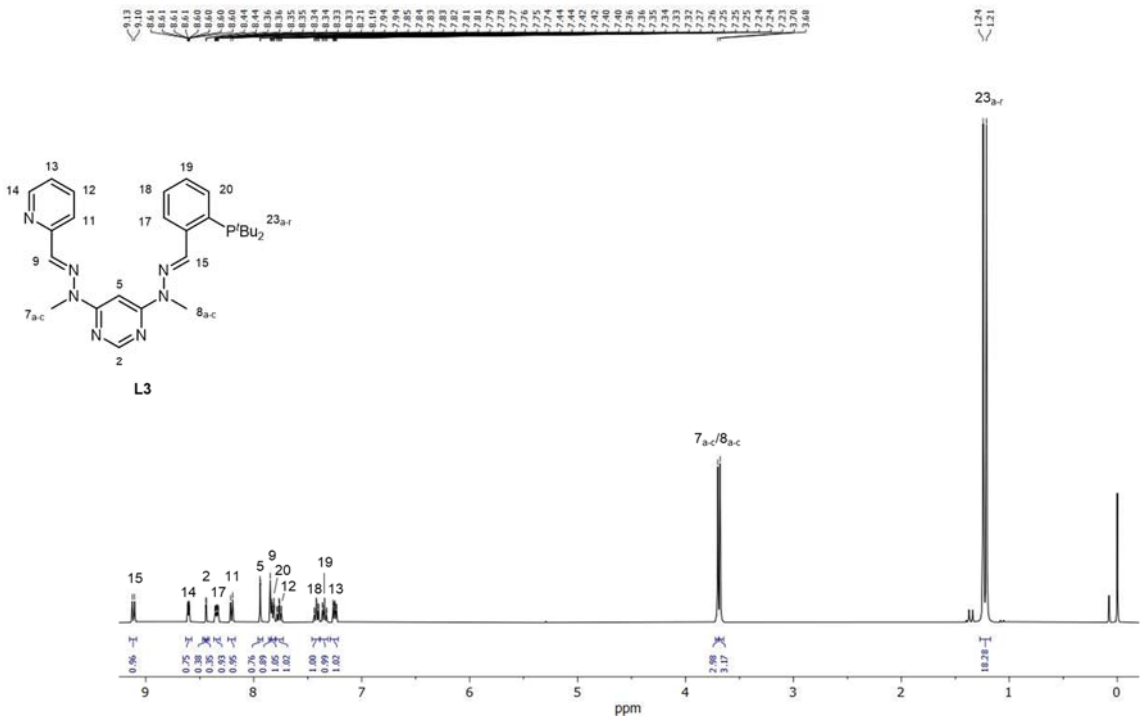

Figure S9. ^{1}H NMR spectrum of ligand **L3** in $CDCl_3$ at 25 °C.

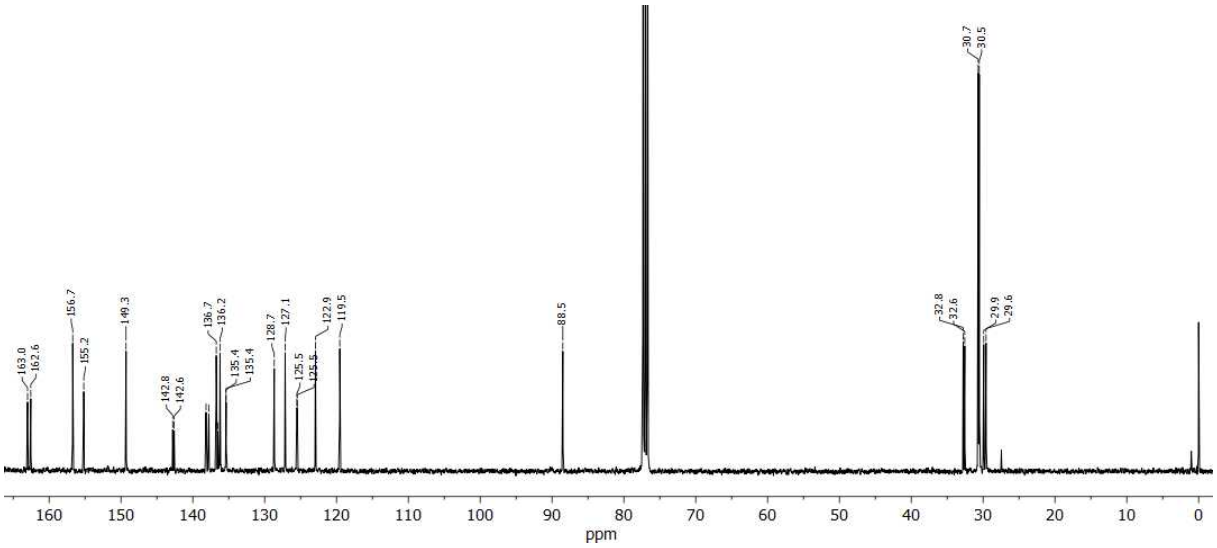

Figure S10. $^{13}C\{^{1}H\}$ NMR spectrum of ligand **L3** in $CDCl_3$ at 25 °C.

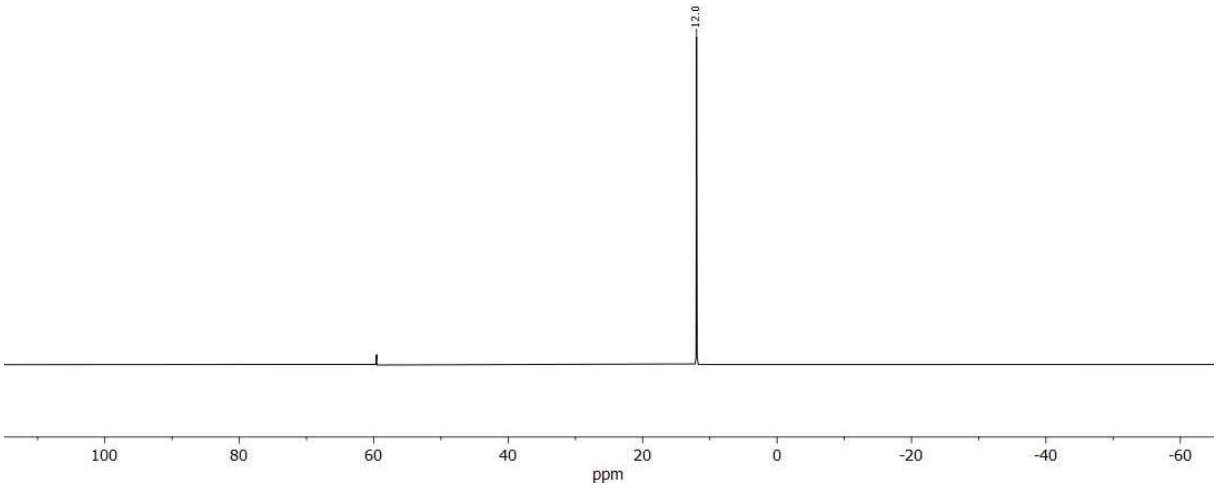

Figure S11. $^{31}P\{^{1}H\}$ NMR spectrum of ligand **L3** in $CDCl_3$ at 25 °C.

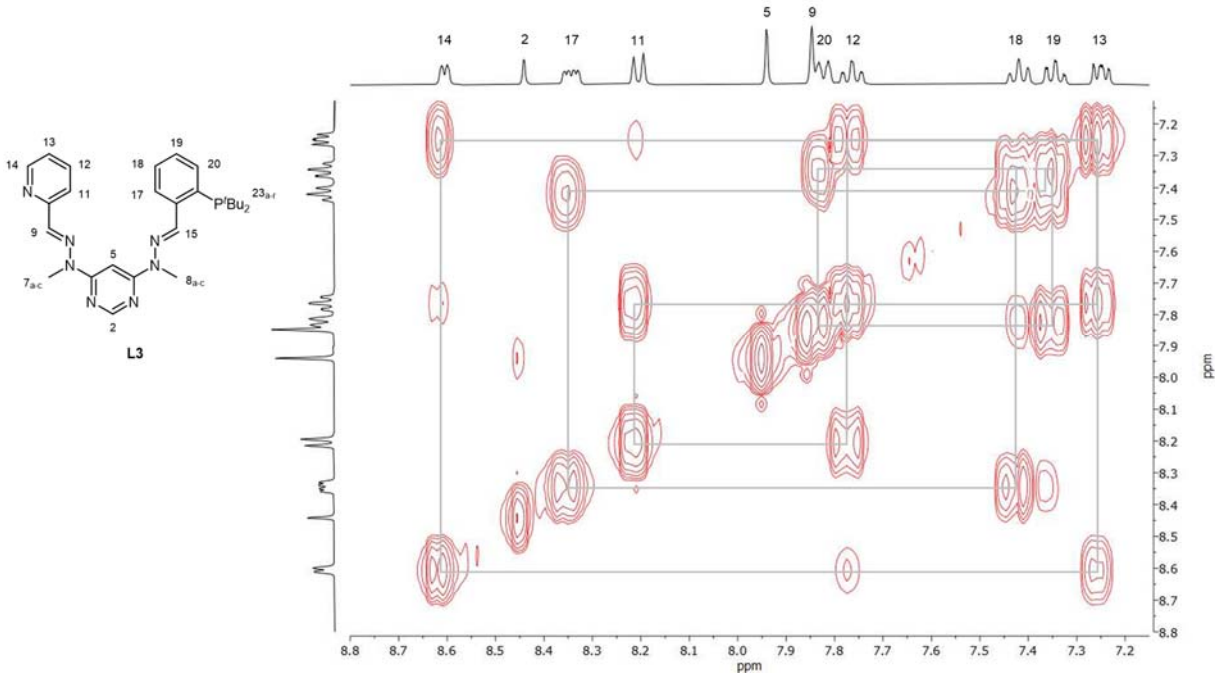

Figure S12. ^{1}H-^{1}H COSY spectrum of ligand **L3** in $CDCl_3$ at 25 °C.

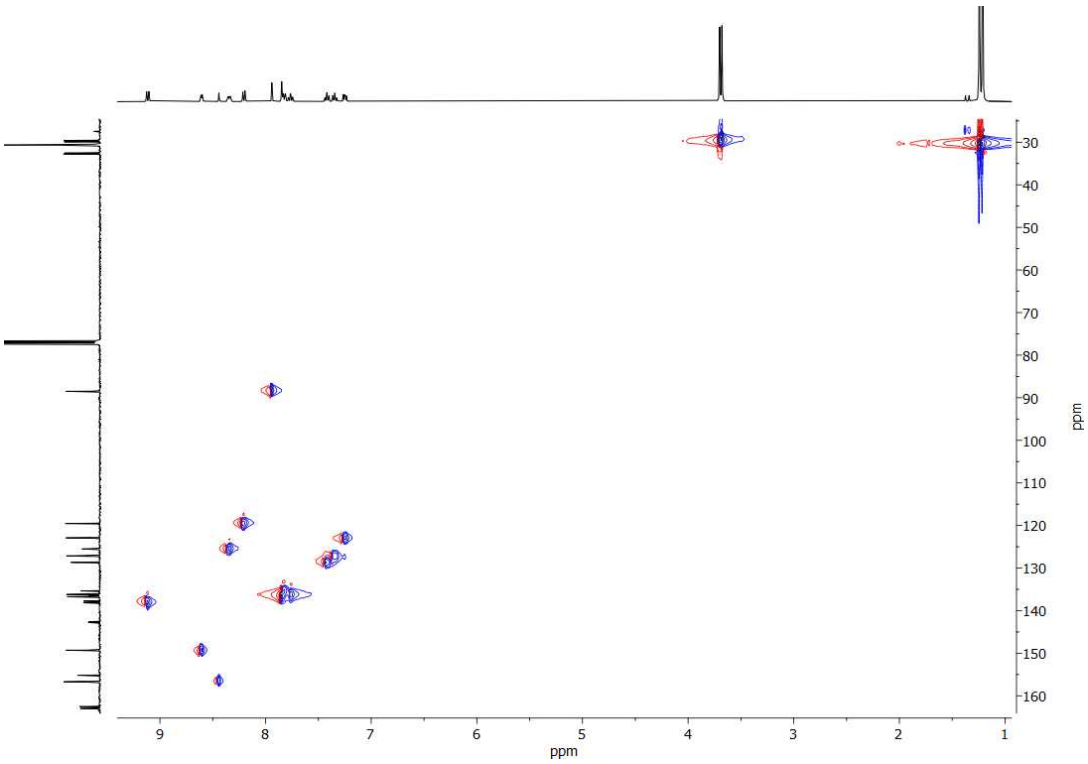

Figure S13. ^{1}H-^{13}C HSQC spectrum of ligand **L3** in $CDCl_3$ at 25 °C.

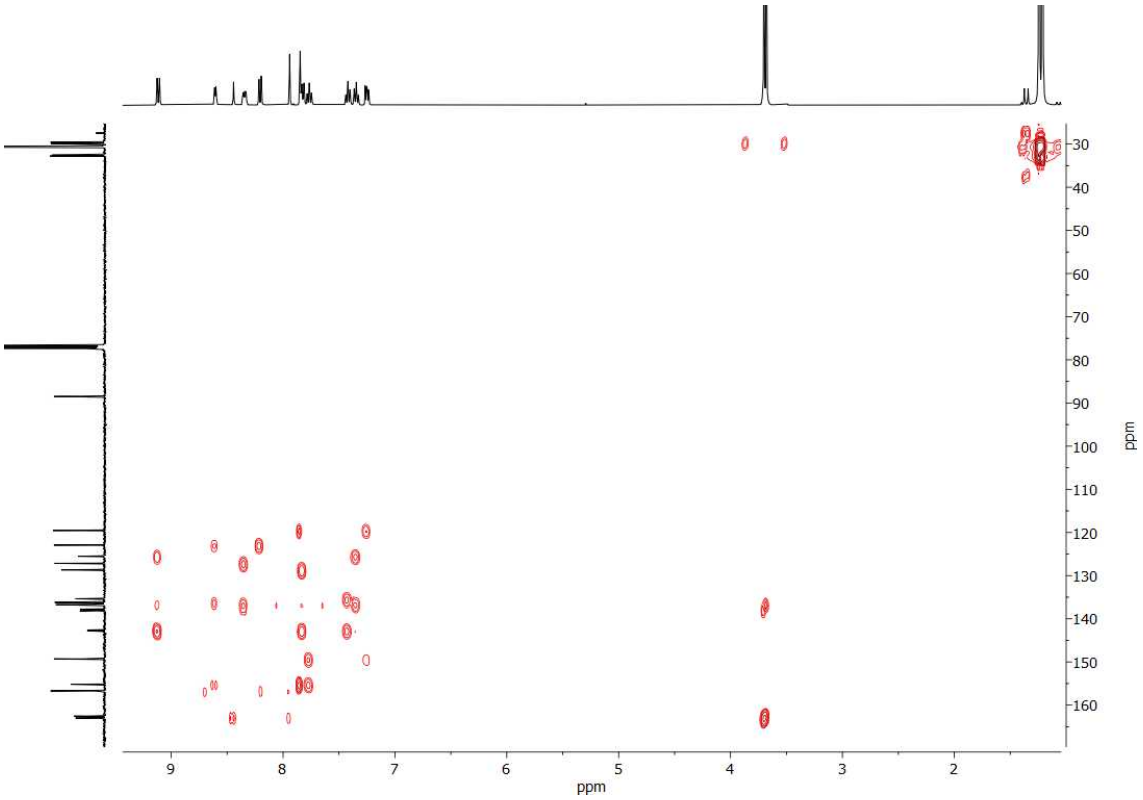

Figure S14. ^{1}H-^{13}C HMBC spectrum of ligand **L3** in $CDCl_3$ at 25 °C.

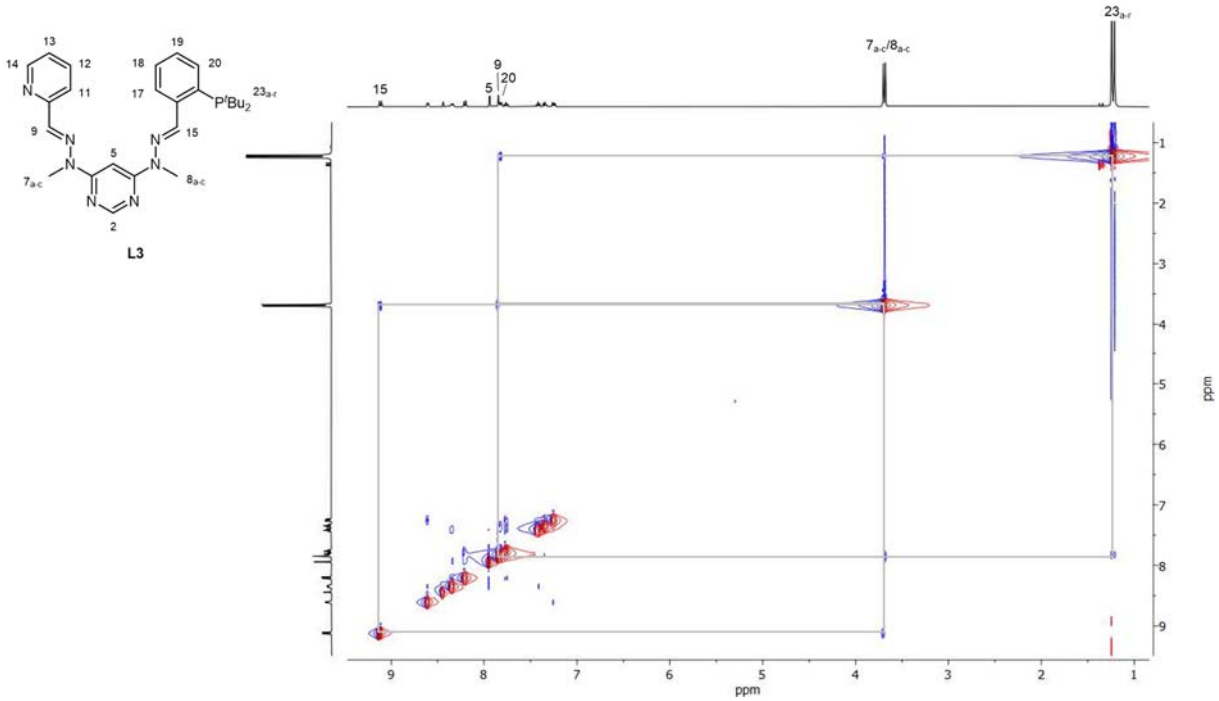

Figure S15. ^{1}H-^{1}H NOESY spectrum of ligand **L3** in $CDCl_3$ at 25 °C.

1.3 **L5** (Molecular Structure in the Solid State; NMR Spectra (^{1}H, $^{13}C\{^{1}H\}$, $^{31}P\{^{1}H\}$))

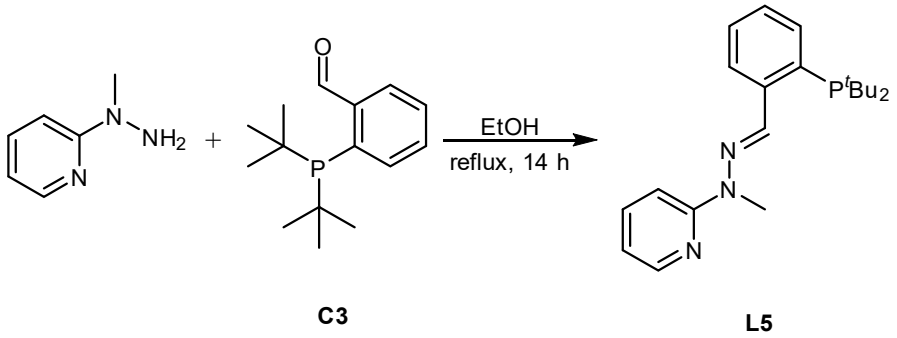

Scheme S3. Synthesis of ligand **L5**.

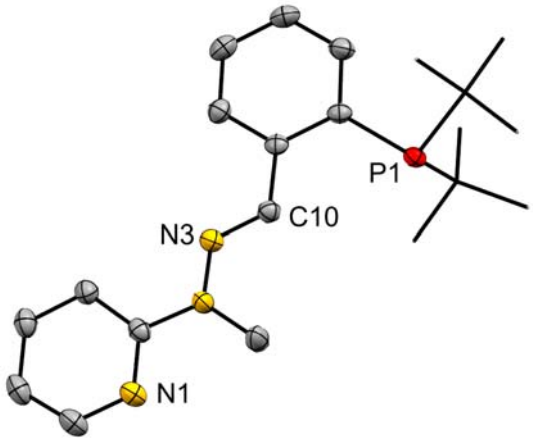

Figure S16. Molecular structure of **L5** (hydrogen atoms are omitted and *tert*-butyl groups are drawn as wireframes for clarity; thermal ellipsoids are set at the 50% probability level).

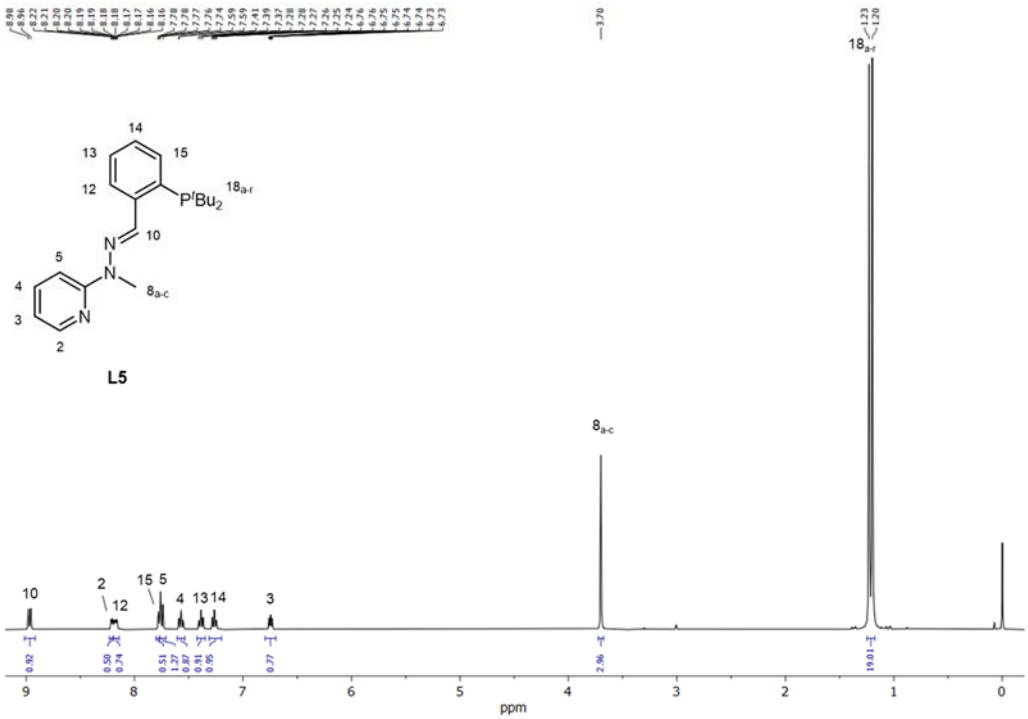

Figure S17. ^{1}H NMR spectrum of ligand **L5** in $CDCl_3$ at 25 °C.

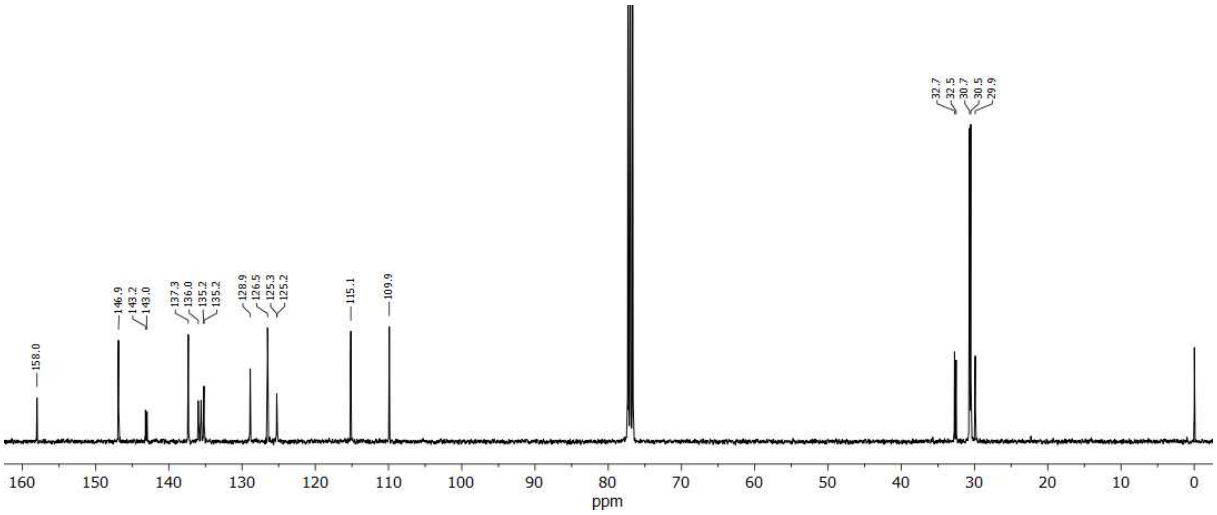

Figure S18. $^{13}C\{^{1}H\}$ NMR spectrum of ligand **L5** in $CDCl_3$ at 25 °C.

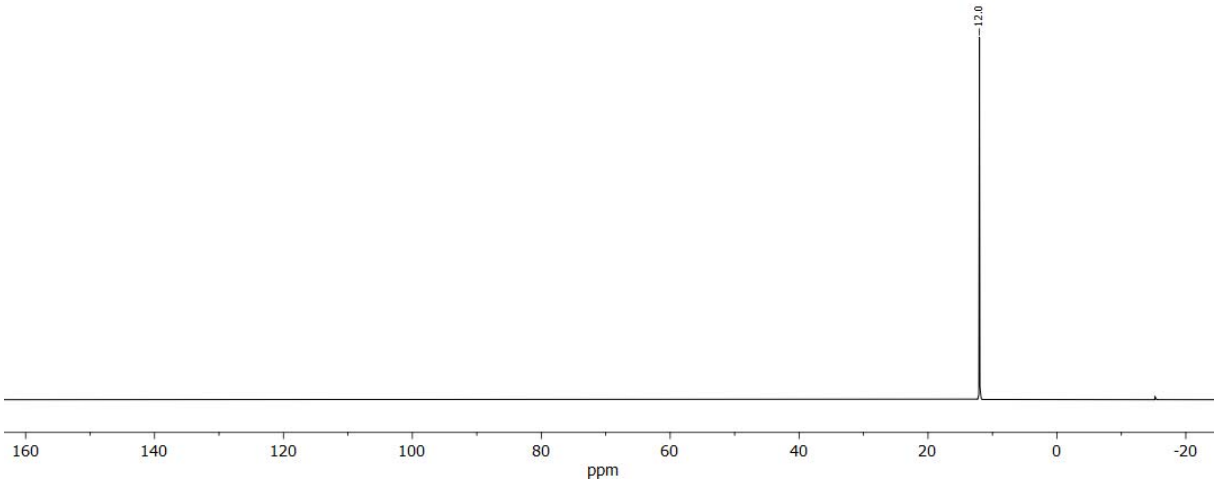

Figure S19. $^{31}P\{^{1}H\}$ NMR spectrum of ligand **L5** in $CDCl_3$ at 25 °C.

2. Monometallic Pd Complexes

2.1 **PdL2** (NMR Spectra (^{1}H, ^{13}C{^{1}H}, ^{31}P{^{1}H}, ^{1}H-^{1}H COSY, ^{1}H-^{13}C HMBC, ^{1}H-^{13}C HSQC))

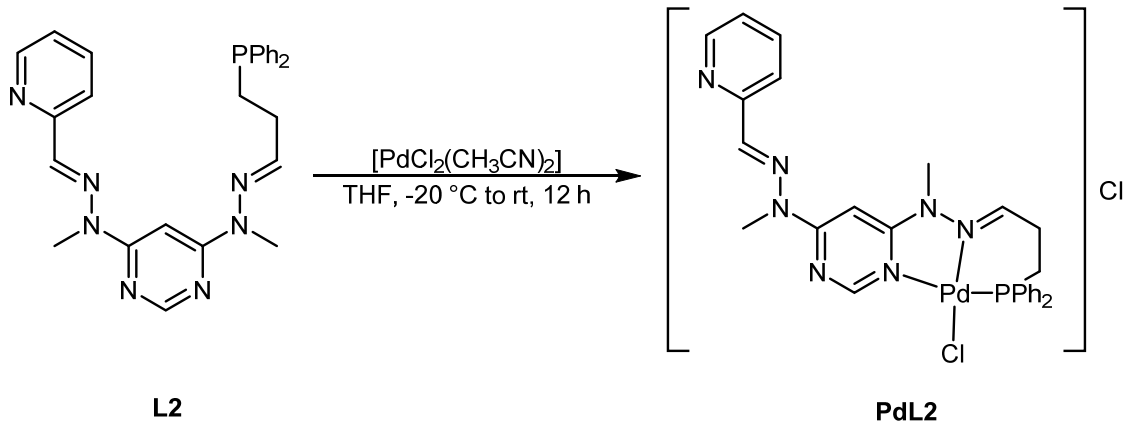

Scheme S4. Synthesis of **PdL2**.

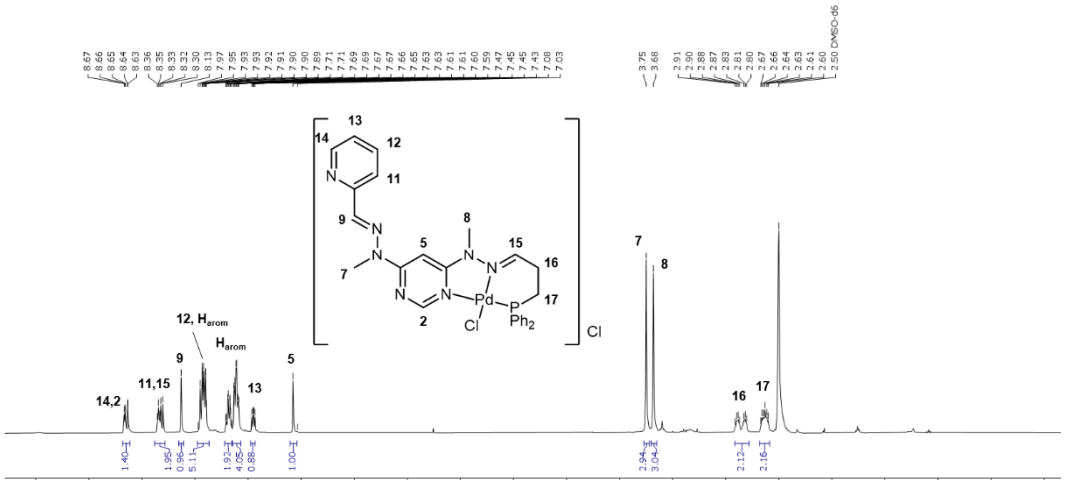

Figure S20. ^{1}H NMR spectrum of **PdL2** in DMSO-d$_6$ at 25 °C.

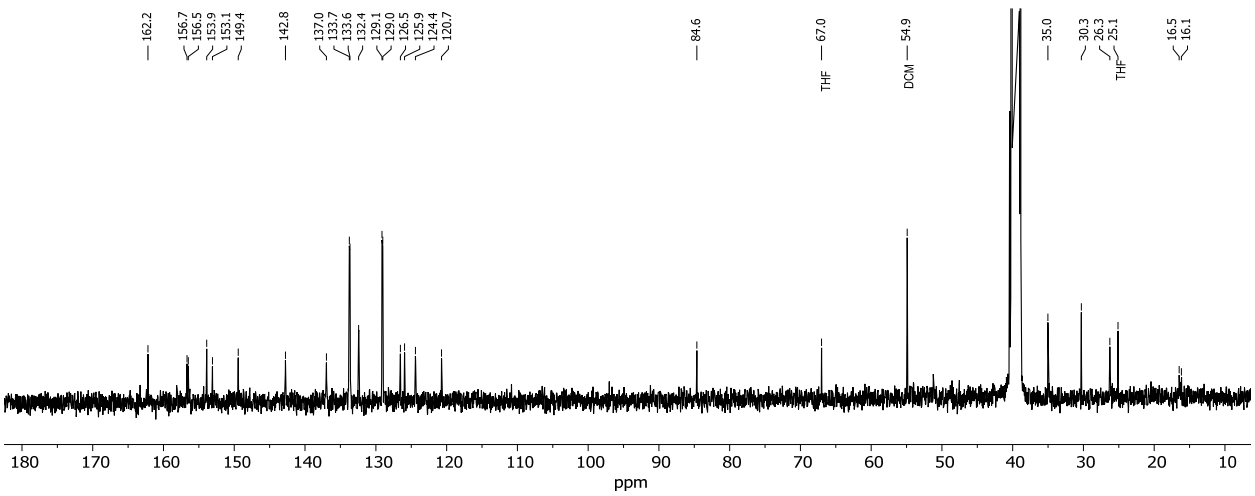

Figure S21. ^{13}C{^{1}H} NMR spectrum of **PdL2** in DMSO-d$_6$ at 25 °C.

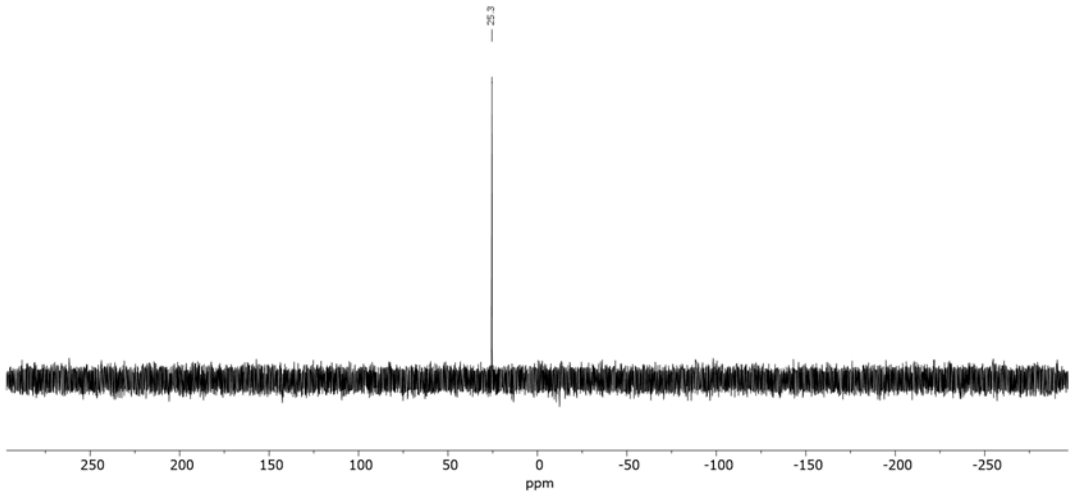

Figure S22. $^{31}P\{^{1}H\}$ NMR spectrum of **PdL2** in DMSO-d_6 at 25 °C.

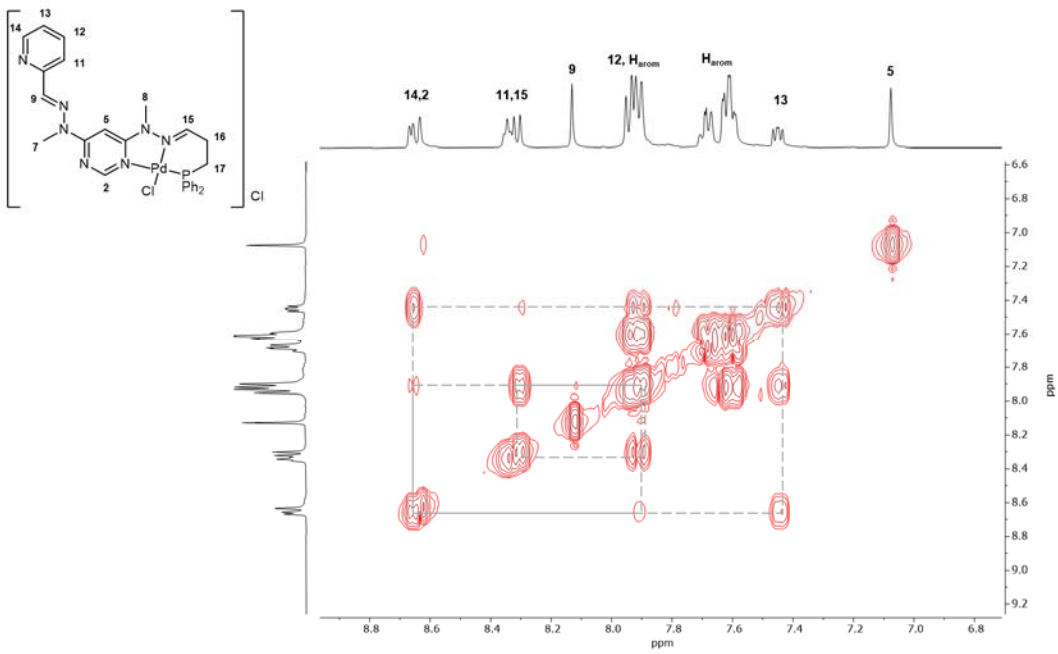

Figure S23. ^{1}H-^{1}H COSY spectrum of **PdL2** in DMSO-d_6 at 25 °C.

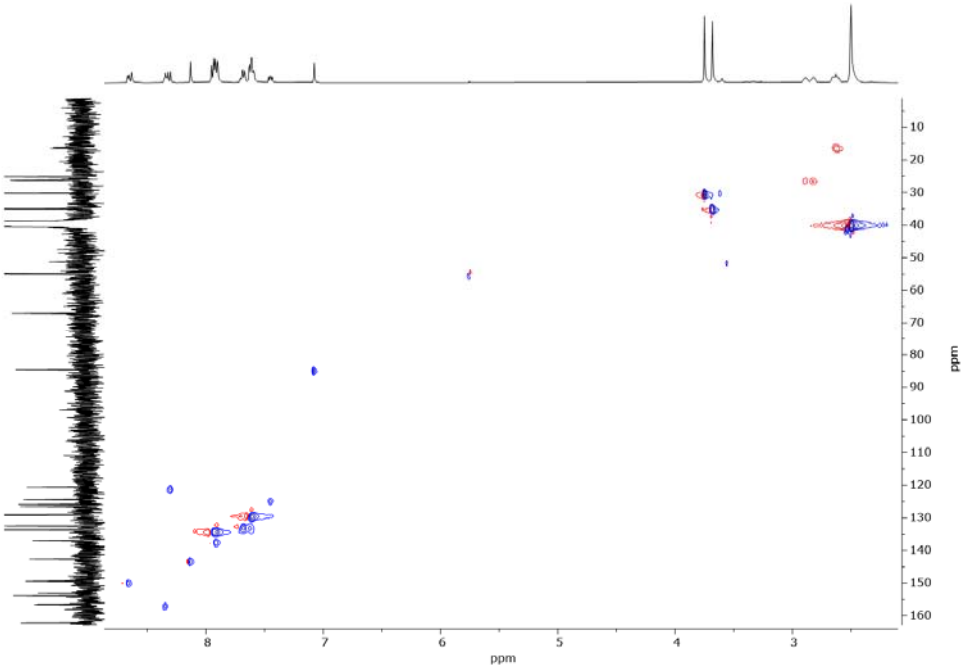

Figure S24. ^{1}H-^{13}C HSQC spectrum of **PdL2** in DMSO-d_6 at 25 °C.

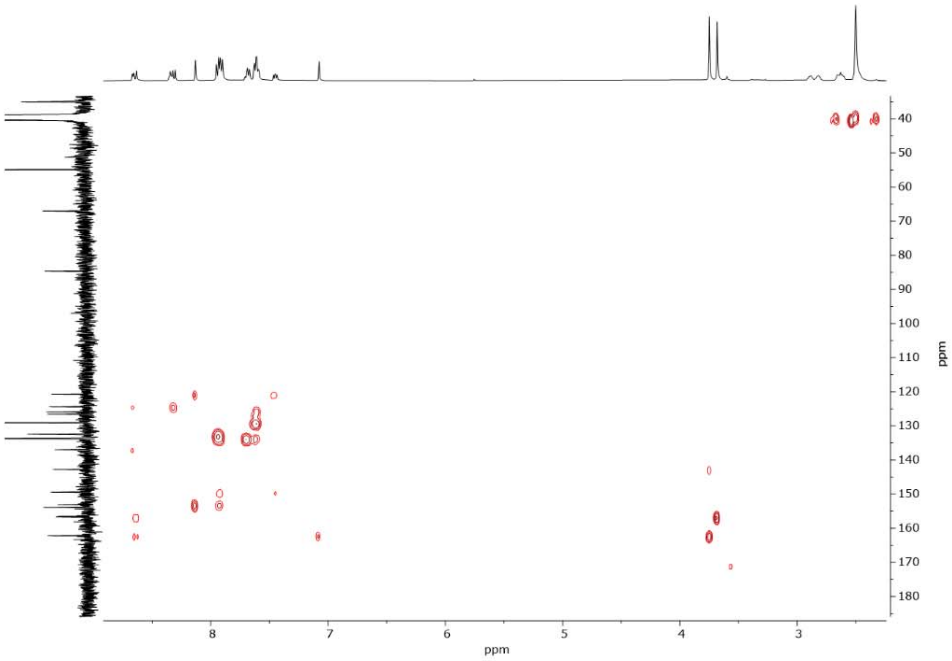

Figure S25. ^{1}H-^{13}C HMBC spectrum of **PdL2** in DMSO-d_6 at 25 °C.

2.2 **PdL3'** (Molecular Structure of **PdL3'** and [PdCl(**L3'**)]·HCl in the Solid State; NMR Spectra (^{1}H, ^{13}C{^{1}H}, ^{31}P{^{1}H}, ^{1}H-^{1}H COSY, ^{1}H-^{13}C HMBC, ^{1}H-^{13}C HSQC, ^{1}H-^{1}H NOESY))

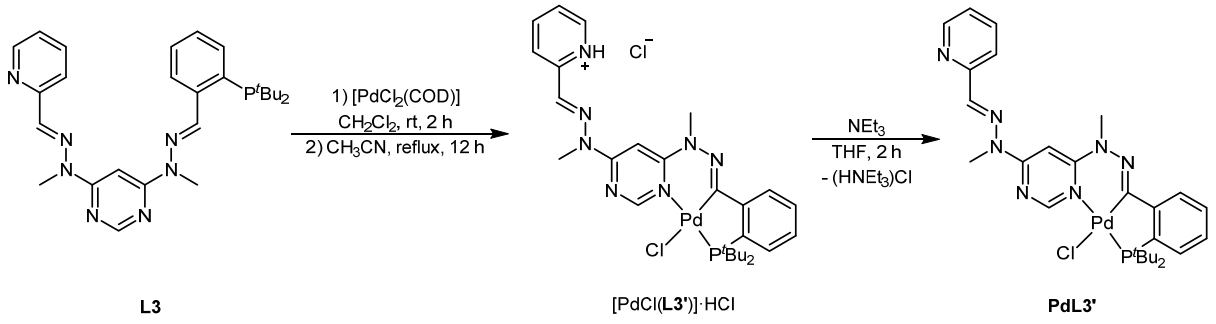

Scheme S5. Synthesis of **PdL3'**.

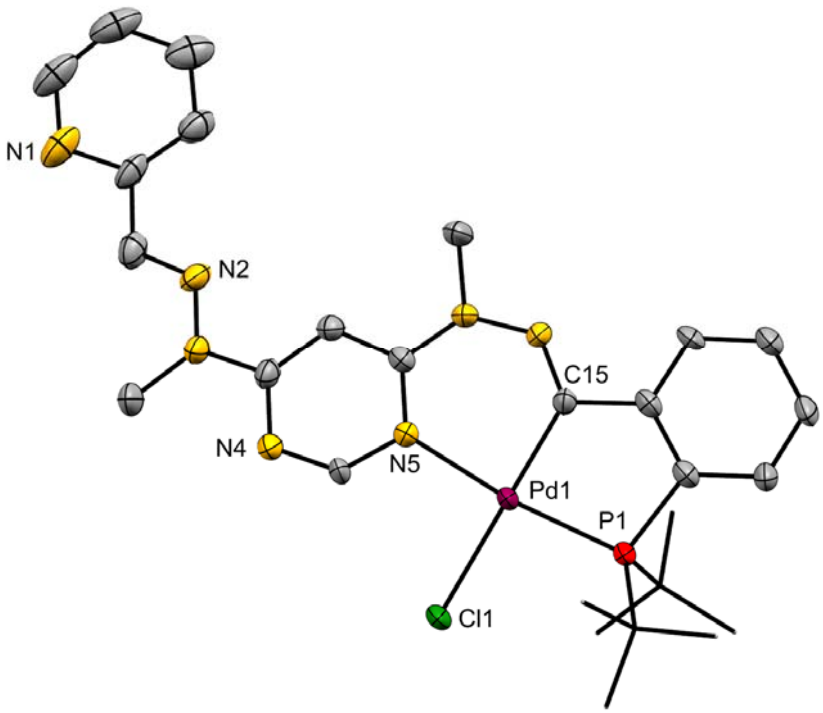

Figure S26. Molecular structure of **PdL3'**·$CHCl_3$·$2H_2O$ (solvent molecules and hydrogen atoms are omitted and *tert*-butyl groups are drawn as wireframes for clarity; thermal ellipsoids are set at the 50% probability level).

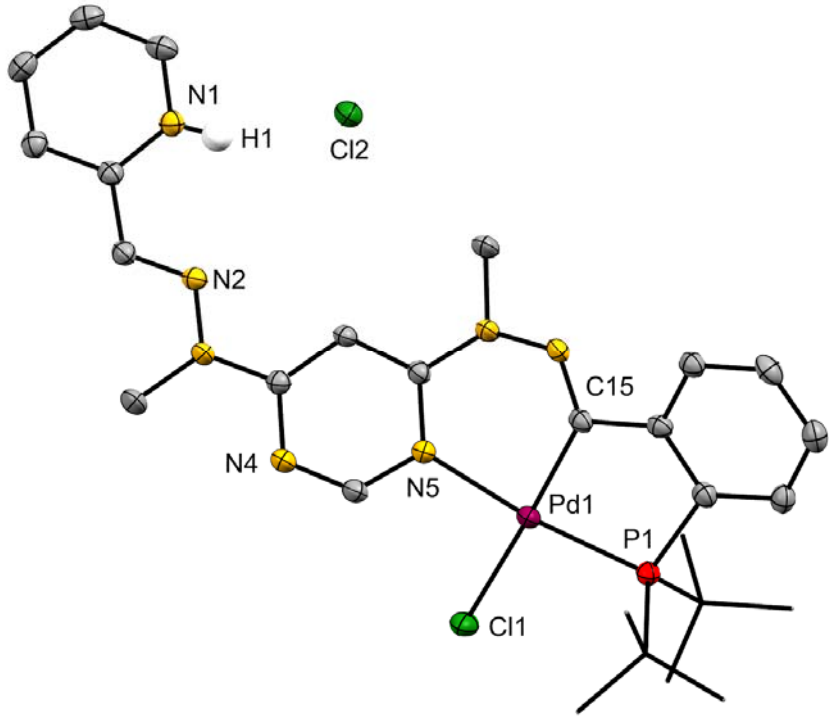

Figure S27. Molecular structure of [PdCl(**L3'**)]·HCl (hydrogen atoms (except H1) are omitted and *tert*-butyl groups are drawn as wireframes for clarity; thermal ellipsoids are set at the 50% probability level).

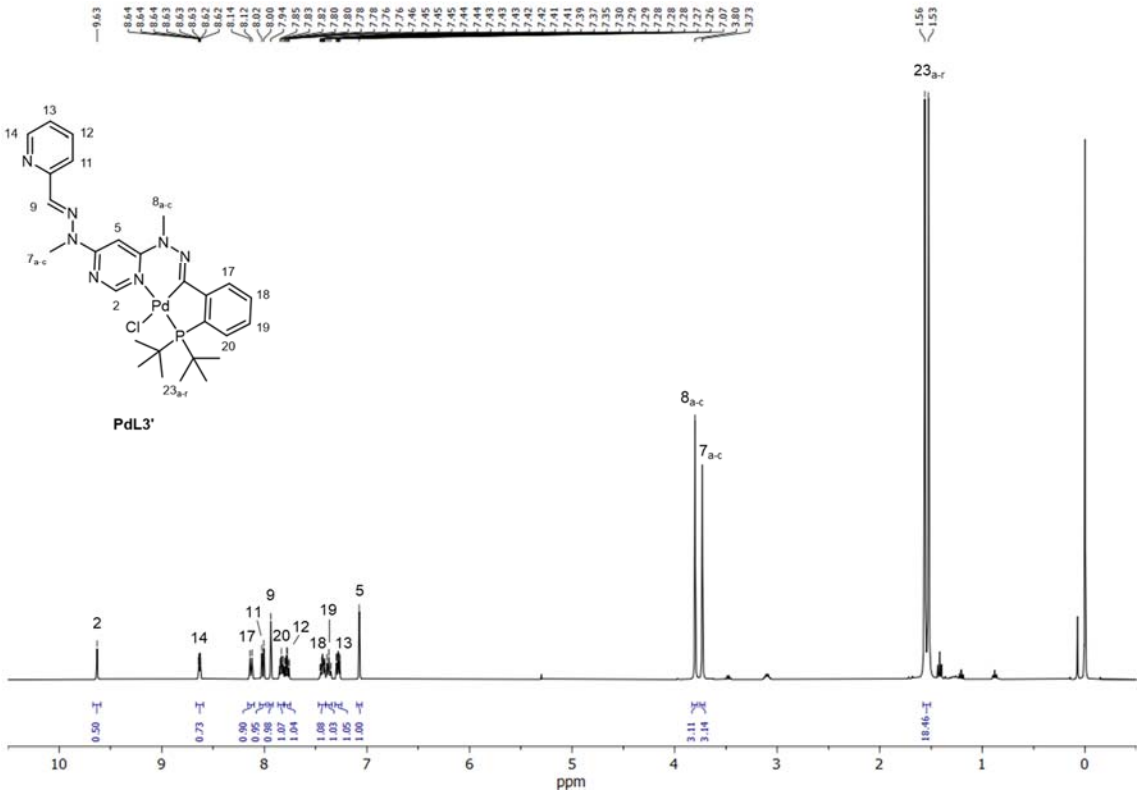

Figure S28. ^{1}H NMR spectrum of **PdL3'** in $CDCl_3$ at 25 °C.

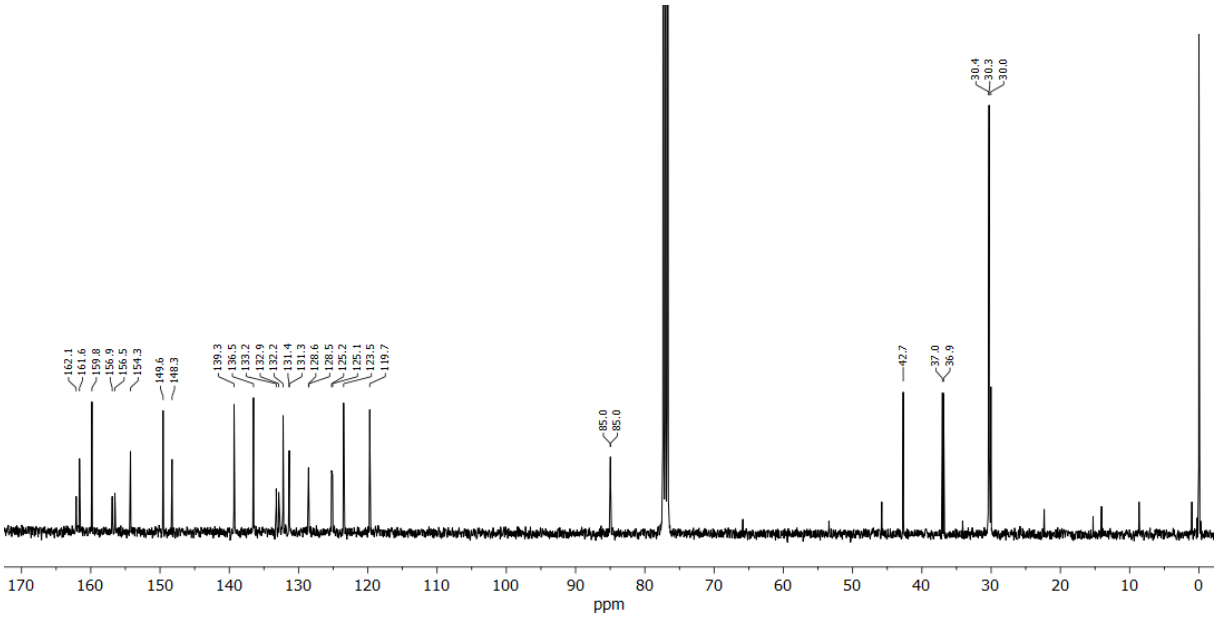

Figure S29. $^{13}C\{^{1}H\}$ NMR spectrum of **PdL3'** in $CDCl_3$ at 25 °C.

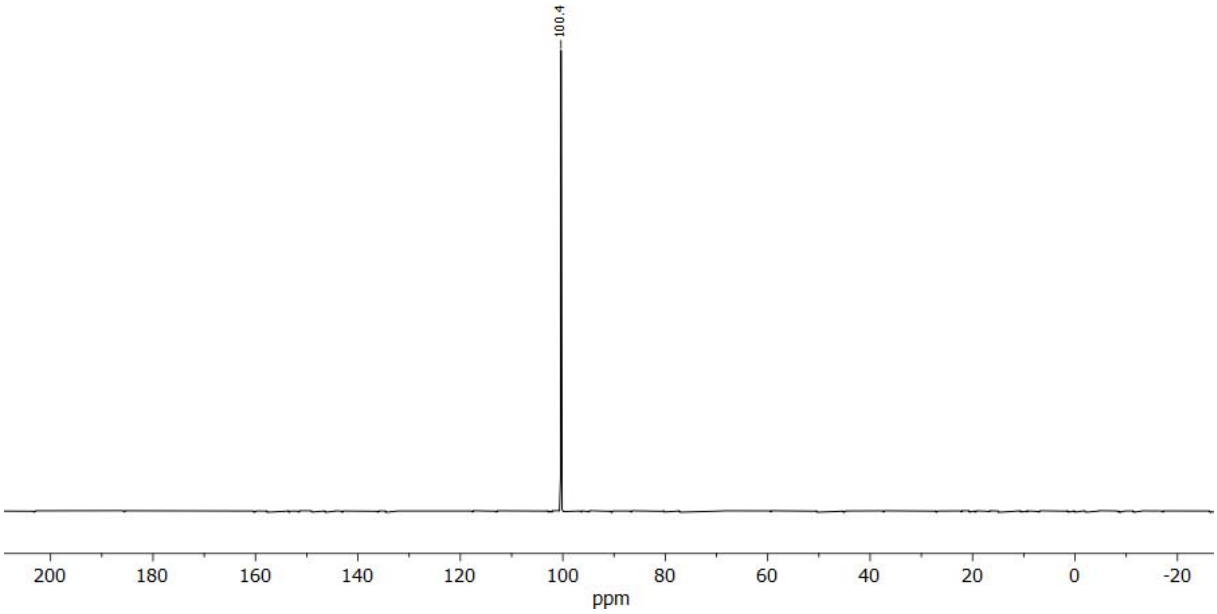

Figure S30. $^{31}P\{^{1}H\}$ NMR spectrum of **PdL3'** in $CDCl_3$ at 25 °C.

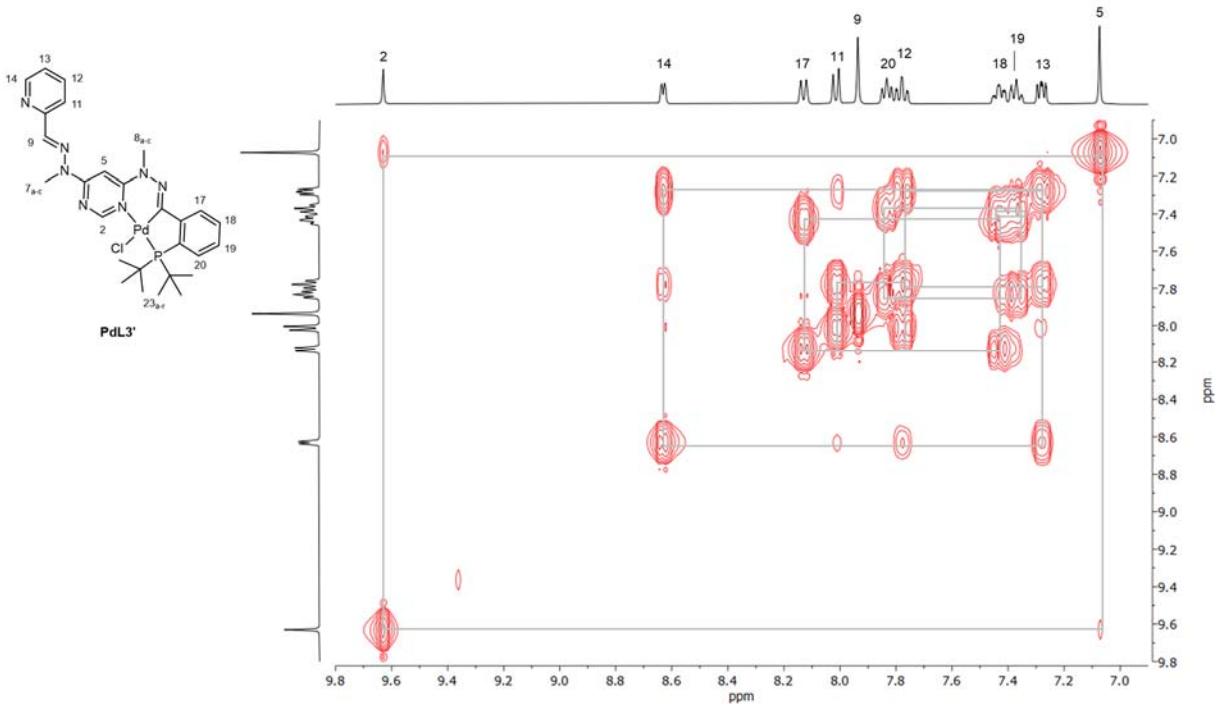

Figure S31. ^{1}H-^{1}H COSY spectrum of **PdL3'** in $CDCl_3$ at 25 °C.

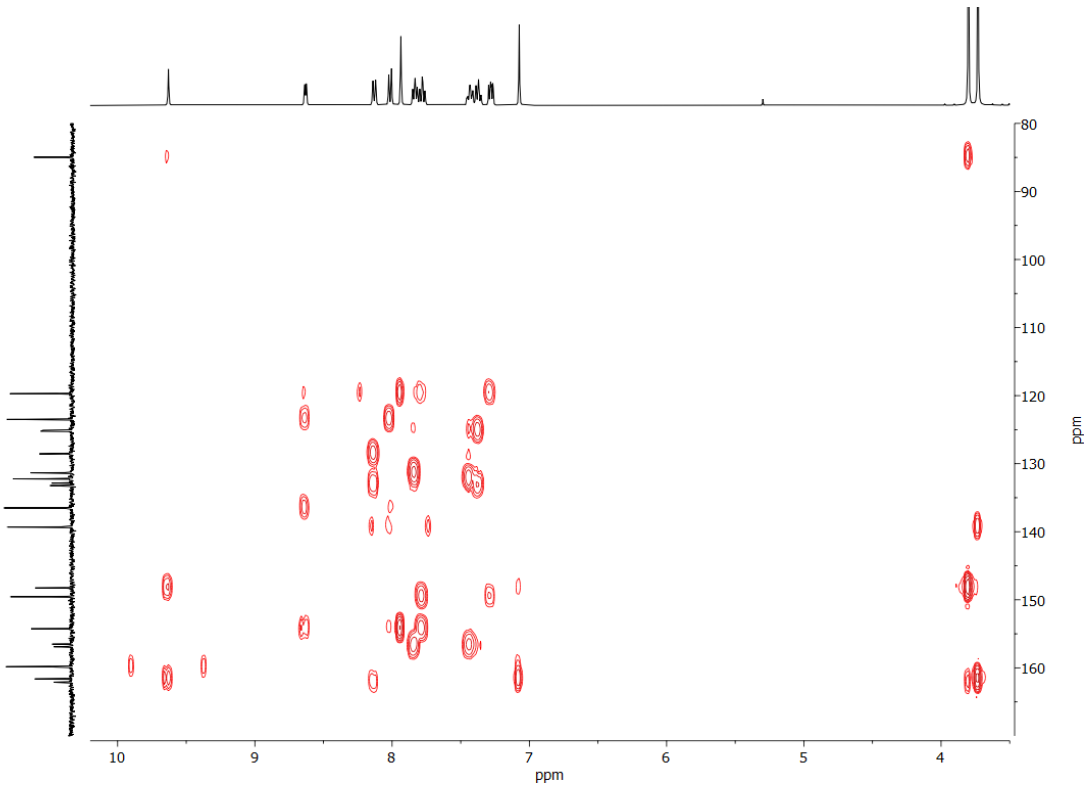

Figure S32. ^{1}H-^{13}C HMBC spectrum of **PdL3'** in $CDCl_3$ at 25 °C.

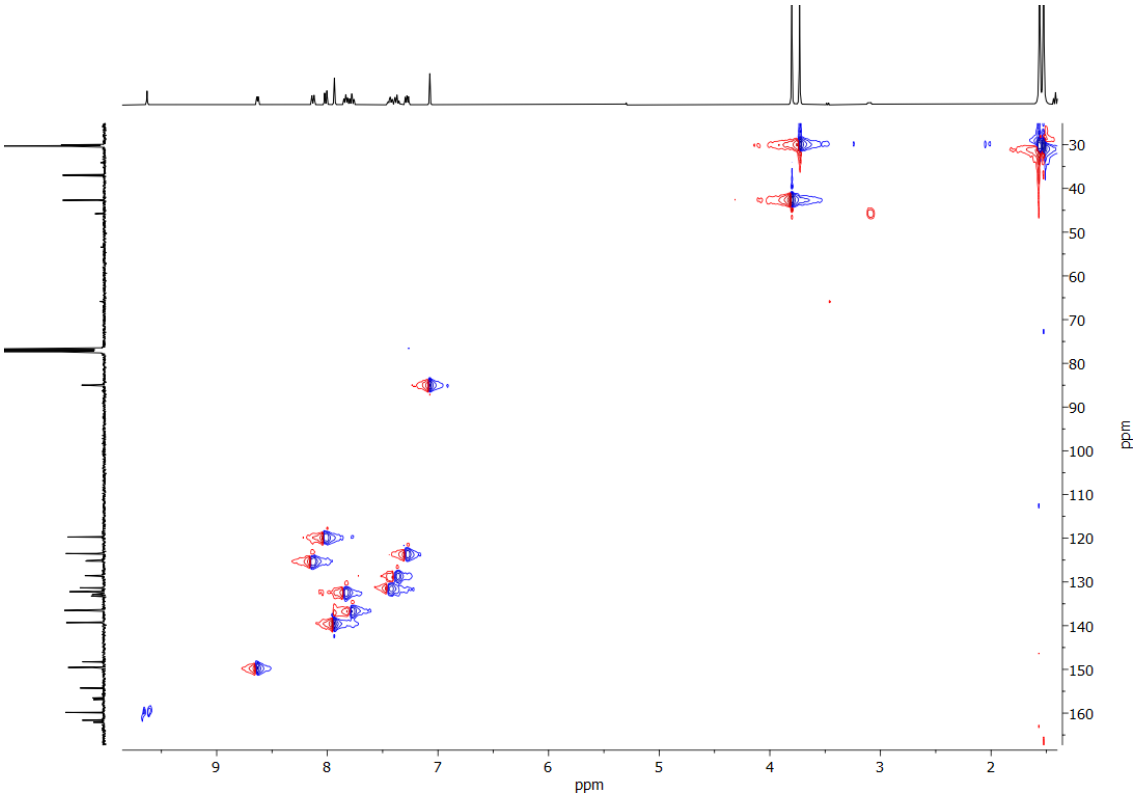

Figure S33. ^{1}H-^{13}C HSQC spectrum of **PdL3'** in $CDCl_3$ at 25 °C.

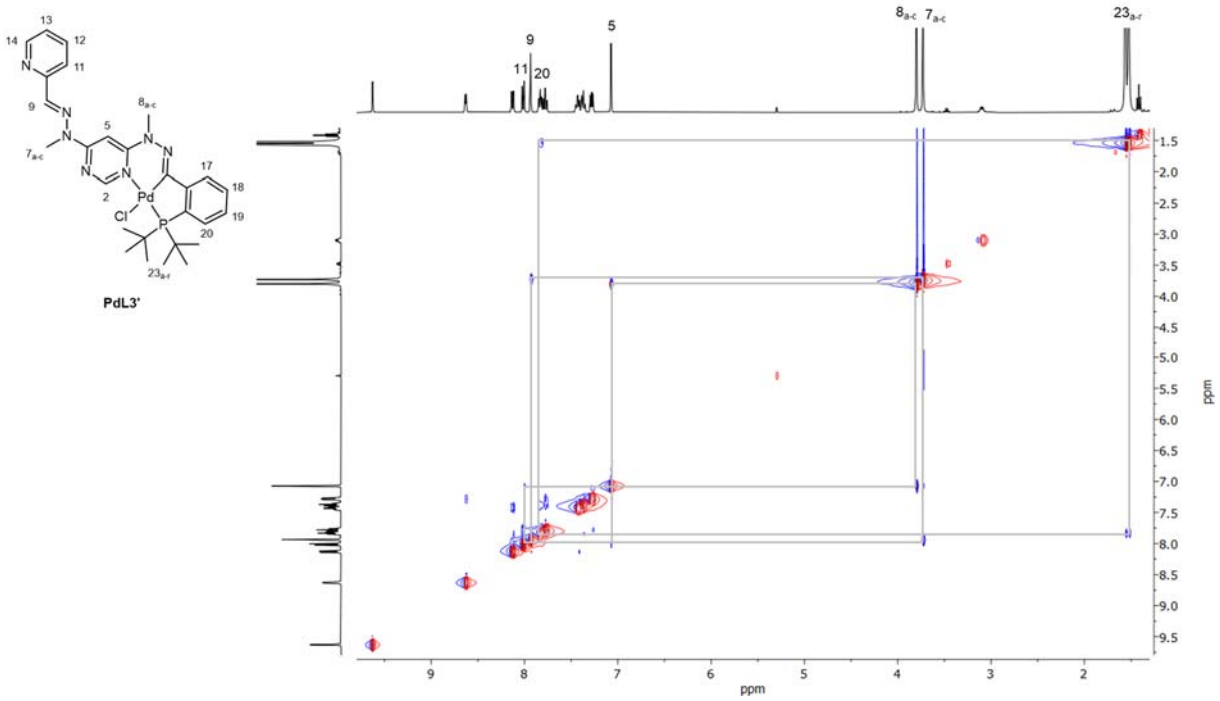

Figure S34. ^{1}H-^{1}H NOESY spectrum of **PdL3'** in $CDCl_3$ at 25 °C.

2.3 **PdL5'** (NMR Spectra (^{1}H, $^{13}C\{^{1}H\}$, $^{31}P\{^{1}H\}$))

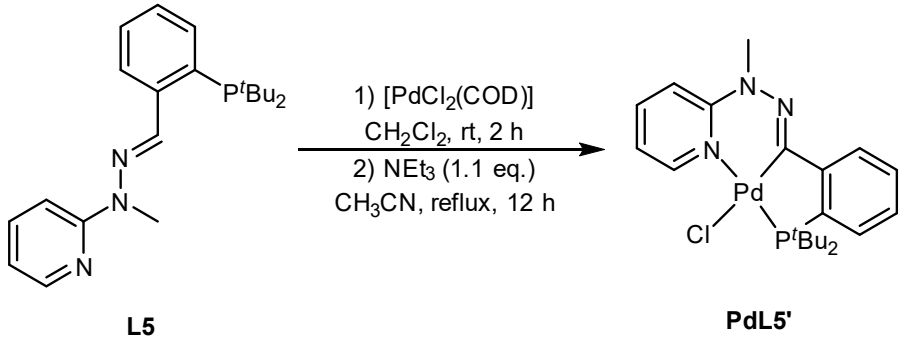

Scheme S6. Synthesis of **PdL5'**.

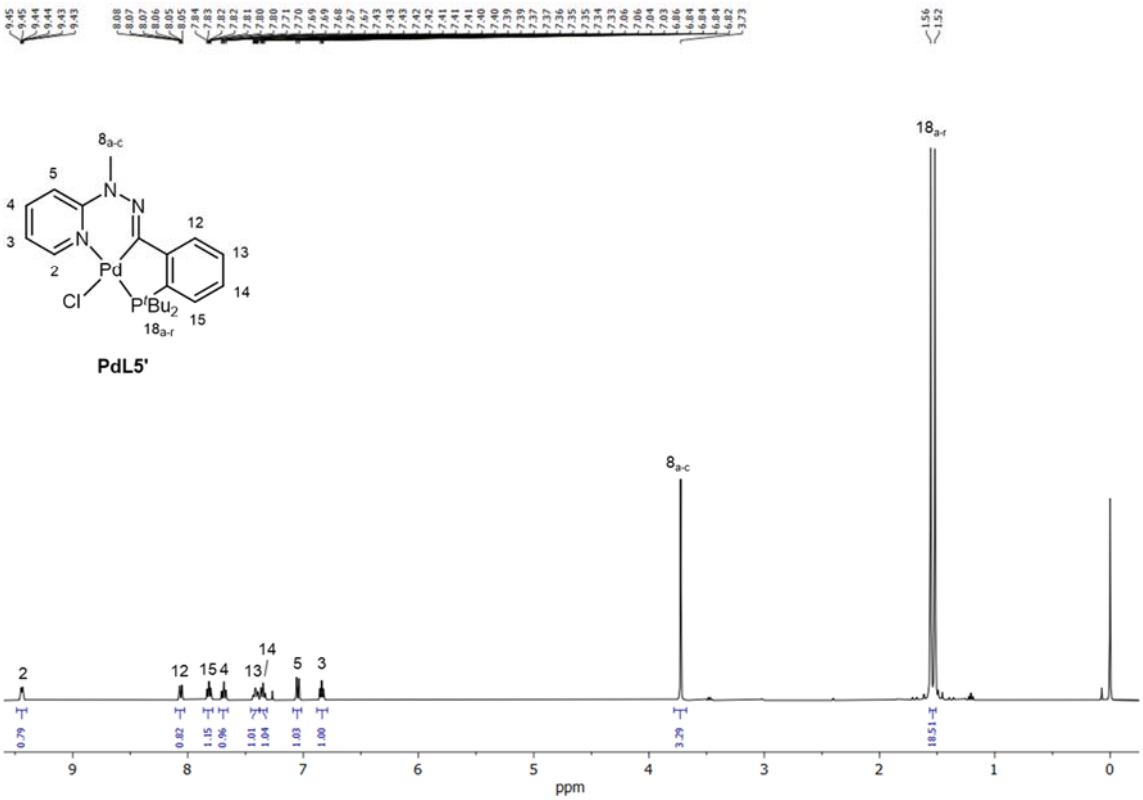

Figure S35. ^{1}H NMR spectrum of **PdL5'** in $CDCl_3$ at 25 °C.

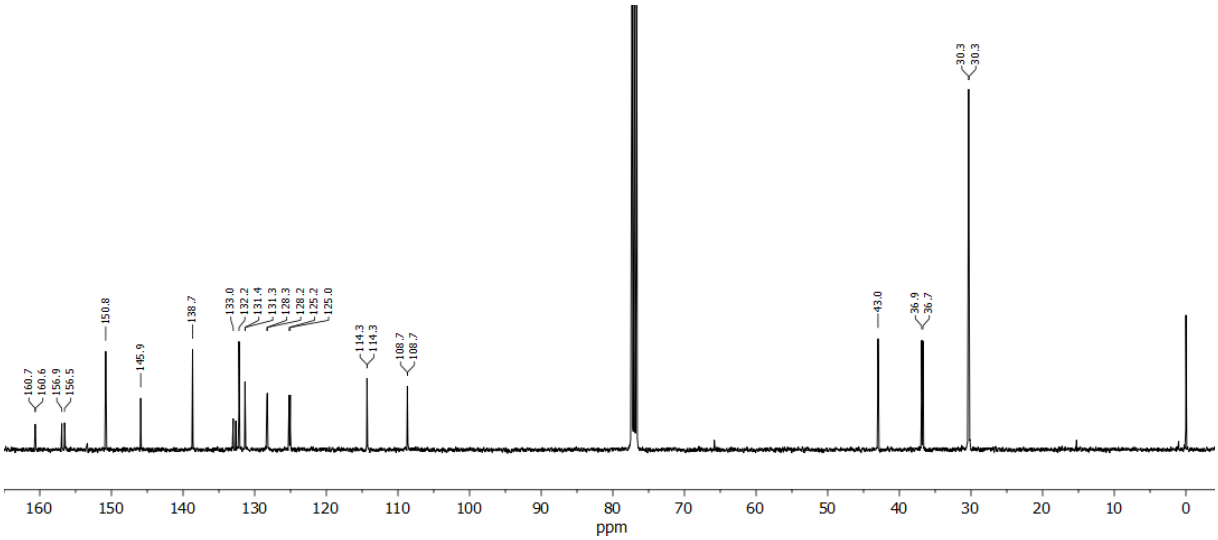

Figure S36. $^{13}C\{^{1}H\}$ NMR spectrum of **PdL5'** in $CDCl_3$ at 25 °C.

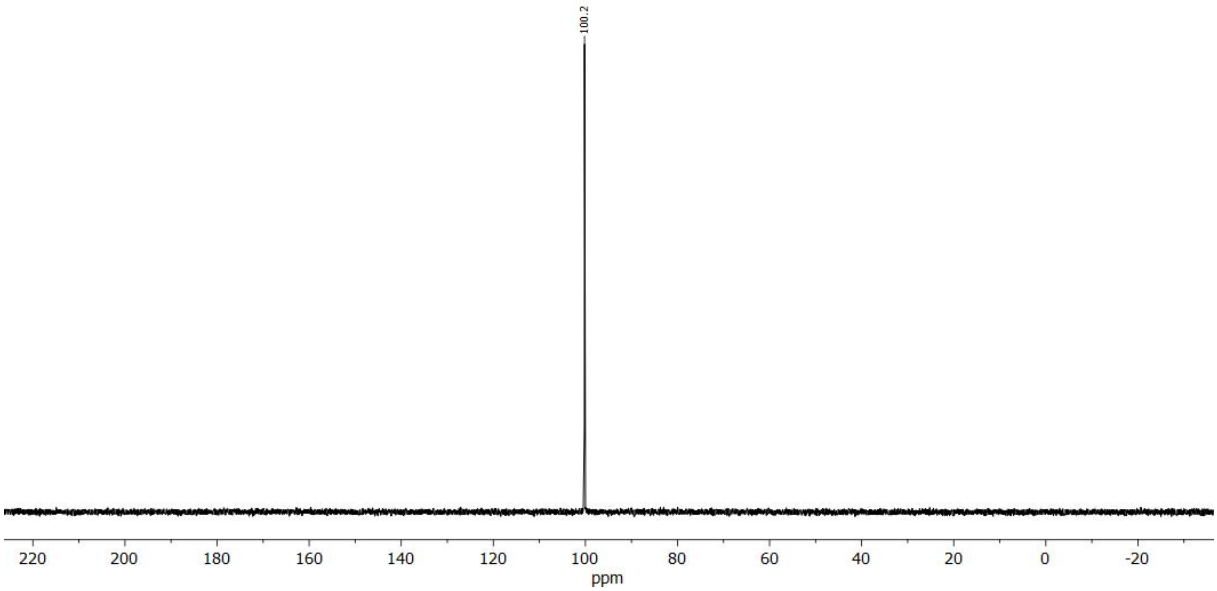

Figure S37. $^{31}P\{^{1}H\}$ NMR spectrum of **PdL5'** in $CDCl_3$ at 25 °C.

3. Monometallic Mn and Co Complex

3.1 MnL4 (Synthesis; NMR Spectra (^{1}H, $^{19}F\{^{1}H\}$))

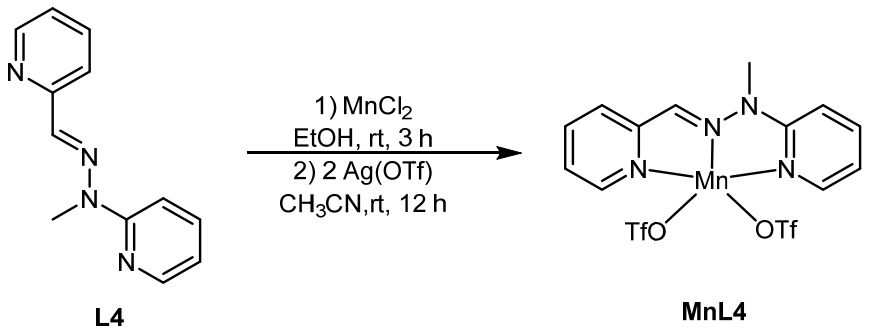

Scheme S7. Synthesis of **MnL4**.

$MnCl_2$ (148 mg, 1.18 mmol, 1.00 eq.) and **L4** (250 mg, 1.18 mmol, 1.00 eq.) were dissolved in EtOH (30 mL). The orange solution was stirred for 3 h at room temperature forming an orange precipitate. The solid was filtered off, washed with EtOH (2 x 20 mL) and dried *in vacuo* to give [$MnCl_2$(**L4**)] as an orange solid (304 mg, 76%). Ag(OTf) (464 mg, 1.81 mmol, 2.01 eq.) and CH_3CN (20 mL) were added to [$MnCl_2$(**L4**)]. The mixture was stirred for 12 h at room temperature. The orange solution was filtered over Celite, and the solvent was removed *in vacuo*. The orange solid was washed with Et_2O (10 mL) and *n*-pentane (10 mL). The solid was dried under vacuum at 40 °C for 3 h to give **MnL4** as an orange solid (410 mg, 81%). Elemental analysis: $C_{14}H_{12}F_6MnN_4O_6S_2$, calculated (%): C 29.74, H 2.14, N 9.91, found (%): C 29.66, H 1.82, N 10.08. HRMS (ESI pos., CH_3CN): *m/z* calculated for $[M–CF_3SO_3]^+$: 415.996, found: 415.993 (100%); calculated for $[[M]_2–CF_3SO_3]^+$: 980.944, found: 980.940 (50%). Selected ATR-IR: $\tilde{\nu}$ (cm^{-1}) = 3045 (w, *v*C–H), 1604 (m, *v*C=N/*v*C=C), 1476 (m, *v*C=C), 1440 (m, *v*C=C), 1210 (s, $v_s CF_3$), 1163 (s, $v_{as} CF_3$), 1027 (s, $v_s SO_3$). ^{1}H NMR (400 MHz, CD_3CN): δ (ppm) = 14.9 (br). Due to the paramagnetic Mn^{II} centre, some protons were not observed in the ^{1}H NMR spectrum. $^{19}F\{^{1}H\}$ NMR (377 MHz, CD_3CN): δ (ppm) = −55.7 (br).

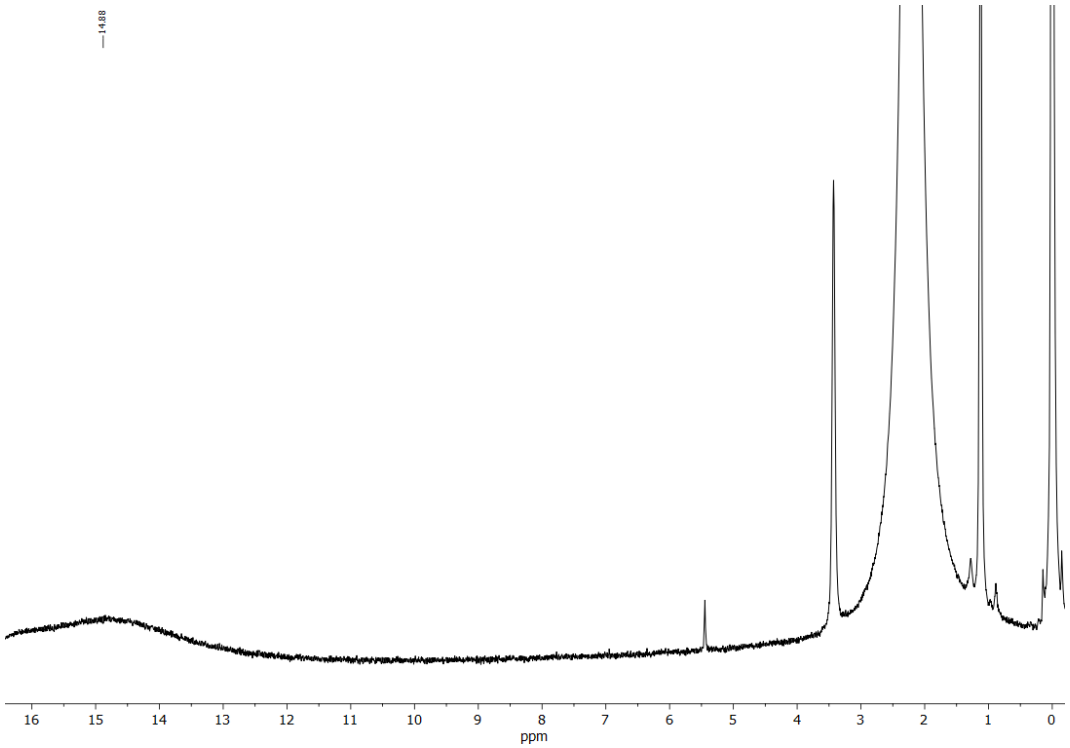

Figure S38. ^{1}H NMR spectrum of **MnL4** in CD_3CN at 25 °C.

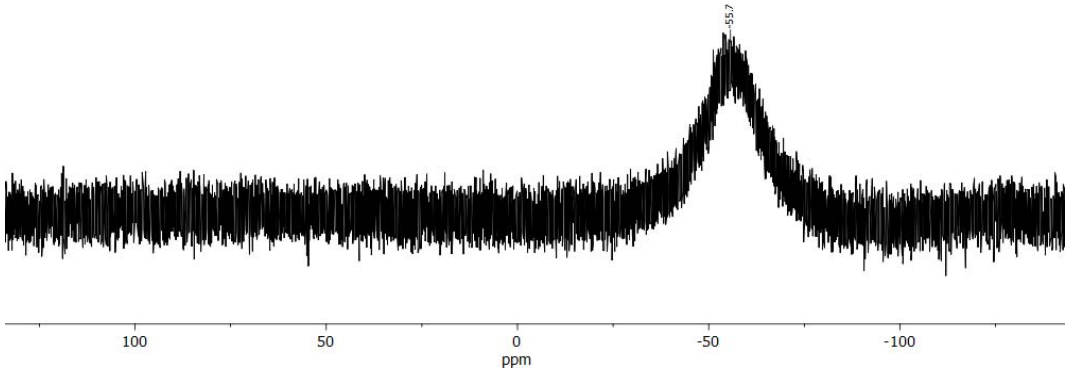

Figure S39. ^{19}F{^{1}H} NMR spectrum of **MnL4** in CD_3CN at 25 °C.

3.2 **CoL4** (Synthesis; NMR Spectra (^{1}H, $^{19}F\{^{1}H\}$))

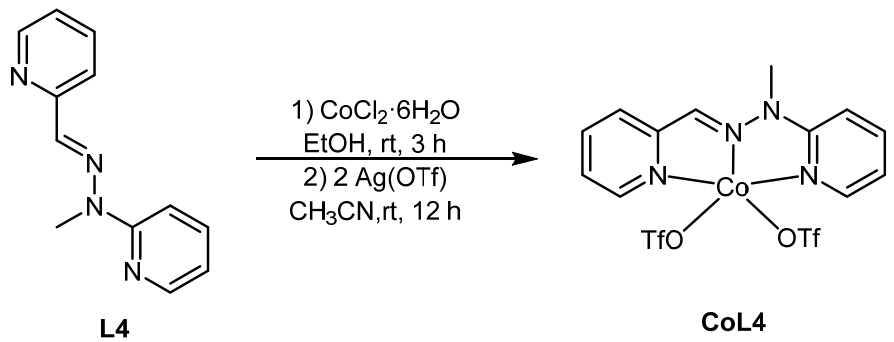

Scheme S8. Synthesis of **CoL4**.

A solution of $CoCl_2 \cdot 6H_2O$ (710 mg, 3.00 mmol, 1.00 eq.) in EtOH (30 mL) was added dropwise to a solution of **L4** (640 mg, 3.00 mmol, 1.00 eq.) in EtOH (30 mL). The dark green solution was stirred for 3 h at room temperature. The green precipitate was filtered, washed with EtOH (2 x 20 mL) and dried *in vacuo* to give [$CoCl_2$(**L4**)] as a dark green solid (739 mg, 72%). Ag(OTf) (150 mg, 0.29 mmol, 2.01 eq.) was added to a suspension of [$CoCl_2$(**L4**)] (100 mg, 0.29 mmol 1.00 eq.) in CH_3CN (10 mL). The mixture was stirred for 12 h at room temperature. The orange solution was filtered over Celite, and the solvent was removed *in vacuo*. The dark red solid was washed with CH_2Cl_2 (5 mL), Et_2O (5 mL) and *n*-pentane (10 mL). The solid was dried under vacuum at 40 °C for 3 h to give **CoL4** as a dark red, hygroscopic solid (134 mg, 81%). Elemental analysis: $C_{14}H_{12}CoF_6N_4O_6S_2 \cdot 2CH_3CN \cdot 0.4C_5H_{12}$, calculated (%): C 35.31, H 3.38, N 12.35, found (%): C 35.62, H 3.12, N 12.48. HRMS (ESI pos., CH_3CN): *m/z* calculated for $[M–CF_3SO_3]^+$: 419.991, found: 419.990 (100%). Selected ATR-IR: $\tilde{\nu}$ (cm^{-1}) = 3068 (w, *v*C–H), 2963 (w, *v*C–H), 1601 (m, *v*C=N/*v*C=C), 1470 (m, *v*C=C), 1440 (m, *v*C=C), 1238 (s, $v_{as}SO_3$), 1223 (s, v_sCF_3), 1145 (s, $v_{as}CF_3$), 1026 (s, v_sSO_3). ^{1}H NMR (400 MHz, CD_3CN): δ (ppm) = 11.53 (s, 1H), 10.90 (s, 3H), 3.54 (s, 1H). Due to the paramagnetic Co^{II} centre, some protons were not observed in the ^{1}H NMR spectrum. $^{19}F\{^{1}H\}$ NMR (377 MHz, CD_3CN): δ (ppm) = −78.5 (s).

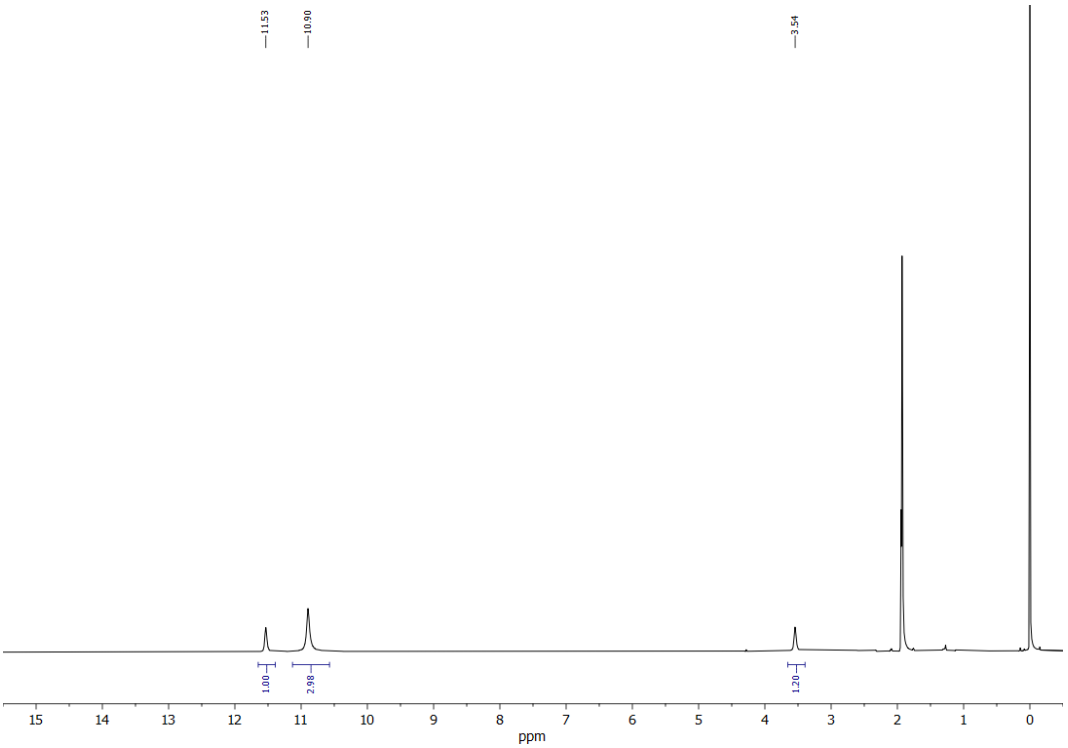

Figure S40. ^{1}H NMR spectrum of **CoL4** in CD_3CN at 25 °C.

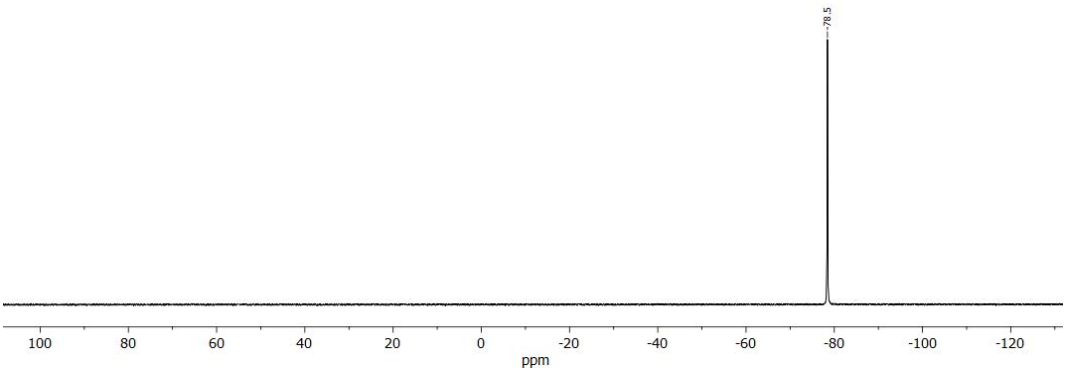

Figure S41. ^{19}F{^{1}H} NMR spectrum of **CoL4** in CD_3CN at 25 °C.

4. Heterobimetallic Pd Complexes

4.1 **CoPdL2** (NMR Spectra (^{1}H, $^{19}F\{^{1}H\}$, $^{31}P\{^{1}H\}$))

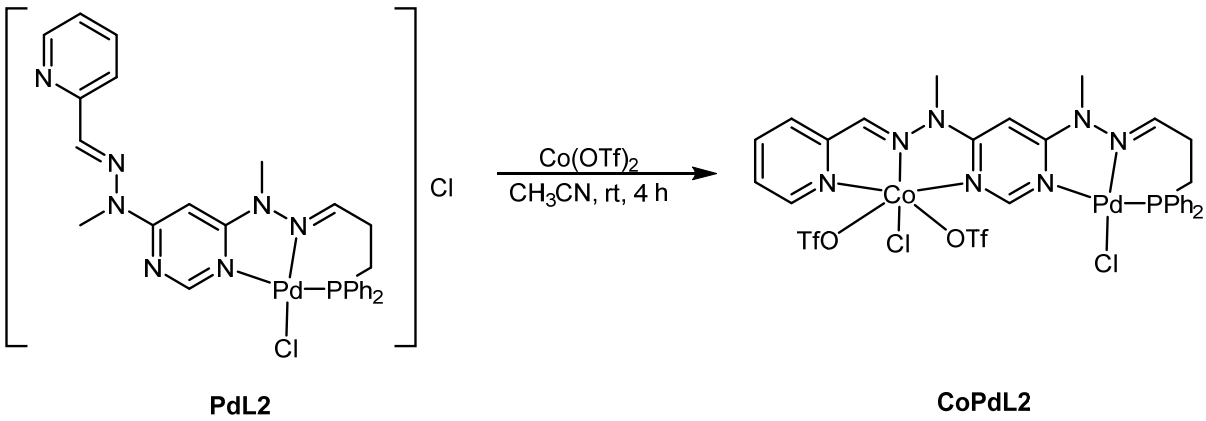

Scheme S9. Synthesis of **CoPdL2**.

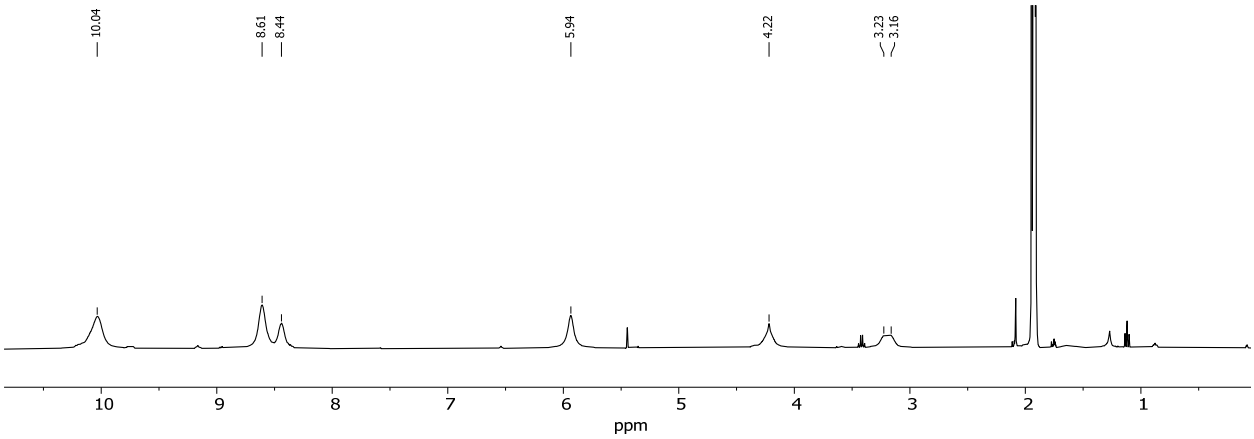

Figure S42. ^{1}H NMR spectrum of **CoPdL2** in CD_3CN at 25 °C.

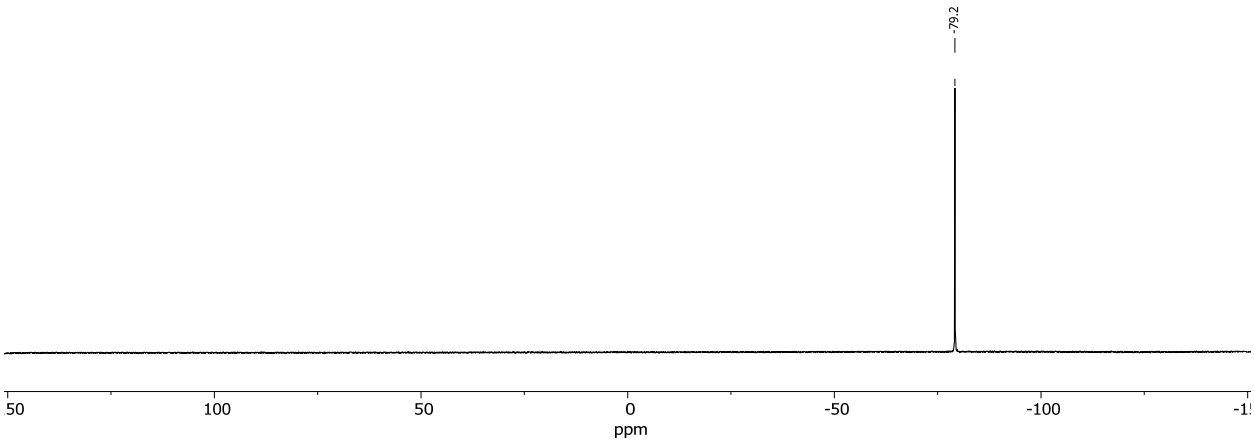

Figure S43. $^{19}F\{^{1}H\}$ NMR spectrum of **CoPdL2** in CD_3CN at 25 °C.

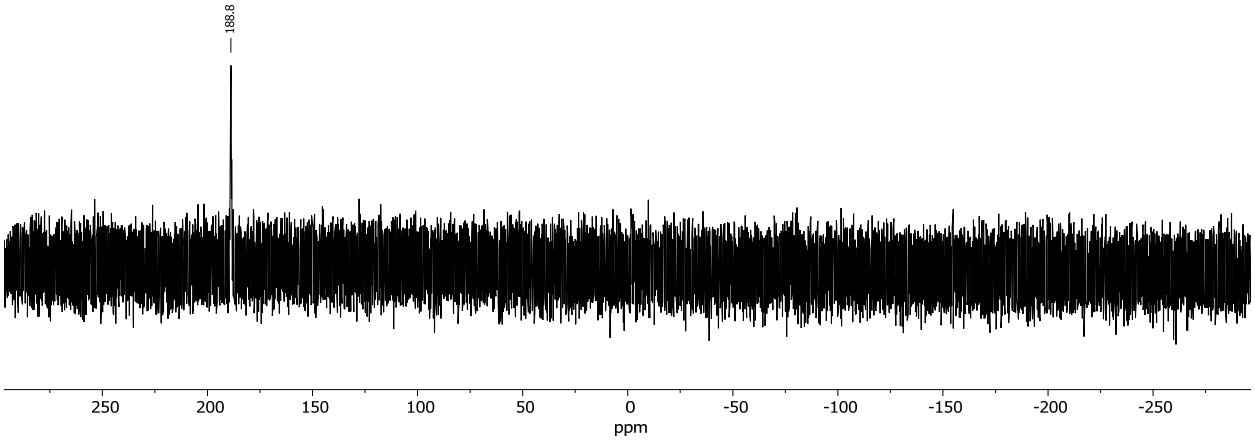

Figure S44. $^{31}P\{^{1}H\}$ NMR spectrum of **CoPdL2** in CD_3CN at 25 °C.

4.2 **MnPdL3'** (NMR Spectra (^{1}H, $^{19}F\{^{1}H\}$, $^{31}P\{^{1}H\}$))

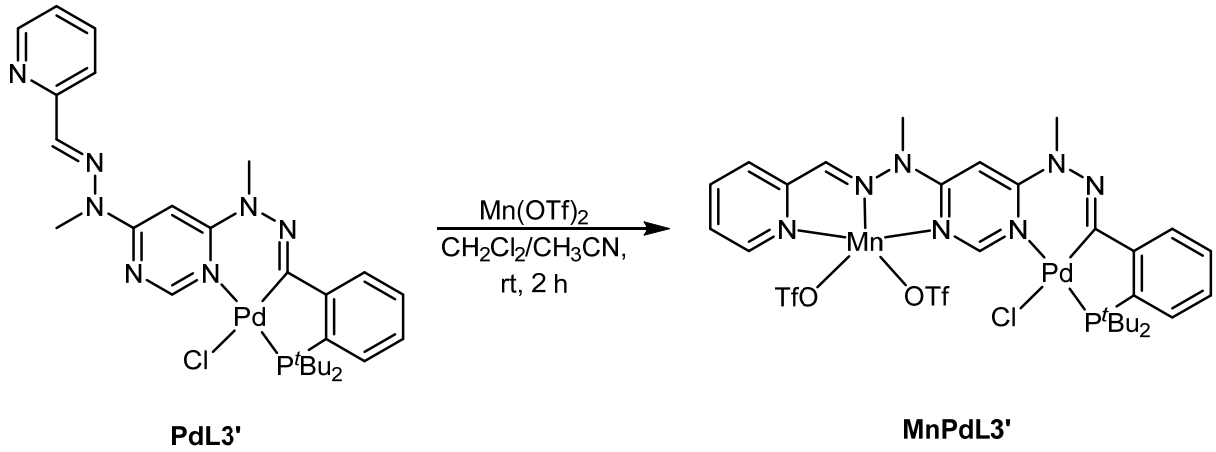

Scheme S10. Synthesis of **MnPdL3'**.

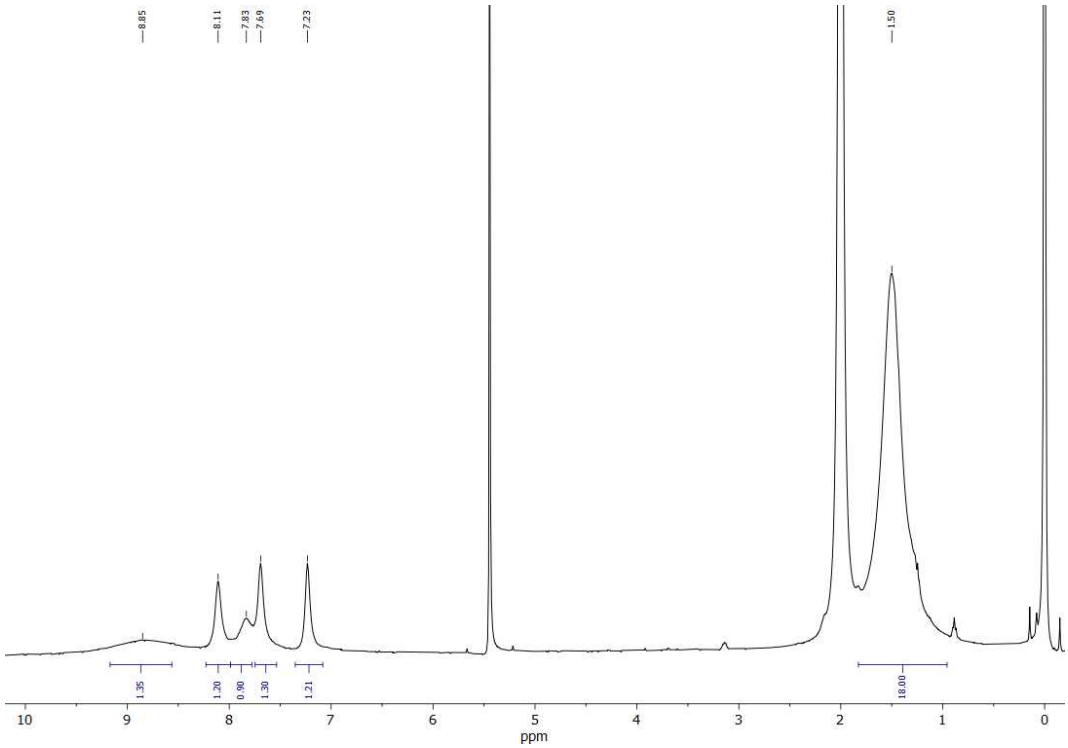

Figure S45. ^{1}H NMR spectrum of **MnPdL3'** in CD_3CN at 25 °C.

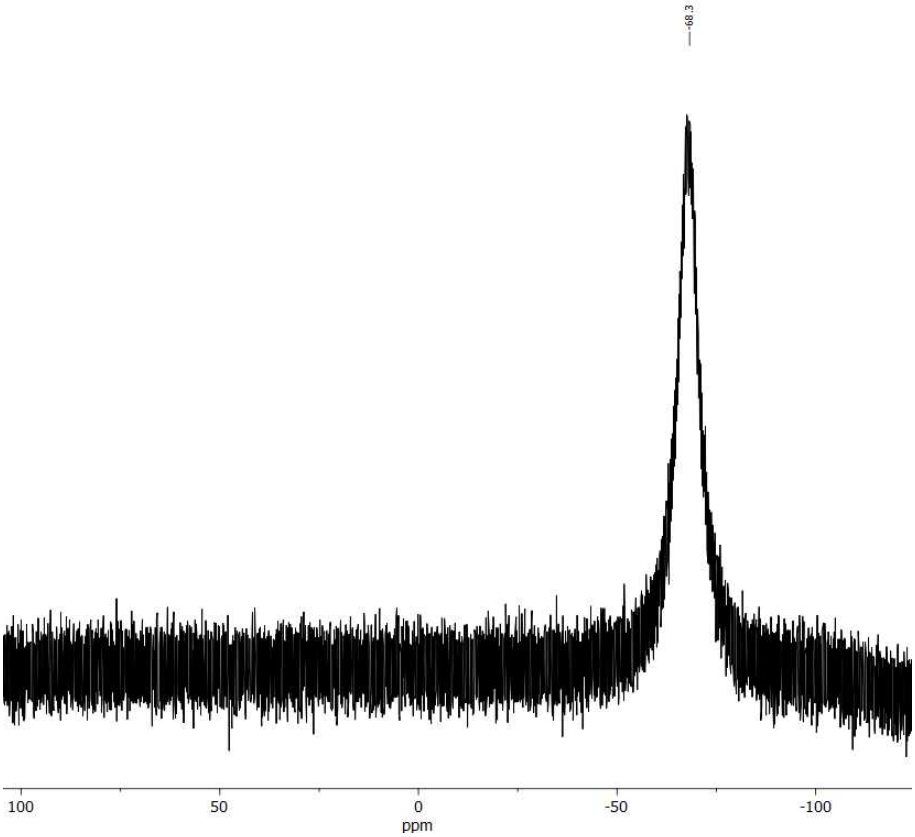

Figure S46. $^{19}F\{^{1}H\}$ NMR spectrum of **MnPdL3'** in CD_3CN at 25 °C.

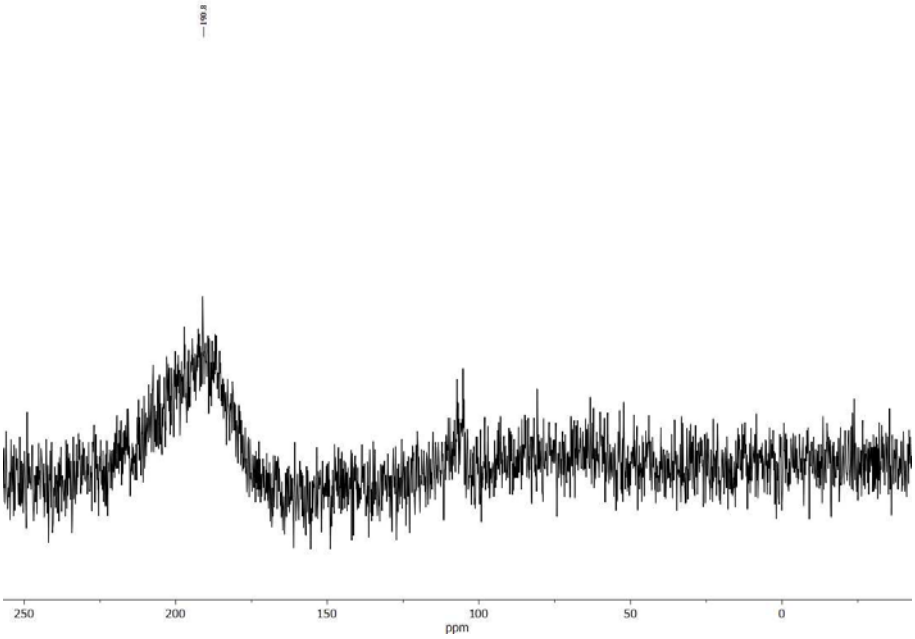

Figure S47. $^{31}P\{^{1}H\}$ NMR spectrum of **MnPdL3'** in CD_3CN at 25 °C.

4.3 **CoPdL3'** (NMR Spectra (^{1}H, $^{19}F\{^{1}H\}$, $^{31}P\{^{1}H\}$))

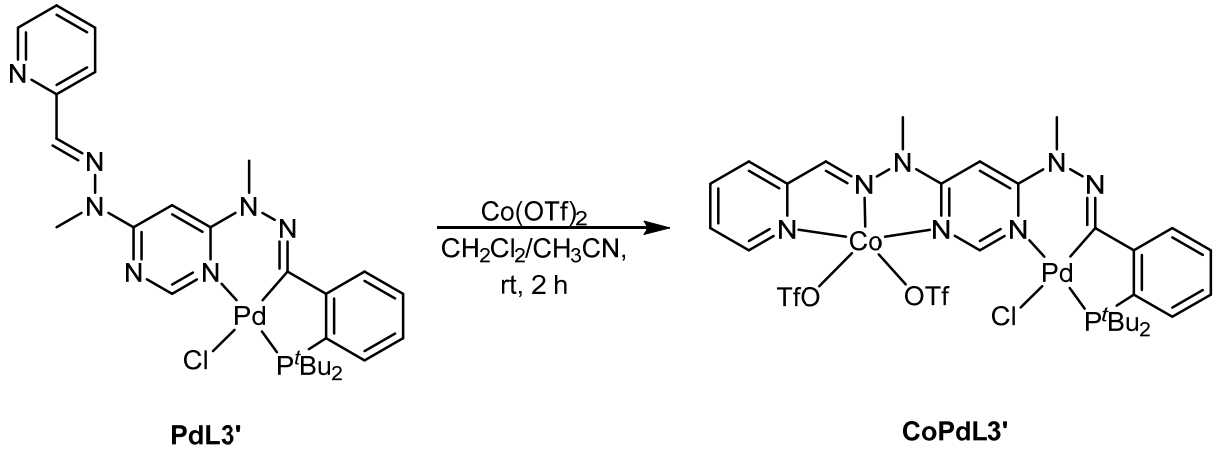

Scheme S11. Synthesis of **CoPdL3'**.

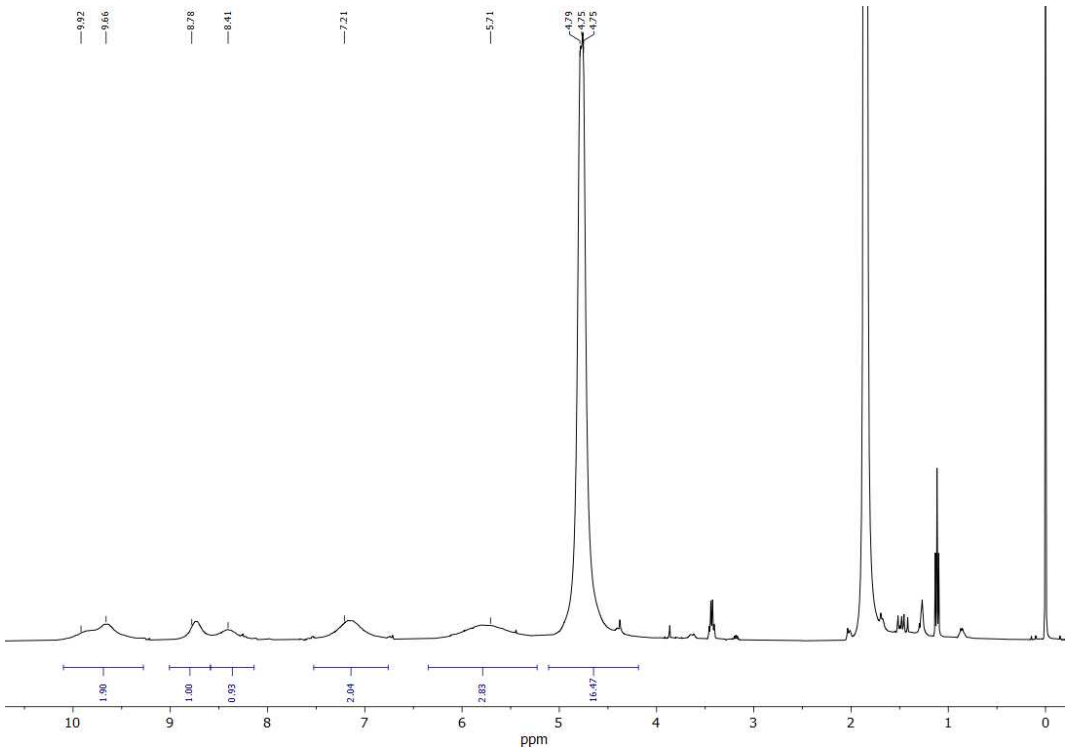

Figure S48. ^{1}H NMR spectrum of **CoPdL3'** in CD_3CN at 25 °C.

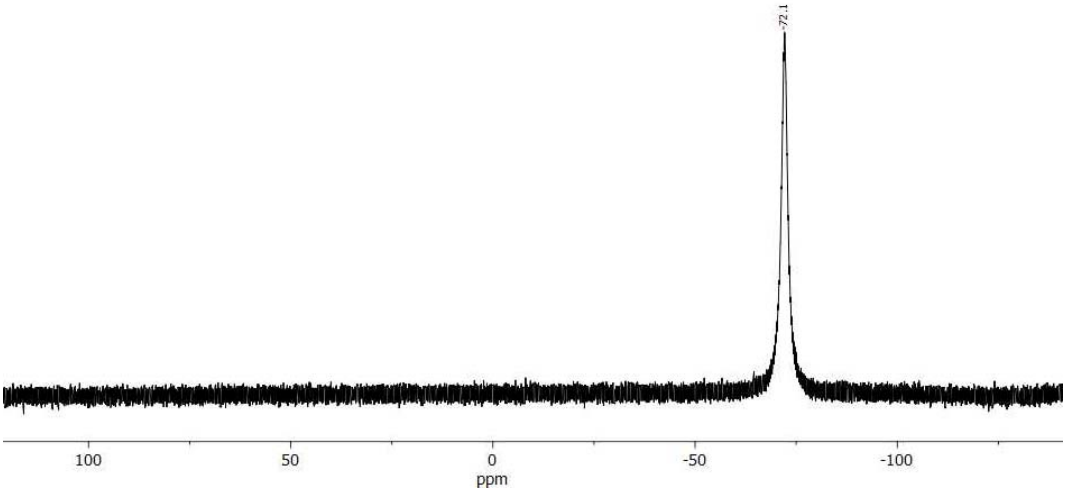

Figure S49. $^{19}F\{^{1}H\}$ NMR spectrum of **CoPdL3'** in CD_3CN at 25 °C.

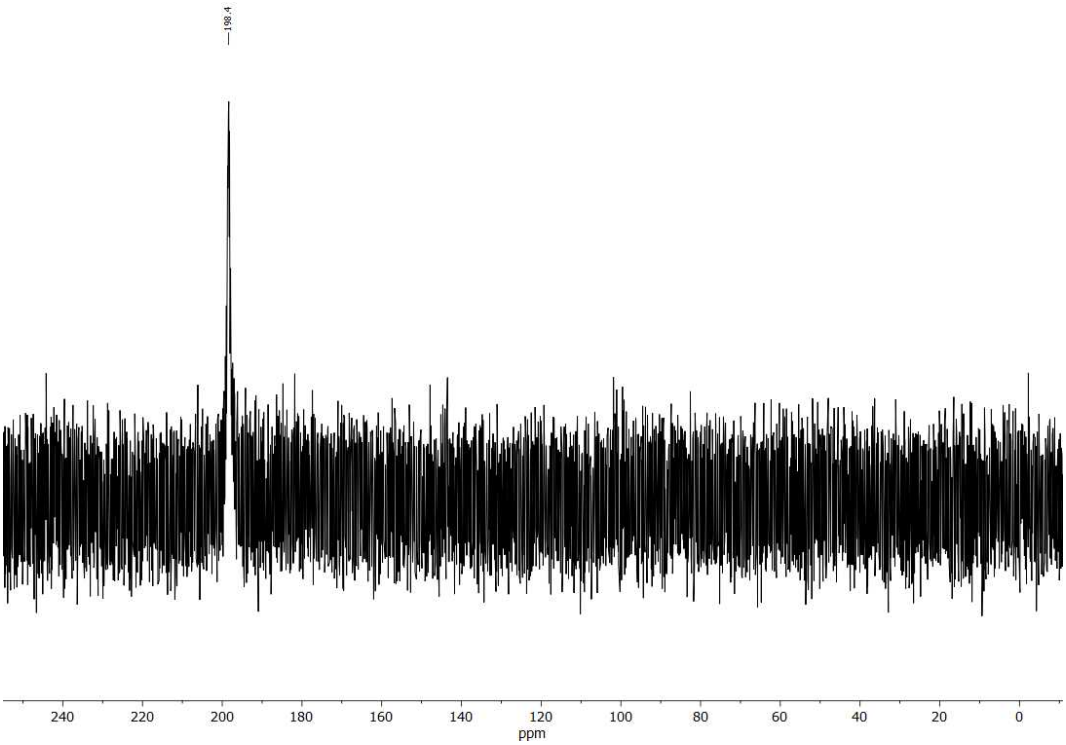

Figure S50. $^{31}P\{^{1}H\}$ NMR spectrum of **CoPdL3'** in CD_3CN at 25 °C.

4.4 Dihedral Angle

Table S1. Dihedral angles [deg] between two planes formed by N1,N2,N4,M1 (M = Mn^{II}, Co^{II}) and N5,N7/C15,P1,Pd1.

Complex	Dihedral angle [deg]
$[MnPdCl_2(OTf)_2(\mathbf{L1})]$	1.2
$[CoPdCl_2(OTf)(\mathbf{L1})]_2(OTf)_2$	10.0
$[CoPdCl_2(CH_3CN)(\mathbf{L2})]_2(OTf)_4$	22.8
$[MnPd(\mathbf{L3'})(OTf)_3(CH_3CN)]$	26.7
$[CoPd(\mathbf{L3'})(OTf)_3(CH_3CN)]$	23.8

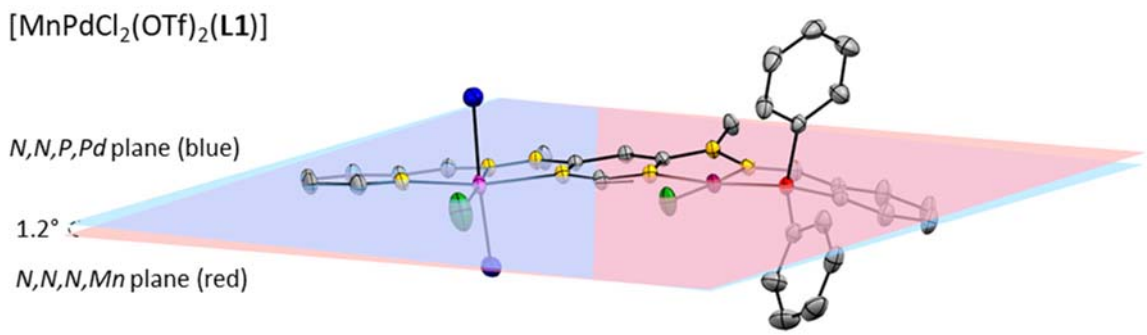

Figure S51. Molecular structure of complex $[MnPdCl_2(OTf)_2(\mathbf{L1})]$ (only the oxygen atoms of the triflate anions are shown; solvent molecules and hydrogen atoms are omitted for clarity). The dihedral angle (1.2°) was determined between the two planes of *N,N,N,Mn* (red) and *N,N,P,Pd* (blue).

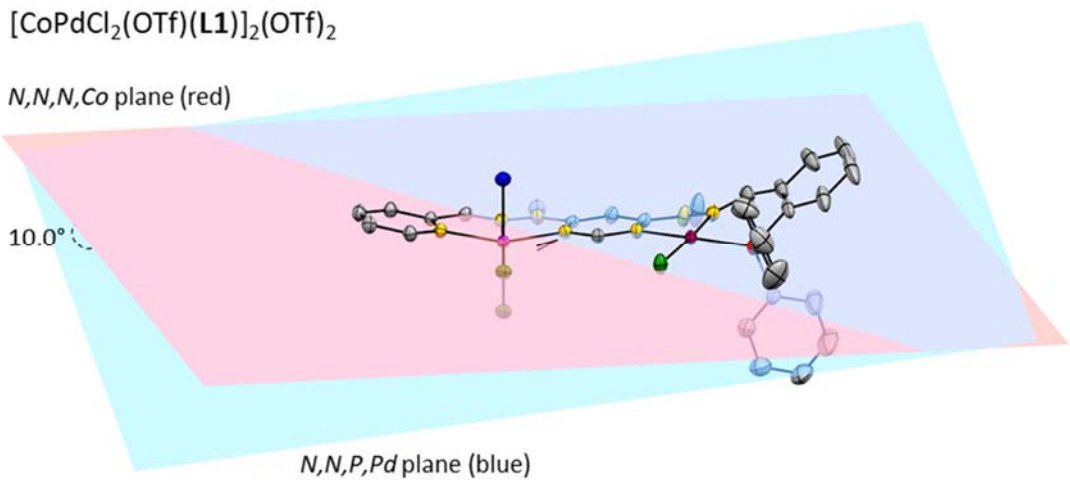

Figure S52. Molecular structure of complex $[CoPdCl_2(OTf)(\mathbf{L1})]_2(OTf)_2$ (only the monomer of the dimeric structure and oxygen atoms of the coordinating triflate anions are shown; solvent molecules, noncoordinating triflate anions, and hydrogen atoms are omitted for clarity). The dihedral angle (10.0°) was determined between the two planes of *N,N,N,Co* (red) and *N,N,P,Pd* (blue).

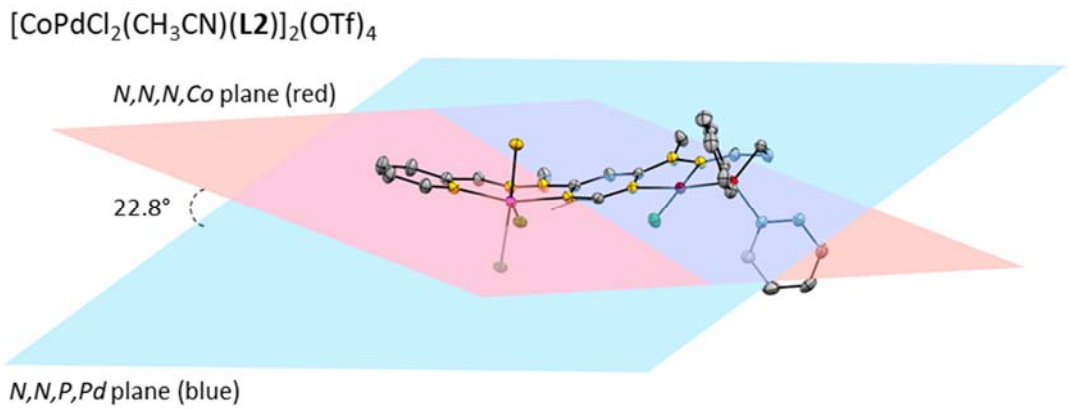

Figure S53. Molecular structure of complex $[CoPdCl_2(CH_3CN)(\mathbf{L2})]_2(OTf)_4$ (only the monomer of the dimeric structure and nitrogen atom of the coordinating CH_3CN molecule are shown; solvent molecules, noncoordinating triflate anions, and hydrogen atoms are omitted for clarity). The dihedral angle (22.8°) was determined between the two planes of *N,N,N,Co* (red) and *N,N,P,Pd* (blue).

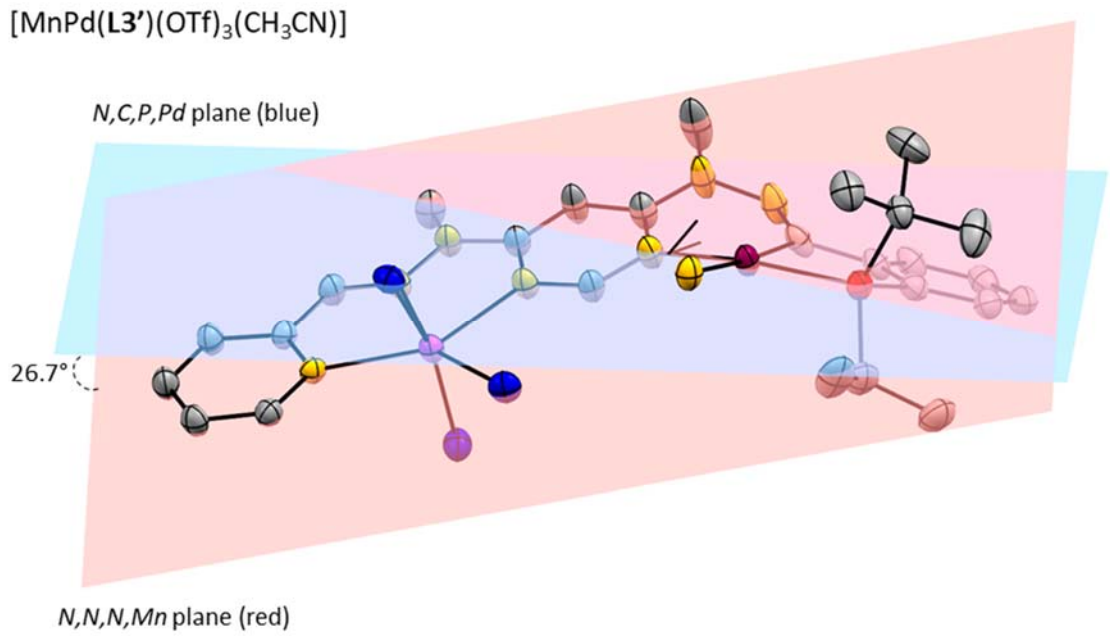

Figure S54. Molecular structure of complex $[MnPd(\mathbf{L3'})(OTf)_3(CH_3CN)]$ (only the oxygen atoms of the coordinating triflate anion and nitrogen atom of the coordinating CH_3CN molecule are shown; solvent molecules and hydrogen atoms are omitted for clarity). The dihedral angle (26.7°) was determined between the two planes of N,N,N,Mn (red) and N,C,P,Pd (blue).

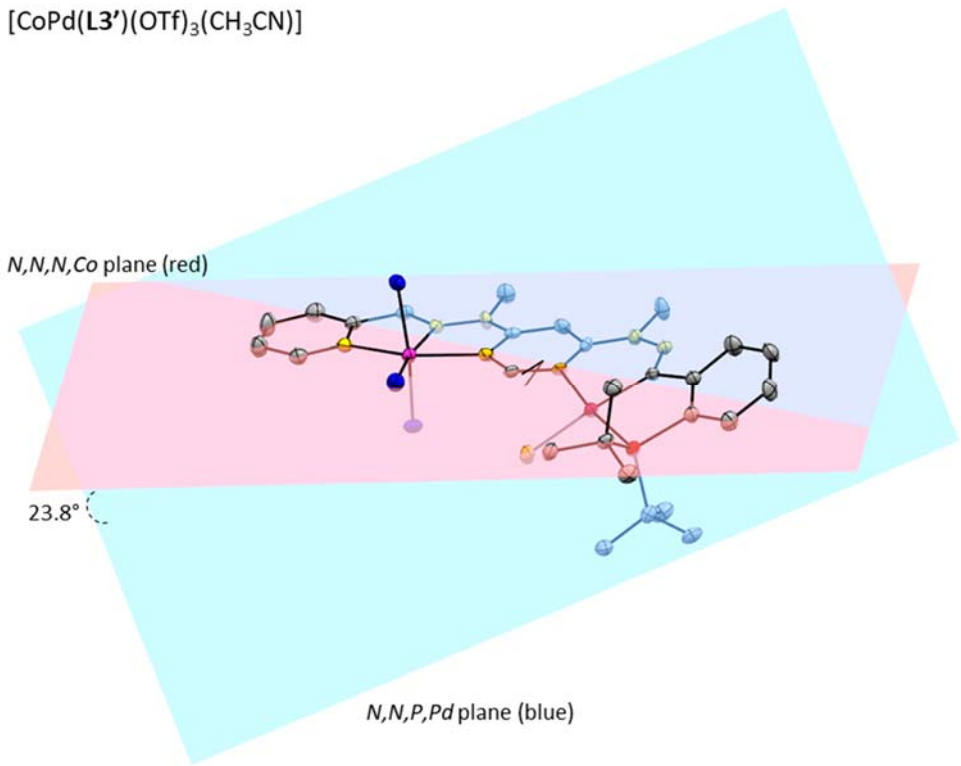

Figure S55. Molecular structure of complex [CoPd(**L3'**)$(OTf)_3(CH_3CN)$] (only the oxygen atoms of the coordinating triflate anion and nitrogen atom of the coordinating CH_3CN molecule are shown; solvent molecules and hydrogen atoms are omitted for clarity). The dihedral angle (26.7°) was determined between the two planes of *N,N,N,Co* (red) and *N,C,P,Pd* (blue).

5. Catalysis

5.1 General Procedure

A mixture of bromobenzene (0.25 mmol, 1.0 eq.), phenylacetylene (0.38 mmol, 1.5 eq.), base (0.50 mmol, 2.0 eq.), precatalyst (0.015 mmol, 6 mol%) and dry, degassed solvent (1.0 mL) were heated under Ar for 4-24 h. The reaction process was monitored by GC-MS. After full conversion of bromobenzene, $NH_3 \cdot BH_3$ (0.25 mmol, 1.0 eq.) was added, and the reaction was continued for 14-24 h at 50 °C. The yields have been determined by GC-MS using naphthalene as an internal standard (4 µL of the reaction solution have been diluted with 1.000 mL of a naphthalene stock solution in acetone).

5.2 Optimisation of the Reaction Conditions

Table S2. Optimisation of the reaction conditions for the Sonogashira cross-coupling reaction. A mixture of bromobenzene (0.25 mmol, 1.0 eq.), phenylacetylene (0.38 mmol, 1.5 eq.), base (0.50 mmol, 2.0 eq.), precatalyst **CoPdL3'** (0.015 mmol, 6 mol%) and dry, degassed solvent (1.0 mL) was heated under Ar for 4-24 h (DABCO = 1,4-diazabicyclo[2.2.2]octane; DIPEA = *N,N*-diisopropylethylamine).

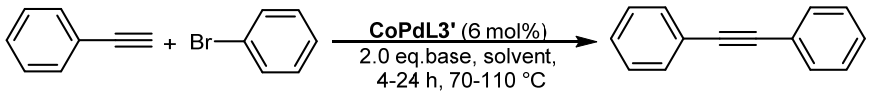

1 **2a** **3a**

Entry	Solvent	Catalyst loading [mol%]	Base	Amount of Base [eq.]	Temperature [°C]	Yield[a] [%] after 4 h	Yield[a] [%] after 24 h
1	CH_3CN	6	DABCO	2.0	90	99	99
2	CH_3CN	6	K_2CO_3	2.0	90	29	99
3	CH_3CN	6	Cs_2CO_3	2.0	90	5	17
4	CH_3CN	6	NEt_3	2.0	90	8	22
5	CH_3CN	6	DIPEA	2.0	90	8	19
6	Toluene	6	DABCO	2.0	110	23	68
7	Dioxane	6	DABCO	2.0	110	78	84
8	THF	6	DABCO	2.0	70	89	90
9	^{t}BuOH	6	DABCO	2.0	90	62	62
10	DMF	6	DABCO	2.0	110	65	65
11	^{t}BuOH	6	K_2CO_3	2.0	90	18	99
12	CH_3CN	3	DABCO	2.0	90	80	81
13	CH_3CN	6	DABCO	1.0	90	72	78

[a] The yields have been determined by GC-MS using naphthalene as an internal standard (4 µL of the reaction solution have been diluted with 1.000 mL of a naphthalene stock solution in acetone).

Table S3. Comparison of monometallic and heterobimetallic Pd^{II} complexes as precatalyst for the transfer semi-hydrogenation. A mixture of diphenylacetylene (0.25 mmol, 1.0 eq.), $NH_3{\cdot}BH_3$ (0.25 mmol, 1.0 eq.), precatalyst (0.015 mmol, 6 mol%) and dry, degassed CH_3CN (1.0 mL) was heated to 50 °C under Ar for 6-24 h.

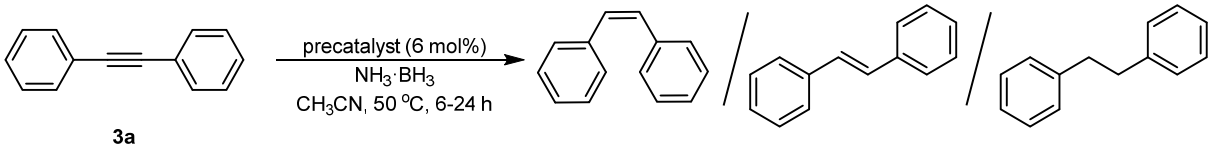

3a

Z/*E*/alkane ratio

Entry	Precatalyst	Yield [%][a] after 6 h *Z*/*E*/alkane (after 24 h)
1	**CoPdL3'**	10/60/30
2	**PdL3'**	3/31/66
3	**CoL4/PdL5'**	32/68/-
4	**CoL4**	9/6/- (24/58/-)
5	**PdL5'**	21/50/28
6	-	-/-/- (-/3/-)

[a] The yields have been determined by GC-MS using naphthalene as internal standard (4 µL of the reaction solution have been diluted with 1.000 mL of a naphthalene stock solution in acetone).

5.3 Reaction Process

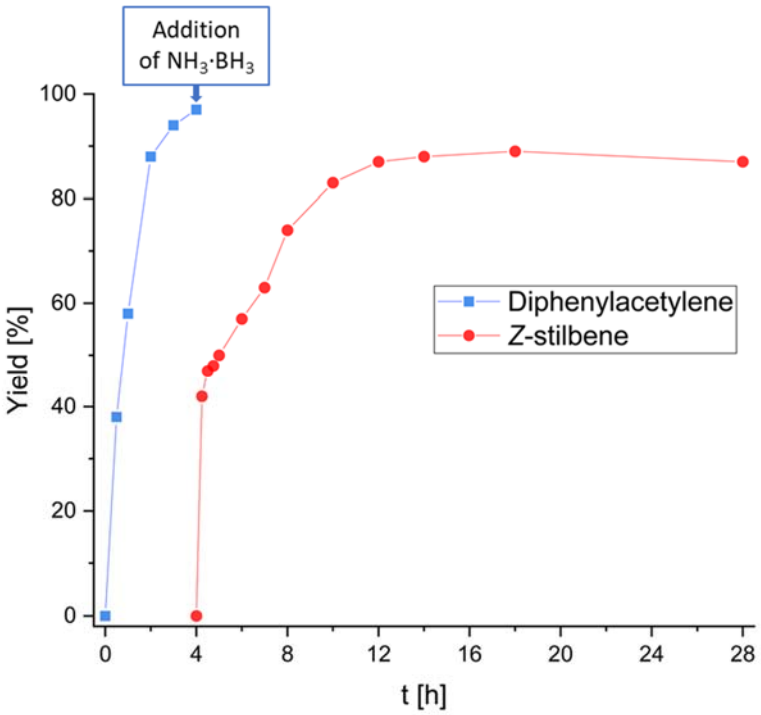

Figure S56. Yield-over-time graph for the formation of diphenylacetylene (blue) in the Sonogashira cross-coupling reaction followed by the formation of *Z*-stilbene (red) after adding $NH_3 \cdot BH_3$ at t = 4 h. The yields have been determined by GC-MS using naphthalene as internal standard.

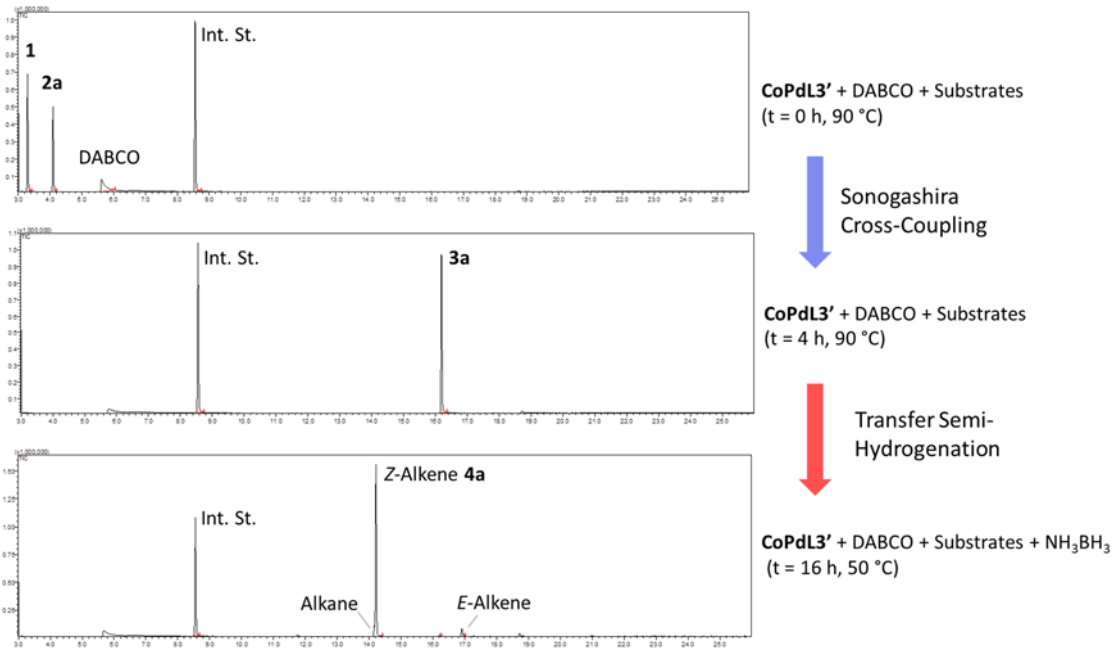

Figure S57. Reaction process followed by GC-MS using naphthalene as an internal standard (Int. St.).

^{1}H NMR (400 MHz, CD_3CN, room temperature)

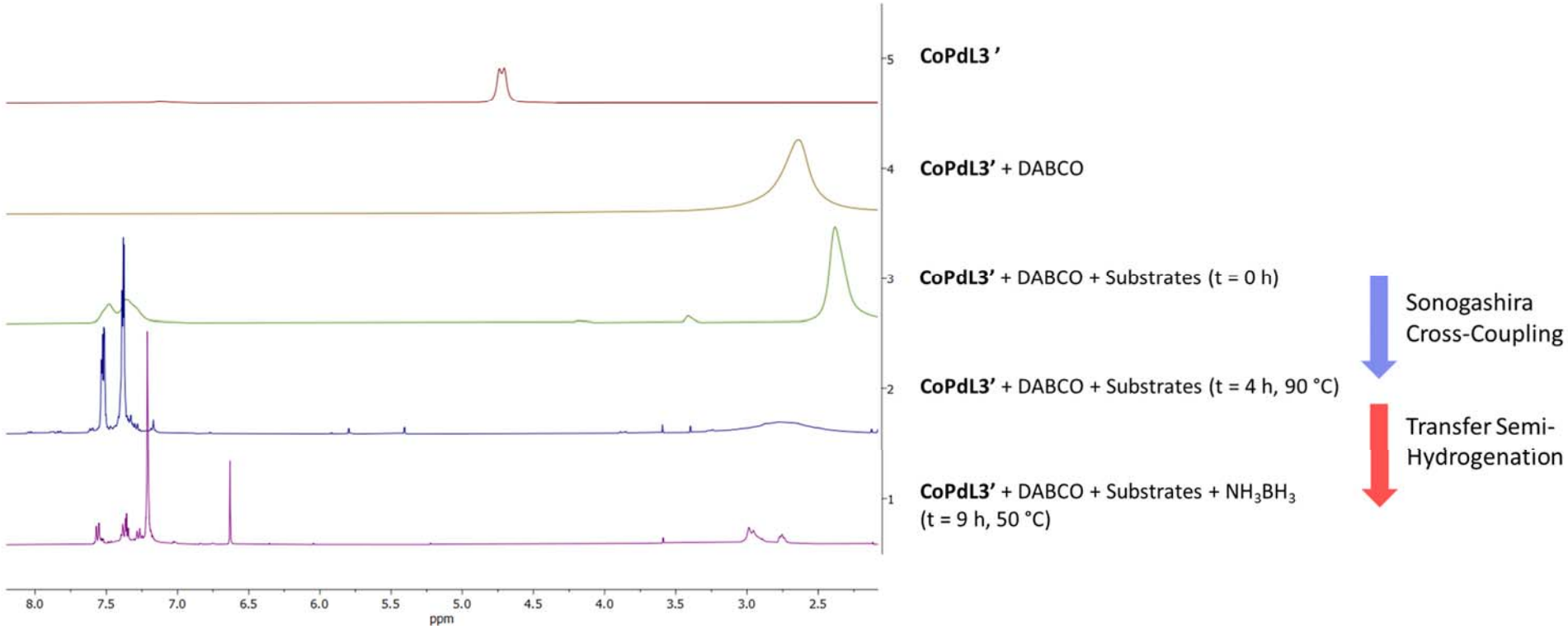

Figure S58. Reaction process followed over time by ^{1}H NMR spectroscopy in CD_3CN at room temperature**.**

$^{31}P\{^{1}H\}$ NMR (162 MHz, CD_3CN, room temperature)

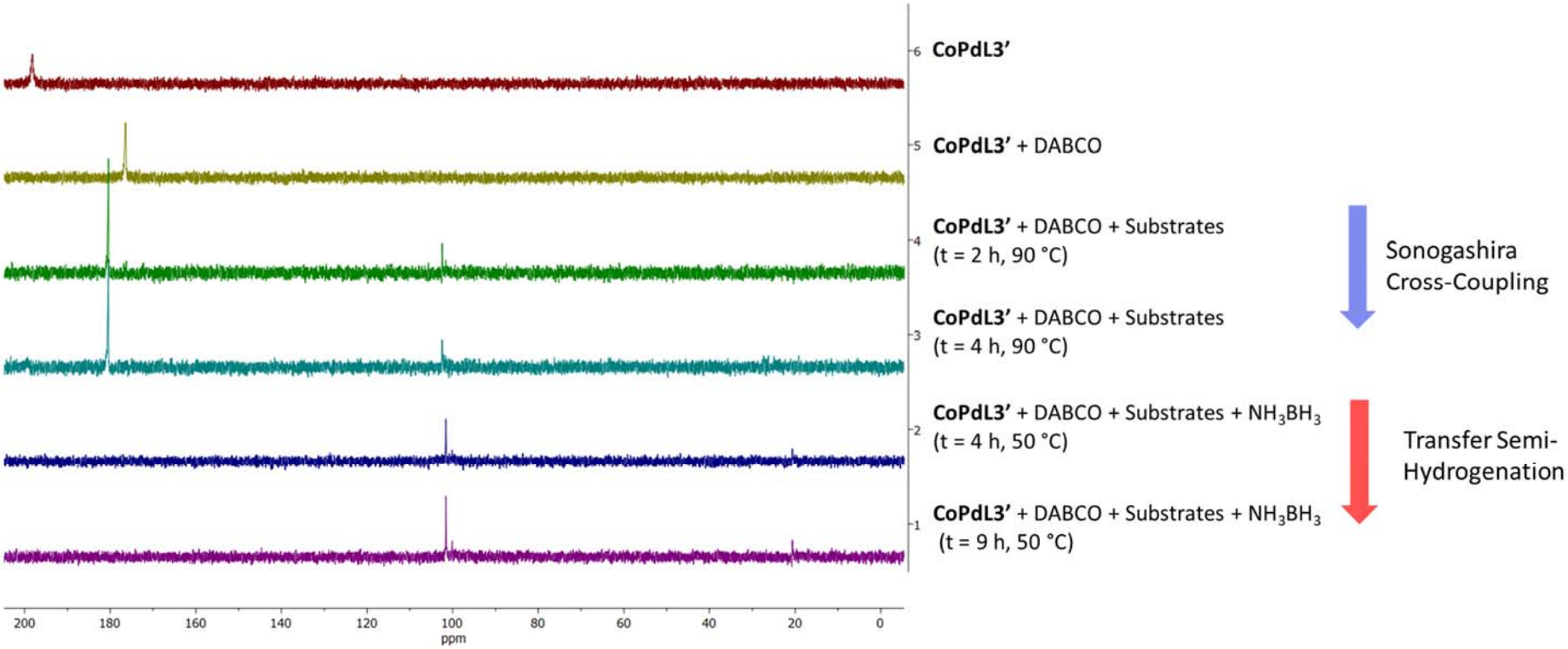

Figure S59. Reaction process followed over time by $^{31}P\{^{1}H\}$ NMR spectroscopy in CD_3CN at room temperature.

^{11}B NMR (128 MHz, CD_3CN, room temperature)

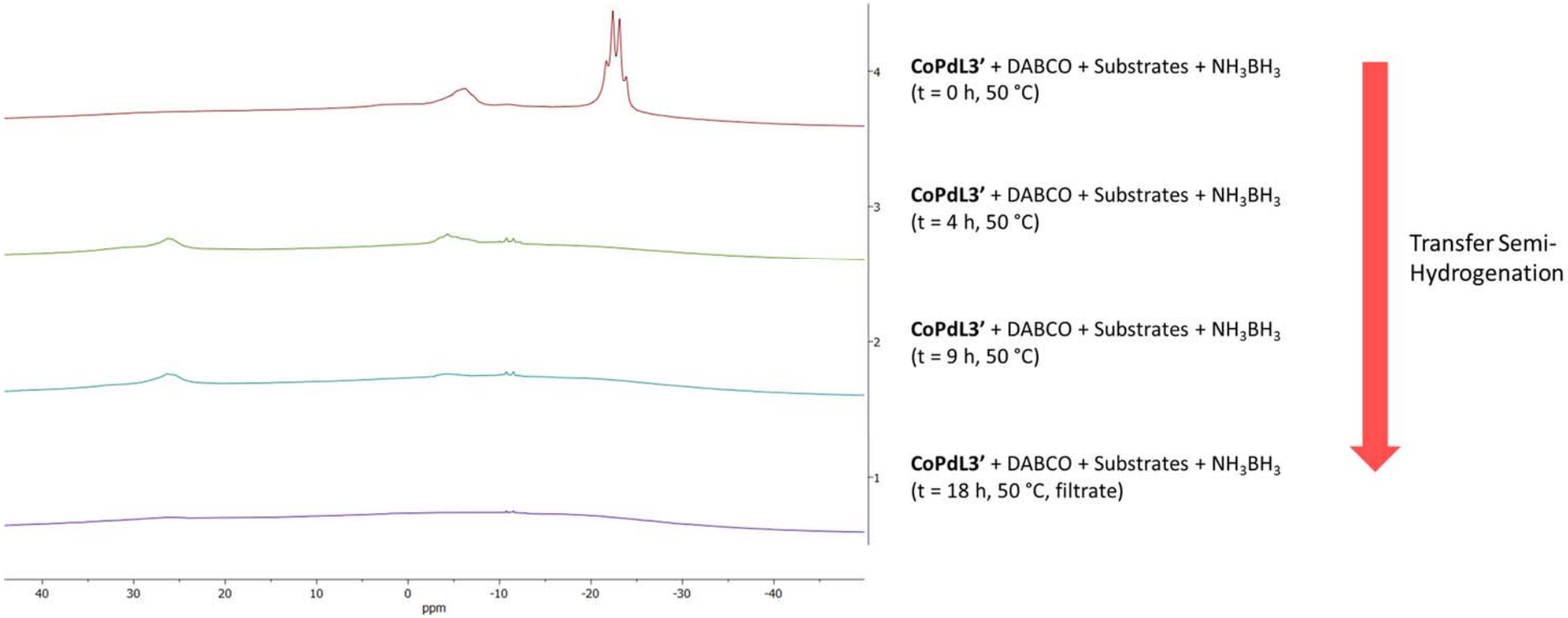

Figure S60. Reaction process of the transfer semi-hydrogenation followed over time by ^{11}B NMR spectroscopy in CD_3CN at room temperature.

5.4 Homogeneous or Heterogeneous?

Furthermore, we have been interested in the true nature of the catalyst. To exclude the formation of catalytically active nanoparticles, several poisoning and kinetic studies have been performed as well as analytical methods (dynamic light scattering (DLS) and high-resolution transmission electron microscopy/energy-dispersive X-ray spectroscopy (TEM/EDX)) to detect potential nanoparticles.[1] The reaction process was monitored over time (Figure S56). The reaction kinetics have not shown a sigmoidal curve indicating that there is no induction period to form catalytically active nanoparticles. In parallel, poisoning studies (mercury test, quantitative ligand poisoning, Crabtree's test[2]) have been carried out for the Sonogashira cross-coupling reaction (Figure S61). The mercury test resulted in a complete inhibition of the catalyst; therefore, a drop of Hg was added directly at the beginning and after 30 min. This result would mean that the precatalyst decomposes into catalytically active nanoparticles which would be inhibited by the amalgam formation. However, the reliability of the mercury test is doubtful for palladacycles.[3] Therefore, the stability of **CoPdL3'** was investigated by heating the complex with mercury for 2 d. No decomposition was observed but the addition of DABCO and mercury resulted in decomposition of the complex (Figure S62, S63). For this reason, the mercury test seems to be a false positive. The addition of 0.1 eq. PMe_2Ph per **CoPdL3'** did not inhibit the catalytic performance. However, the addition of 0.5 eq. PMe_2Ph per **CoPdL3'** caused a complete inhibition. This might underline the homogeneous nature of the catalytically active species. The limitations of this test are reaction temperatures over 50 °C because PMe_2Ph might dissociate from the heterogeneous catalyst surface. On the other hand, the Crabtree's test is used to poison a homogeneous catalyst. However, a possible homogeneous catalyst was not inhibited by the addition of dibenzo[*a*,*e*]cyclooctatetraene (DCT) even if the reaction mixture was stirred for 3 h at room temperature before continuing with heating at 90 °C. In general, the DCT did not react with **CoPdL3'** at room temperature for 24 h nor at 90 °C for 24 h (Figure S64, S65). Therefore, the Crabtree's test is not suitable for this complex. Moreover, the Maitlis' test was performed after completion of the Sonogashira cross-coupling reaction. The hot reaction mixture was filtered over Celite and fresh substrates and solvent were added. The filtrate was still catalytically active giving diphenylacetylene with a yield of 71% after 4 h. Since these tests could not fully prove the nature of the catalytically active species, DLS and TEM-EDX measurements were carried out. The DLS measurement has shown nanoparticles with a size of 10 nm and 26 nm though the count rate was relatively low (77 kcps, should be 100–500 kcps (kilo counts per second)) and the baseline index was 5.7 (should be ≥8). Both values suggest a low quality of the DLS measurement and a possible contamination by dust (Chapter 5.4.2). Therefore, we tried to track potential nanoparticles by TEM-EDX measurements, but no nanoparticles have been found (Chapter 5.4.3). Finally, the reaction process was followed by ^{1}H and $^{31}P\{^{1}H\}$ NMR spectroscopy (Figure S58, S59) indicating the complex identity during the Sonogashira cross-coupling. However, the phosphorus signal shifts from 180.4 ppm to 101.6 ppm during the transfer semi-hydrogenation which is comparable to the monometallic complex **PdL3'** (100.2 ppm). This suggests the potential loss of Co from the heterobimetallic complex. It is worth mentioning, that the complexes **CoPdL3'**, **PdL3'**, **CoL4** and **PdL5'** have been tested for the direct transfer hydrogenation of diphenylacetylene but none of the complexes have shown similar reactivity and selectivity as **CoPdL3'** after the Sonogashira cross-coupling reaction (Table S3). Therefore, we propose that the catalytically active species for the transfer semi-hydrogenation was formed during the Sonogashira cross-coupling reaction. However, there is no clear evidence if Co or Pd is catalysing the transfer semi-hydrogenation. Nevertheless, we conclude that the catalytically active species is homogeneous.

5.4.1 Poisoning Studies

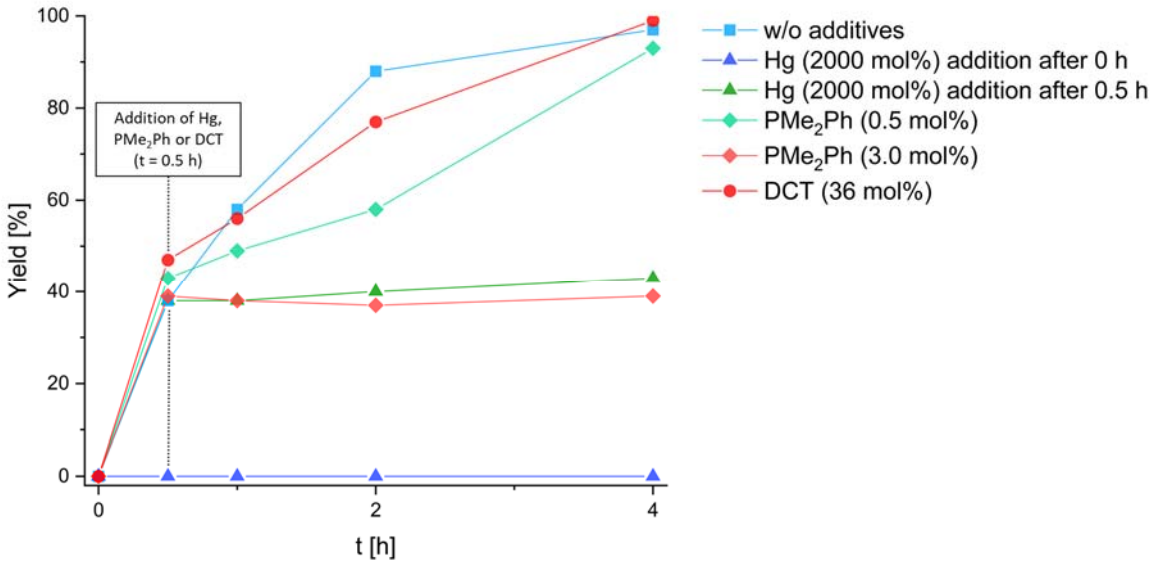

Figure S61. Catalyst poisoning during the Sonogashira cross-coupling reaction with Hg (330 eq. per **CoPdL3'**), PMe_2Ph (0.1 eq. and 0.5 eq. per **CoPdL3'**) and DCT (6.0 eq. per **CoPdL3'**). The yields have been determined by GC-MS using naphthalene as internal standard.

Hg Poisoning

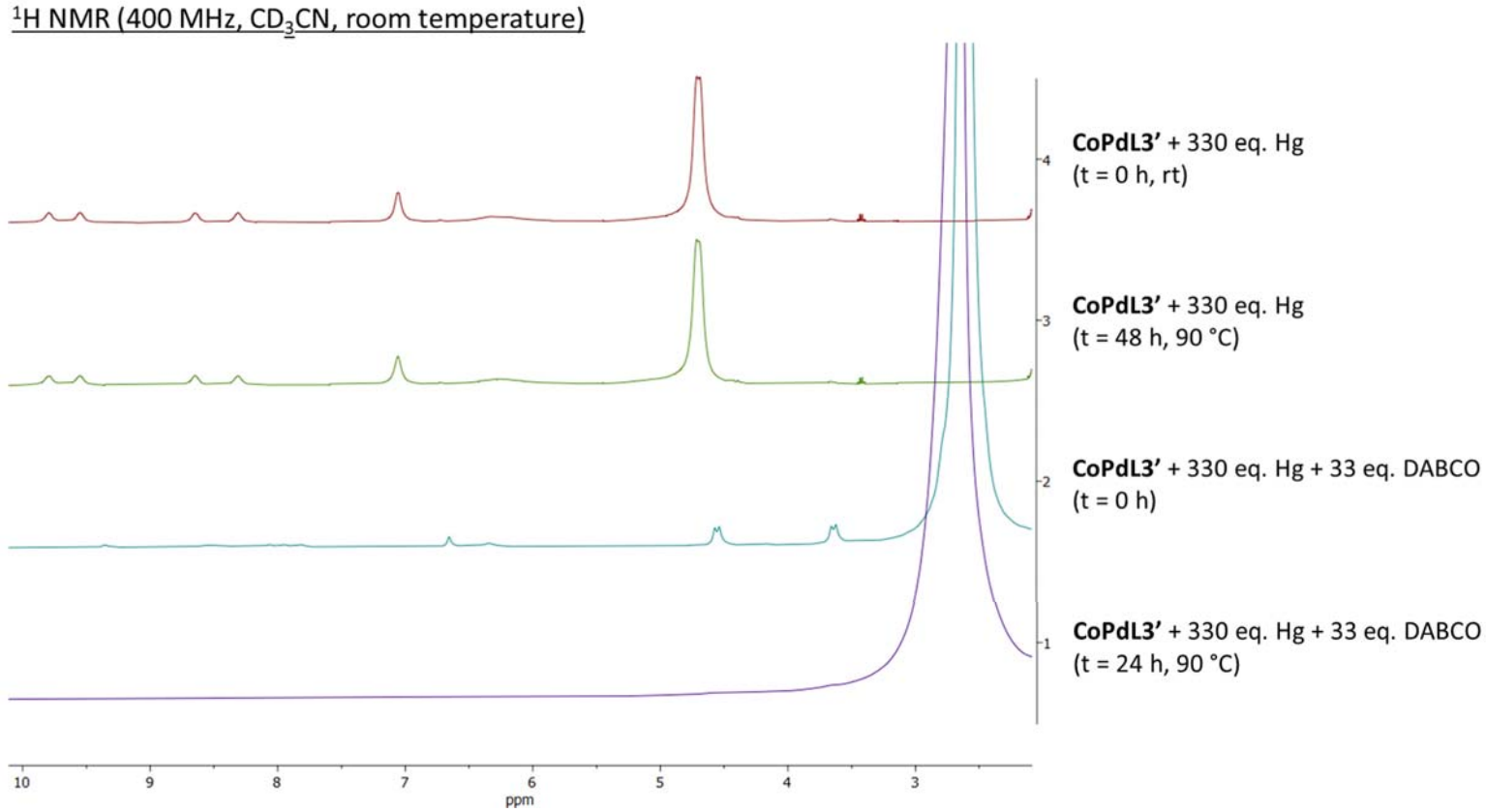

Figure S62. ^{1}H NMR spectra of the complex **CoPdL3'** reacting with Hg and DABCO.

$^{31}P\{^{1}H\}$ NMR (162 MHz, CD_3CN, room temperature)

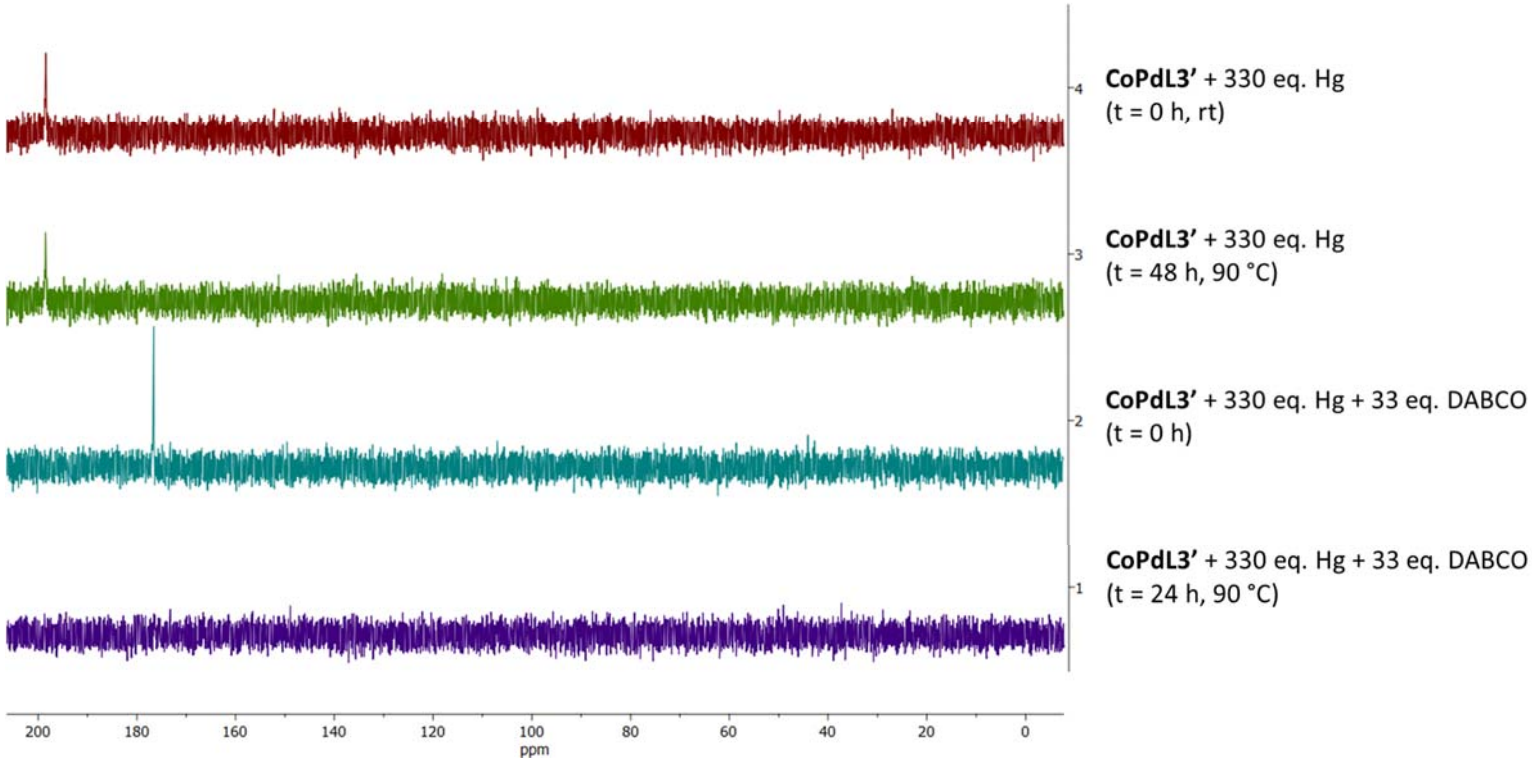

Figure S63. $^{31}P\{^{1}H\}$ NMR spectra of the complex **CoPdL3'** reacting with Hg and DABCO.

DCT Poisoning

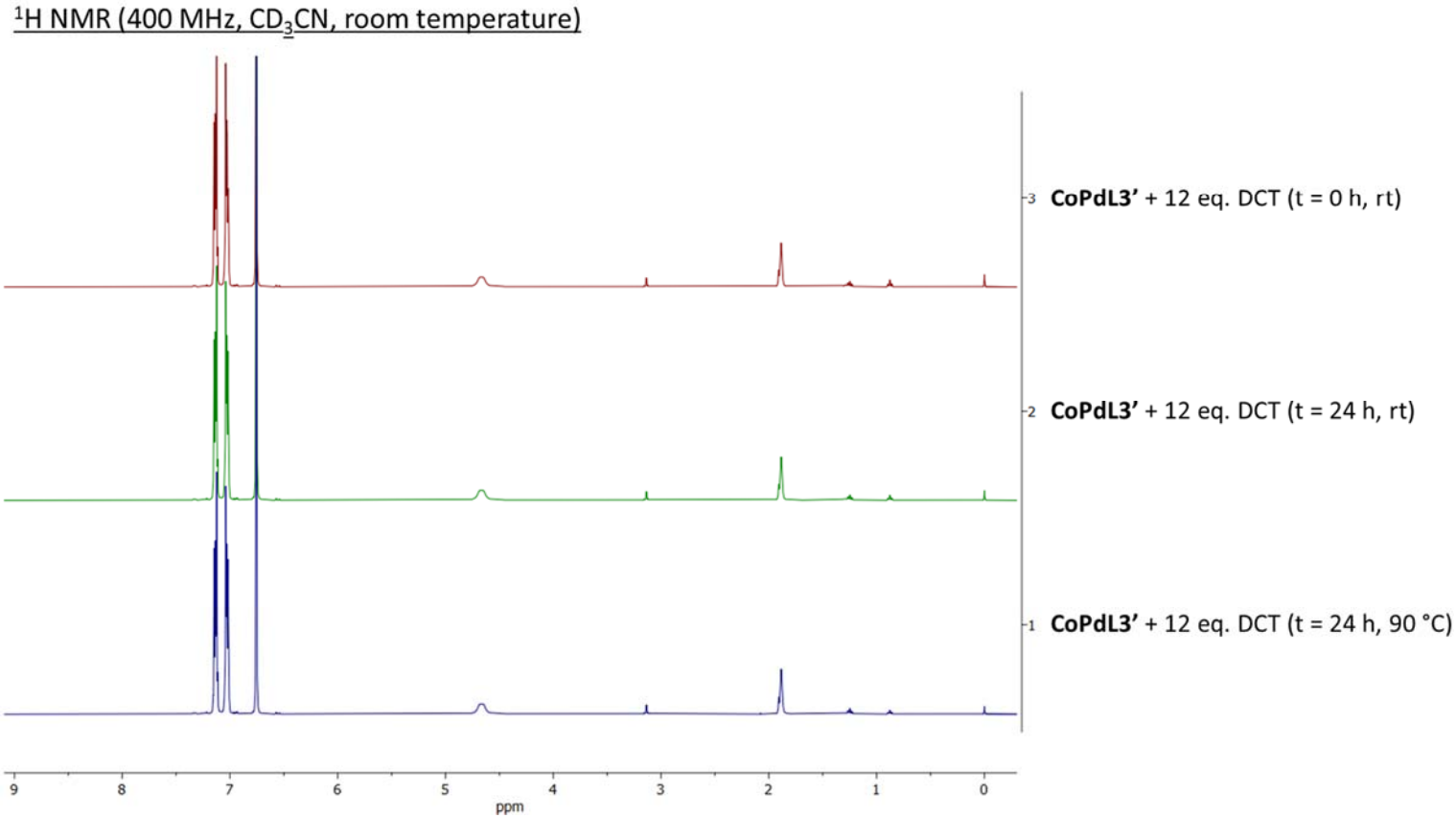

Figure S64. ^{1}H NMR spectra of the complex **CoPdL3'** not reacting with DCT.

$^{31}P\{^{1}H\}$ NMR (162 MHz, CD_3CN, room temperature)

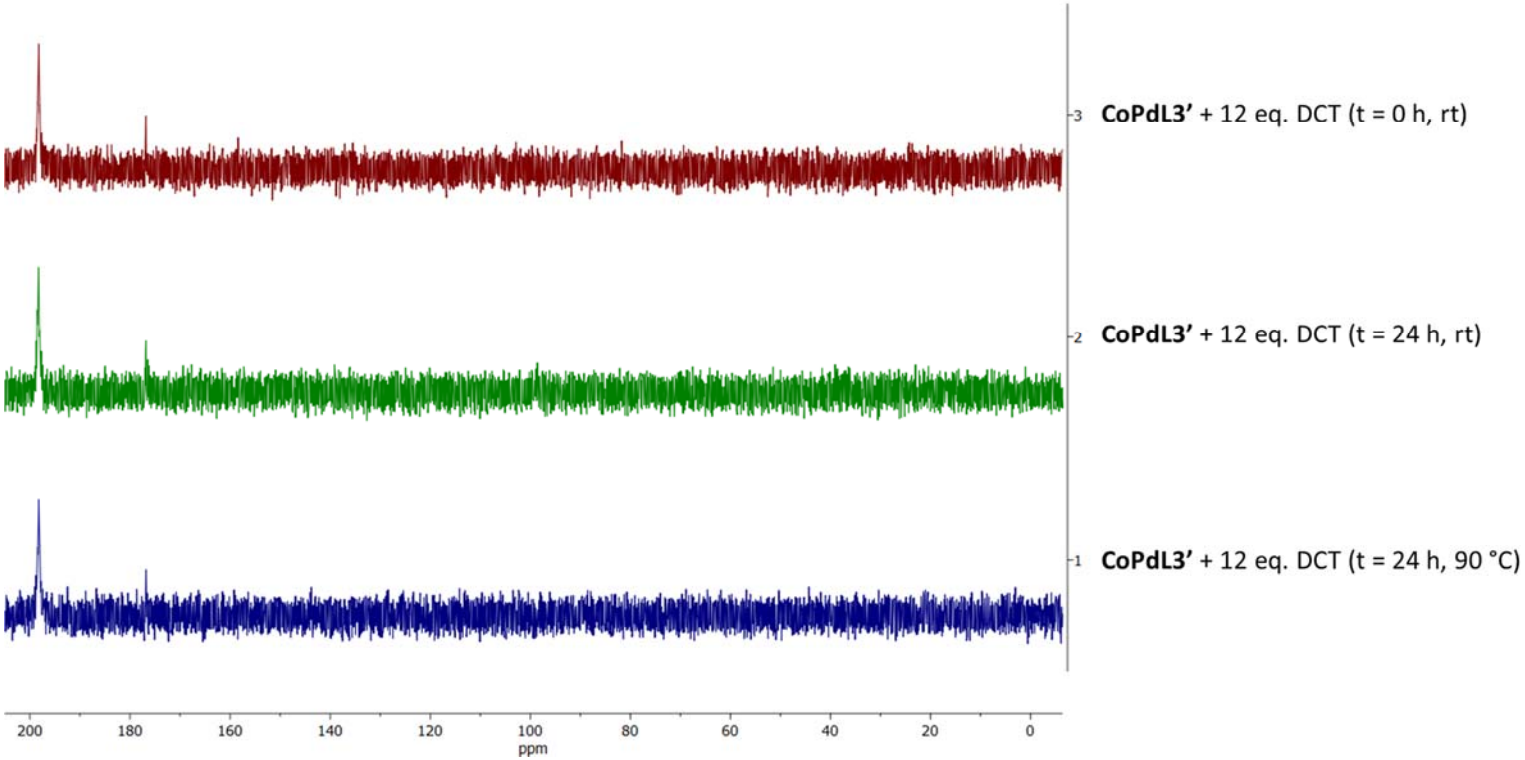

Figure S65. $^{31}P\{^{1}H\}$ NMR spectra of the complex **CoPdL3'** not reacting with DCT.

5.4.2 DLS (dynamic light scattering)

Measurement Parameters:

Temperature	= 25.0 deg. C	Runs Completed	= 5
Liquid	= Unspecified	Run Duration	= 00:00:30
Viscosity	= 0.334 cP	Total Elapsed Time	= 00:02:30
Ref.Index Fluid	= 1.344	Average Count Rate	= 76.9 kcps
Angle	= 90.00	Ref.Index Real	= 1.590
Wavelength	= 659.0 nm	Ref.Index Imag	= 0.000
Baseline	= Auto (Slope Analysis)	Dust Filter Setting	= 5.00

RC_78_H12st_dust5_100x diluted (Combined)

Effective Diameter: 16.4 nm

Polydispersity: 0.158

Baseline Index: 5.7/ 37.50%

Elapsed Time: 00:02:30

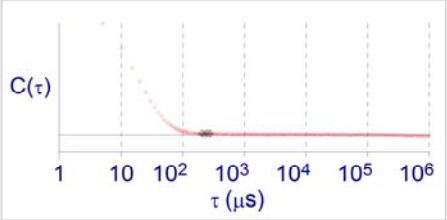

Correlation Function

Run	Eff. Diam. (nm)	Half Width (nm)	Polydispersity	Baseline Index
1	16.0	6.6	0.171	2.4/ 43.06%
2	16.0	6.6	0.171	8.9/ 32.64%
3	16.3	6.7	0.171	8.9/ 38.19%
4	16.6	7.2	0.189	6.3/ 37.50%
5	16.4	6.3	0.146	5.5/ 36.11%
Mean	16.3	6.7	0.170	6.4/ 37.50%
Std. Error	0.1	0.2	0.007	1.2/ 1.69
Combined	16.4	6.5	0.158	5.7/ 37.50%

Elapsed Time	00:02:30
Mean Diam.	19.6 nm
Rel. Var.	0.187
Skew	-0.239

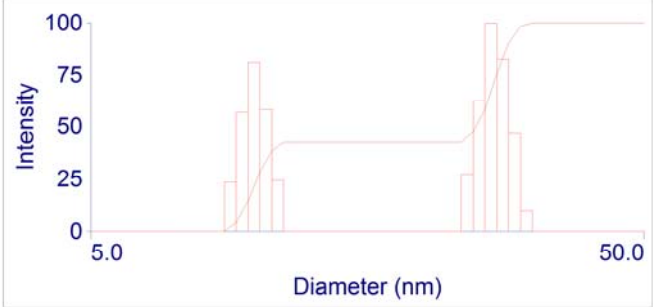

Multimodal Size Distribution

d(nm)	G(d)	C(d)	d(nm)	G(d)	C(d)	d(nm)	G(d)	C(d)
7.3	0	0	12.6	0	43	21.7	0	43
7.7	0	0	13.2	0	43	22.8	0	43
8.1	0	0	13.9	0	43	23.9	27	47
8.5	0	0	14.6	0	43	25.2	62	58
8.9	23	4	15.4	0	43	26.4	100	76
9.4	57	14	16.1	0	43	27.8	82	90
9.9	81	28	17.0	0	43	29.2	47	98
10.4	58	38	17.8	0	43	30.6	9	100
10.9	24	43	18.7	0	43	32.2	0	100
11.4	0	43	19.7	0	43	33.8	0	100
12.0	0	43	20.6	0	43	35.5	0	100

5.4.3 Transmission Electron Microscopy/Energy-dispersive X-ray Spectroscopy (TEM/EDX analysis)

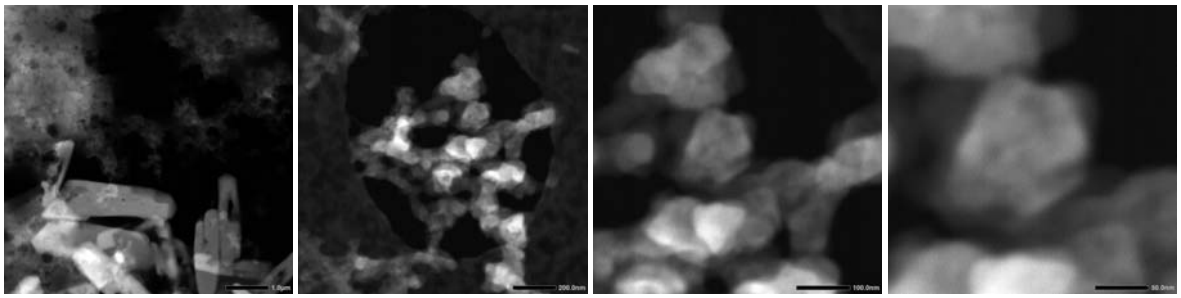

kV: 200; Mag: 80000; Takeoff: 12.4; Live Time (s): 42; Amp Time (µs): 3.84; Resolution (eV): 126.8.

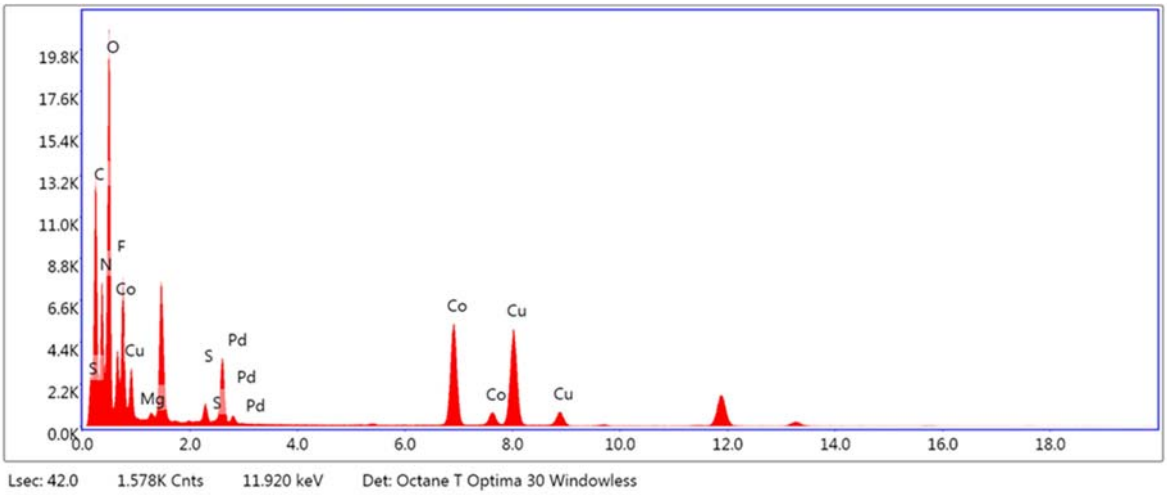

Element	Weight %	Atomic %	Net Int.	Net Error%	kAB Factor[1]
C K	21.7	36.3	2140.7	0.4	1.27
N K	9.2	13.1	1210.8	0.6	0.94
O K	27.0	33.9	3364.7	0.5	1
F K	2.0	2.1	154.1	10.8	1.61
Mg K	0.9	0.7	96.3	4.2	1.13
S K	2.5	1.6	276.8	1.7	1.12
Pd L	1.9	0.4	69.9	2.0	3.36
Co K	34.9	11.9	2079.4	0.5	2.09

[1] The number kAB, normally called the k-factor, relates the compositions of A and B. It is not a proper constant, but it is referred to as a sensitivity factor. It depends on the particular AEM system, the voltage, and analysis conditions in general.

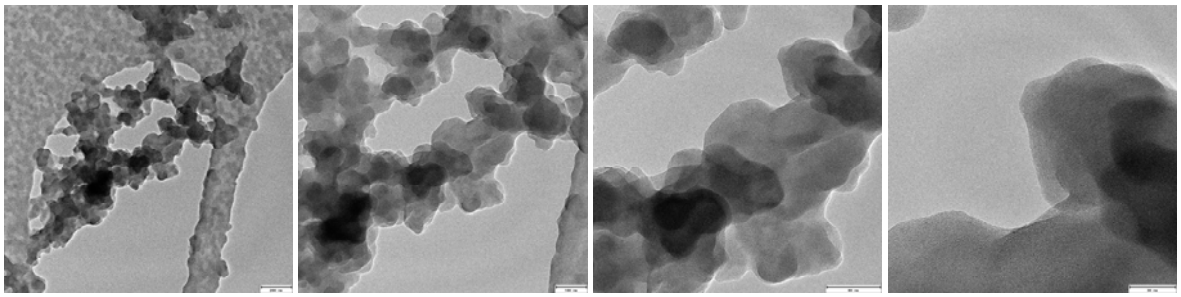

kV: 200; Mag: 100000; Takeoff: 12.4; Live Time (s): 45.7; Amp Time (µs): 3.84; Resolution (eV): 126.8.

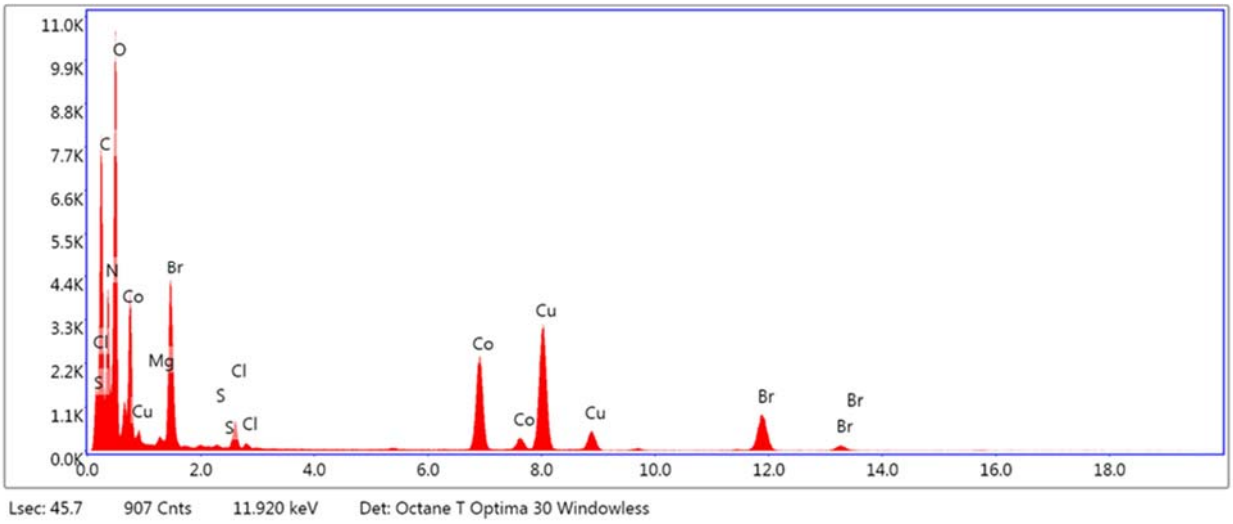

Element	Weight %	Atomic %	Net Int.	Net Error%	kAB Factor[1]
C K	20.2	38.6	1176.6	0.5	1.27
N K	7.6	12.5	594.0	0.9	0.94
O K	21.5	30.8	1581.9	0.7	1
Mg K	0.0	0.0	2.4	100.0	1.13
S K	0.4	0.3	23.3	15.4	1.12
Cl K	2.7	1.7	166.9	2.2	1.19
Co K	23.7	9.2	834.4	0.9	2.09
Br K	23.9	6.9	420.6	1.4	4.2

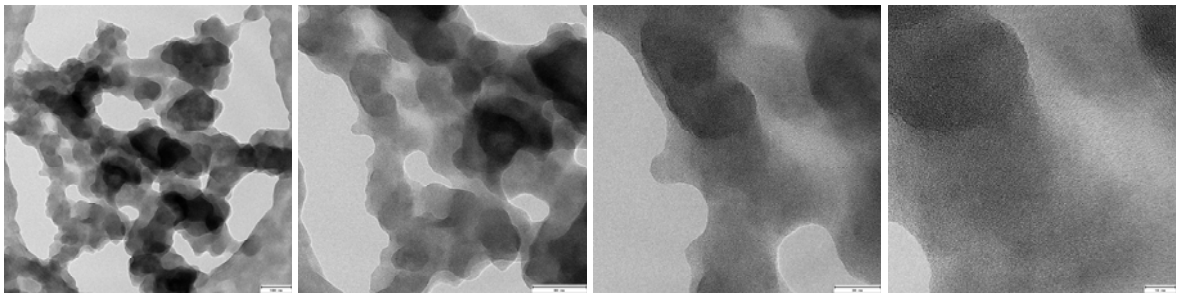

kV: 200; Mag: 40000; Takeoff: 12.4; Live Time (s): 45.9; Amp Time (µs): 3.84; Resolution (eV): 126.8.

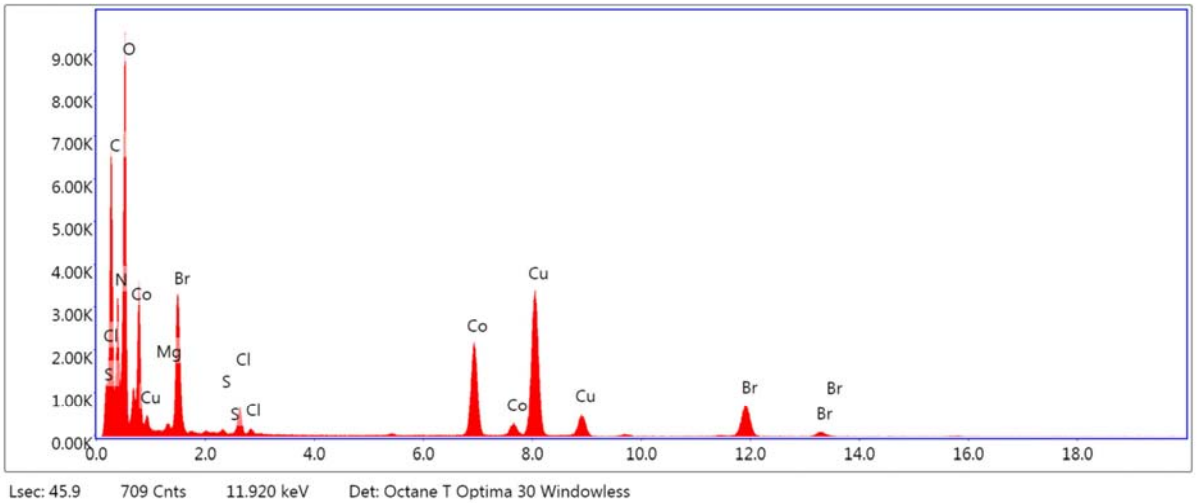

Element	Weight %	Atomic %	Net Int.	Net Error%	kAB Factor[1]
C K	20.1	38.5	1032.3	0.6	1.27
N K	6.9	11.3	473.8	1.1	0.94
O K	21.9	31.5	1423.4	0.7	1
Mg K	0.0	0.0	0.0	100.0	1.13
S K	0.4	0.3	26.0	12.4	1.12
Cl K	2.9	1.9	156.9	2.3	1.19
Co K	25.7	10.0	798.3	0.9	2.09
Br K	22.2	6.4	344.0	1.5	4.2

5.5 Substrate Scope

General procedure for sequential Sonogashira cross-coupling reaction followed by transfer semi-hydrogenation. **4a-4m**:

Substituted bromobenzene derivative (0.5 mmol, 1 eq.), phenylacetylene (1.0 mmol, 110 µl, 2 eq.), **CoPdL3'** (0.03 mmol, 30 mg, 6 mol%), DABCO (1.0 mmol, 112 mg, 2 eq.) and acetonitrile (2 mL) were added. The reaction mixture was degassed by freeze-pump-thaw and heated in an oil bath at 90 °C. After 4 hours, the progress of the reaction was checked using GC-MS which was followed by addition of ammonia borane (31 mg, 1.0 mmol, 2 eq.) mixed in 1:1 ratio with $MgSO_4$ to ease the process of weighing in the solid and additionally acetonitrile (2 mL) was added. The flask was covered completely in aluminium foil and was heated in a water bath at 50 °C for 15 hours. The reaction was monitored by GC-MS, the reaction mixture was passed over Celite and the precipitate was washed with dichloromethane (3 × 10 mL). The crude reaction mixture filtrate was purified using a Biotage Isolera (25 g SNAP Ultra cartridge, EtOAc (EA)/*n*-hexane (Hex) or *n*-pentane) to afford the corresponding compounds (**4a-4m**) and isolated yields are reported.

Procedure for synthesis of combretastatin A-4 (**4n**) by sequential Sonogashira cross-coupling reaction followed by transfer semi-hydrogenation:

In a Schlenk flask under argon, 5-iodo-2-methoxyphenol (125 mg, 0.5 mmol, 1 eq.), 5-ethynyl-1,2,3-trimethoxybenzene (192 mg, 1.0 mmol, 2 eq.), **CoPdL3'** (0.03 mmol, 30 mg, 6 mol%), DABCO (1.0 mmol, 112 mg, 2 eq.) and acetonitrile (2 mL) were added. The reaction mixture was degassed by freeze-pump-thaw and heated in an oil bath at 90 °C. After 5 hours, ammonia borane (31 mg, 1.0 mmol, 2 eq.) was weighed in and additionally acetonitrile (2 mL) was added. The flask was covered completely in aluminium foil and was heated in a water bath at 50 °C for 24 hours. The reaction mixture was cooled down and passed over Celite and washed with dichloromethane (3 × 10 mL). The crude reaction mixture was purified using a silica gel column eluted with *n*-pentane/ethyl acetate (7:3) to afford the combretastatin A-4 as a viscous oil that solidified on cooling (82 mg, 26 mmol, 52%).

4a: (*Z*)-1,2-diphenylethene[4]

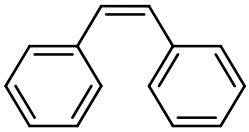

Product was isolated via column chromatography (Hex) as a colourless liquid (71 mg, 0.39 mmol, 79%).

^{1}H NMR (400 MHz, $CDCl_3$) δ = 7.28 – 7.13 (m, 10H), 6.59 (s, 2H).

^{13}C{^{1}H} NMR (101 MHz, $CDCl_3$) δ = 137.2, 130.2, 128.9, 128.2, 127.1.

4b: (*Z*)-1-methyl-4-styrylbenzene[4]

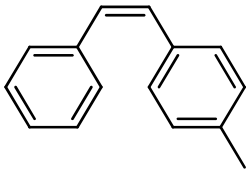

Product was isolated via column chromatography (Hex/EA – 200:3) as a colourless liquid (64 mg, 0.33 mmol, 66%).

^{1}H NMR (400 MHz, $CDCl_3$) δ (ppm) = 7.29 – 7.16 (m, 5H), 7.16 – 7.12 (m, 2H), 7.02 (d, J=7.9, 2H), 6.55 (s, 2H), 2.30 (s, 3H).

^{13}C{^{1}H} NMR (101 MHz, $CDCl_3$) δ (ppm) = 137.6, 137.0, 134.4, 130.3, 129.7, 129.0, 129.0, 128.9, 128.3, 127.1, 21.4.

4c: (*Z*)-1-methyl-3-styrylbenzene[4]

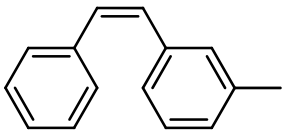

Product was isolated via column chromatography (Hex/EA – 50:1) as a colourless liquid (69 mg, 0.35 mmol, 71%).

^{1}H NMR (400 MHz, $CDCl_3$) δ (ppm) = 7.26 – 7.16 (m, 5H), 7.11 – 6.98 (m, 4H), 6.56 (s, 2H), 2.25 (s, 3H).

^{13}C{^{1}H} NMR (101 MHz, $CDCl_3$) δ (ppm) = 137.9, 137.5, 137.3, 130.5, 130.2, 129.7, 129.0, 128.3, 128.2, 128.0, 127.2, 126.0, 21.5.

4d: (*Z*)-1-methyl-2-styrylbenzene[4]

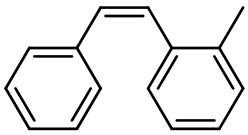

Product was isolated via column chromatography (Hex/EA – 50:1) as a colourless liquid (65 mg, 0.33 mmol, 67%).

^{1}H NMR (400 MHz, $CDCl_3$) δ (ppm) = 7.22 – 6.98 (m, 9H), 6.62 (m, 2H), 2.26 (s, 3H).

^{13}C{^{1}H} NMR (101 MHz, $CDCl_3$) δ (ppm) = 137.1, 137.0, 136.1, 130.5, 130.0, 129.5, 128.9, 128.8, 128.0, 127.2, 127.0, 125.7, 19.8.

4e: (*Z*)-1-chloro-4-styrylbenzene[4]

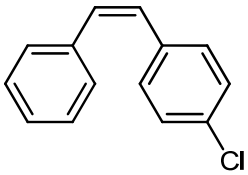

Product was isolated via column chromatography (Hex/EA – 49:1) as a colourless liquid (82 mg, 0.38 mmol, 76%).

^{1}H NMR (400 MHz, $CDCl_3$) δ (ppm) = 7.28 – 7.10 (m, 9H), 6.62 (d, *J* = 12.2 Hz, 1H), 6.52 (d, *J* = 12.2 Hz, 1H).

^{13}C{^{1}H} NMR (101 MHz, $CDCl_3$) δ (ppm) = 136.8, 135.6, 132.7, 130.9, 130.2, 128.9, 128.8, 128.4, 128.3, 127.3.

4f: (*Z*)-1-fluoro-4-styrylbenzene[4]

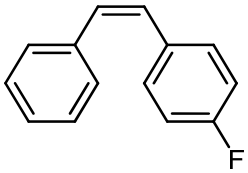

Product was isolated via column chromatography (Hex/EA – 100:3) as a colourless liquid (62 mg, 0.31 mmol, 63%).

^{1}H NMR (400 MHz, $CDCl_3$) δ (ppm) = 7.28 – 7.15 (m, 7H), 6.90 (t, *J* = 8.8 Hz, 2H), 6.59 (d, *J* = 12.2 Hz, 1H), 6.54 (d, *J* = 12.2 Hz, 1H).

^{13}C{^{1}H} NMR (101 MHz, $CDCl_3$) δ (ppm) = 162.0 (d, J_{CF} = 246.6 Hz), 137.2, 133.3 (d, J_{CF} = 3.5 Hz), 130.7 (d, J_{CF} = 7.9 Hz), 130.4 (d, J_{CF} = 1.3 Hz), 129.2, 129.0, 128.4, 127.3, 115.3 (d, J_{CF} = 21.4 Hz).

^{19}F NMR (377 MHz, $CDCl_3$) δ = –114.7 (tt, J_{FH} = 9.0, 5.4 Hz).

4g: (*Z*)-trimethyl(4-styrylphenyl)silane[5]

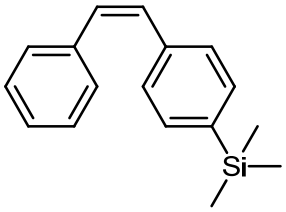

Product was isolated via column chromatography (Hex/EA – 100:3) as a colourless liquid (81 mg, 0.32 mmol, 64%).

^{1}H NMR (400 MHz, $CDCl_3$) δ (ppm) = 7.32 – 7.26 (m, 2H), 7.23 – 7.07 (m, 7H), 6.56 – 6.44 (m, 2H), 0.16 (s, 9H).

^{13}C{^{1}H} NMR (101 MHz, $CDCl_3$) δ (ppm) = 139.5, 137.7, 137.5, 133.3, 130.5, 130.4, 129.0, 128.4, 128.3, 127.2, –1.0.

4h: (*Z*)-ethyl 4-styrylbenzoate[6]

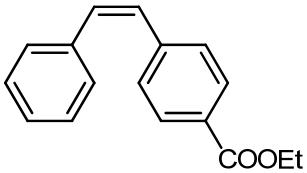

Product was isolated via column chromatography (Hex/EA – 100:3) as a white solid (93 mg, 0.37 mmol, 74%).

^{1}H NMR (400 MHz, $CDCl_3$) δ (ppm) = 7.89 (d, *J* = 8.4 Hz, 1H), 7.30 (d, *J* = 8.2 Hz, 1H), 7.24 – 7.19 (m, 2H), 6.71 (d, *J* = 12.2 Hz, 1H), 6.61 (d, *J* = 12.3 Hz, 1H), 4.36 (q, *J* = 7.1 Hz, 1H), 1.38 (t, *J* = 7.1 Hz, 2H).

^{13}C{^{1}H} NMR (101 MHz, $CDCl_3$) δ (ppm) = 166.4, 142.0, 136.7, 132.1, 129.5, 129.3, 128.9, 128.8, 128.8, 128.3, 127.5, 60.9, 14.3.

4i: (*Z*)-1-styrylnaphthalene[7]

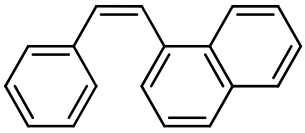

Product was isolated via column chromatography (*n*-pentane) as a colourless oil (79 mg, 0.34 mmol, 69%).

^{1}H NMR (400 MHz, $CDCl_3$) δ (ppm) = 8.11 – 8.06 (m, 1H), 7.92 – 7.84 (m, 1H), 7.83 – 7.71 (m, 1H), 7.57 – 7.41 (m, 2H), 7.41 – 7.30 (m, 2H), 7.13 – 7.02 (m, 6H), 6.84 (d, *J* = 12.2 Hz, 1H).

^{13}C{^{1}H} NMR (101 MHz, $CDCl_3$) δ (ppm) = 136.7, 135.2, 133.6, 131.9, 131.5, 129.0, 128.4, 128.3, 127.9, 127.4, 127.0, 126.4, 125.9, 125.9, 125.5, 124.8.

4j: (*Z*)-2-styrylthiophene[8]

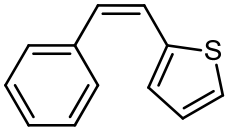

Product was isolated via column chromatography (*n*-pentane) as a colourless oil (59 mg, 0.32 mmol, 63%).

^{1}H NMR (400 MHz, $CDCl_3$) δ (ppm) = 7.40 – 7.29 (m, 5H), 7.11 (dd, *J* = 5.1, 1.2 Hz, 1H), 6.99 (d, *J* = 3.6 Hz, 1H), 6.90 (dd, *J* = 5.1, 3.6 Hz, 1H), 6.72 (d, *J* = 11.9 Hz, 1H), 6.60 (d, *J* = 11.9 Hz, 1H).

^{13}C{^{1}H} NMR (101 MHz, $CDCl_3$) δ (ppm) = 139.8, 137.3, 128.9, 128.8, 128.5, 128.1, 127.5, 126.4, 125.5, 123.3.

4k: (*Z*)-5-styrylpyrimidine[4]

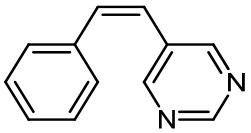

Product was isolated via column chromatography (Hex/EA – 7:3) as a yellow oil (67 mg, 0.37 mmol, 74%).

^{1}H NMR (400 MHz, $CDCl_3$) δ (ppm) = 9.01 (s, 1H), 8.56 (s, 2H), 7.32 – 7.17 (m, 6H), 6.89 (d, *J* = 12.1 Hz, 1H), 6.47 (d, *J* = 12.1 Hz, 1H).

^{13}C{^{1}H} NMR (101 MHz, $CDCl_3$) δ (ppm) = 156.9, 156.7, 135.9, 135.1, 131.3, 129.0, 128.6, 128.2, 122.8.

4l: (*Z*)-2-styrylpyridine[9]

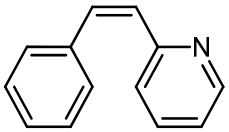

Product was isolated via column chromatography (Hex/EA – 8:2) as a yellow oil (61 mg, 0.33 mmol, 67%).

^{1}H NMR (400 MHz, $CDCl_3$) δ (ppm) = 8.58 – 8.55 (m, 1H), 7.44 – 7.38 (m, 1H), 7.27 – 7.19 (m, 5H), 7.16 – 7.11 (m, 1H), 7.09 – 7.03 (m, 1H), 6.81 (d, *J* = 12.4 Hz, 1H), 6.67 (d, *J* = 12.4 Hz, 1H).

^{13}C{^{1}H} NMR (101 MHz, $CDCl_3$) δ (ppm) = 156.5, 149.7, 136.8, 135.8, 133.4, 130.7, 129.0, 128.4, 127.7, 124.0, 121.9.

4m: (*E*)-4-styrylaniline[1]

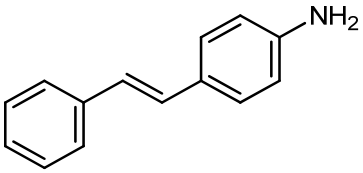

Product was isolated via column chromatography (*n*-pentane/EA – 7:3) as a yellow solid (61 mg, 0.31 mmol, 62%).

^{1}H NMR (400 MHz, $CDCl_3$) δ (ppm) = 7.50 – 7.42 (m, 2H), 7.36 – 7.28 (m, 4H), 7.25 – 7.16 (m, 1H), 7.02 (d, *J* = 16.3 Hz, 1H), 6.91 (d, *J* = 16.3 Hz, 1H), 6.70 – 6.60 (m, 2H), 3.71 (br, 1H).

$^{13}C\{^1H\}$ NMR (101 MHz, $CDCl_3$) δ (ppm) = 146.1, 137.9, 128.7, 128.6, 128.0, 127.7, 126.9, 126.1, 125.1, 115.2.

4n: (*Z*)-2-methoxy-5-(3,4,5-trimethoxystyryl)phenol - Combretastatin A-4[10]

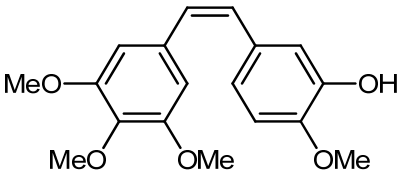

Product was isolated via column chromatography (*n*-pentane/EA-7:3) as a viscous oil that solidified on cooling (82 mg, 26 mmol, 52%).

^1H NMR (400 MHz, $CDCl_3$) δ (ppm) = 6.92 (d, *J* = 2.0 Hz, 1H), 6.80 (dd, *J* = 8.4, 2.0 Hz, 1H), 6.73 (d, *J* = 8.4 Hz, 1H), 6.53 (s, 2H), 6.44 (dd, *J* = 12.2 Hz, 2H), 5.51 (s, 1H), 3.87 (s, 3H), 3.84 (s, 3H), 3.70 (s, 6H).

$^{13}C\{^1H\}$ NMR (101 MHz, $CDCl_3$) δ (ppm) = 153.0, 145.9, 145.4, 137.3, 132.9, 130.8, 129.6, 129.2, 121.3, 115.2, 110.5, 106.2, 61.1, 56.1.

4a: (*Z*)-1,2-diphenylethene

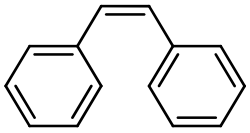

^{1}H NMR (400 MHz, $CDCl_3$)

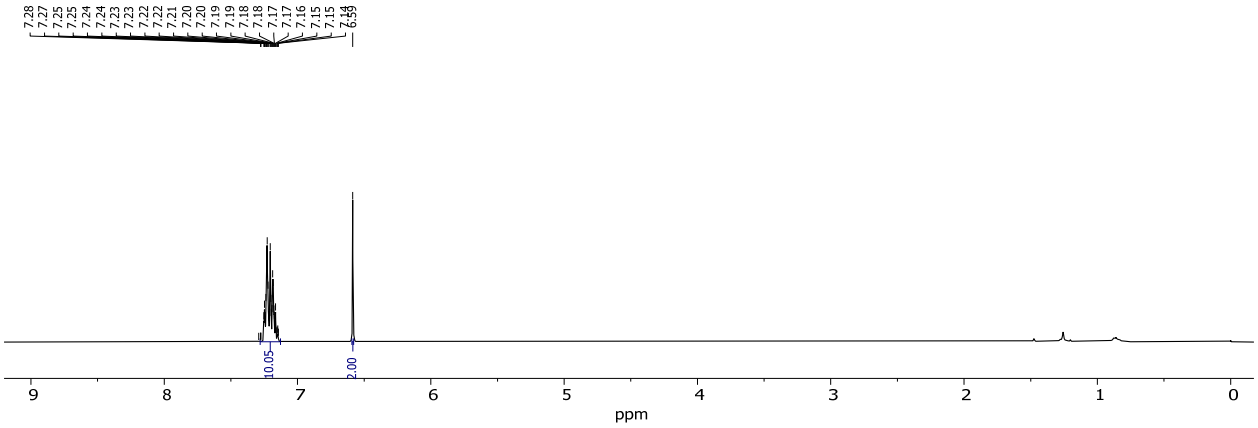

^{13}C{^{1}H} NMR (101 MHz, $CDCl_3$)

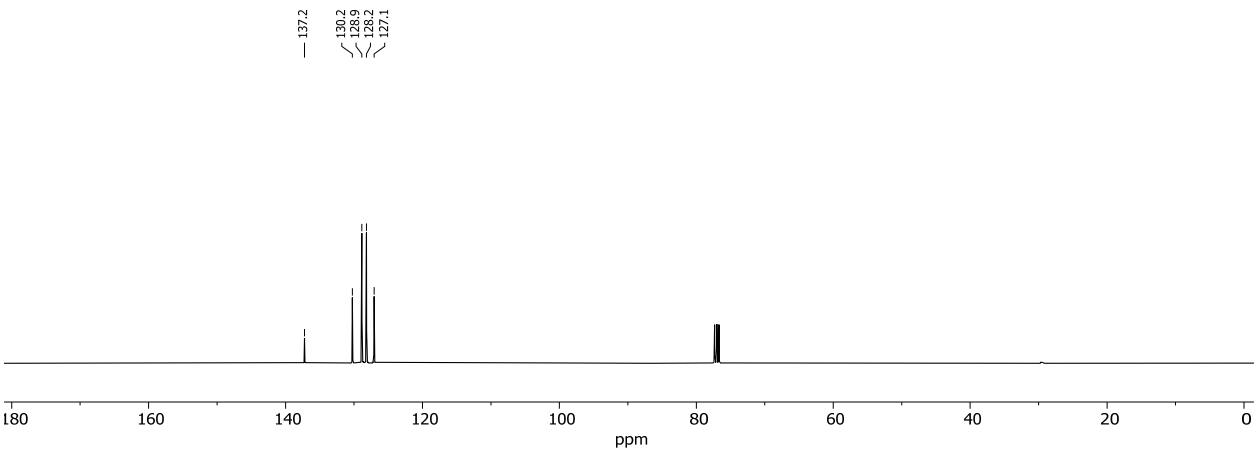

4b: (*Z*)-1-methyl-4-styrylbenzene

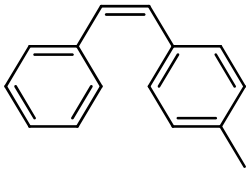

^{1}H NMR (400 MHz, $CDCl_3$)

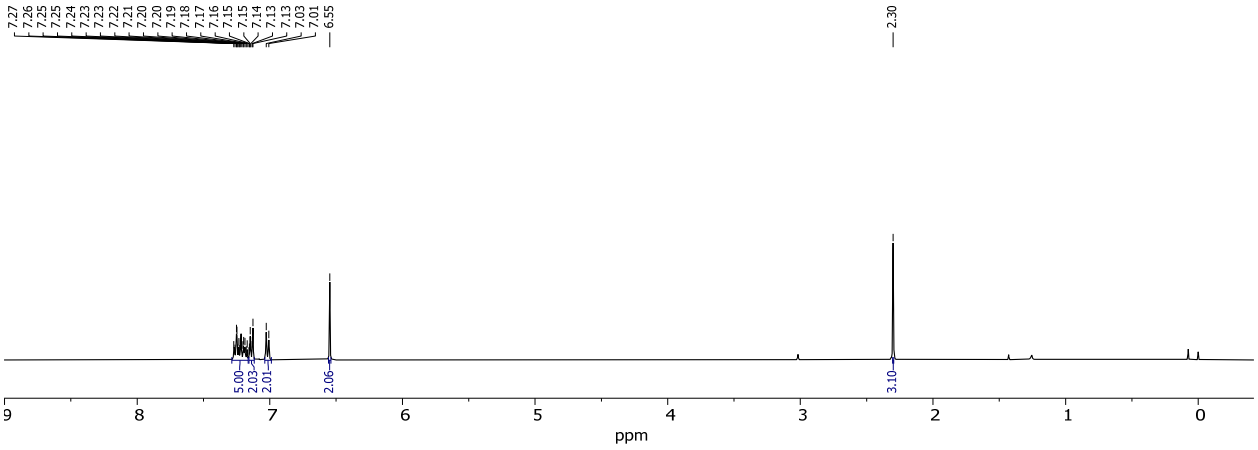

^{13}C{^{1}H} NMR (101 MHz, $CDCl_3$)

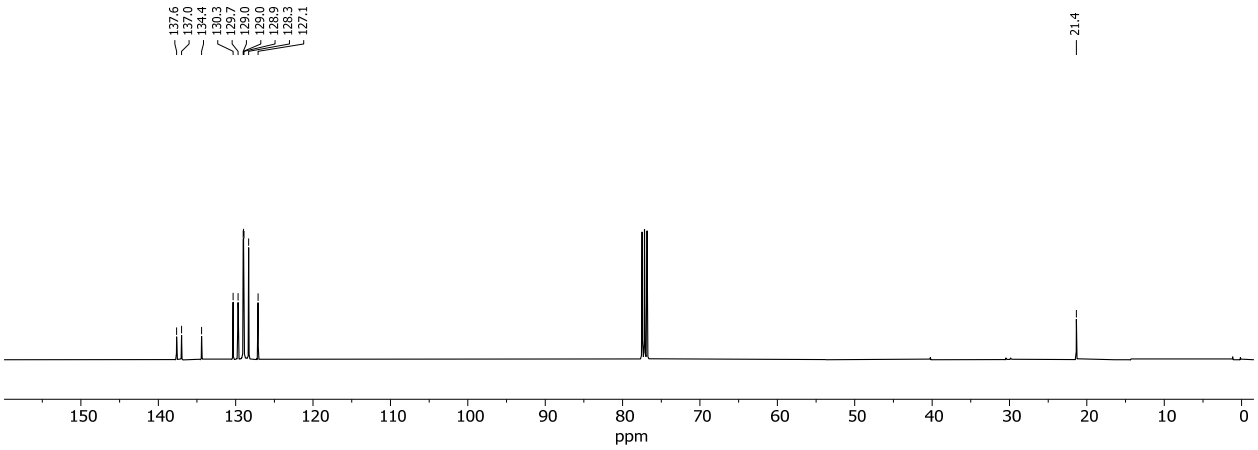

4c: (*Z*)-1-methyl-3-styrylbenzene

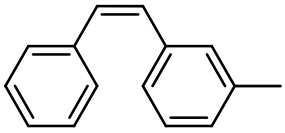

^{1}H NMR (400 MHz, $CDCl_3$)

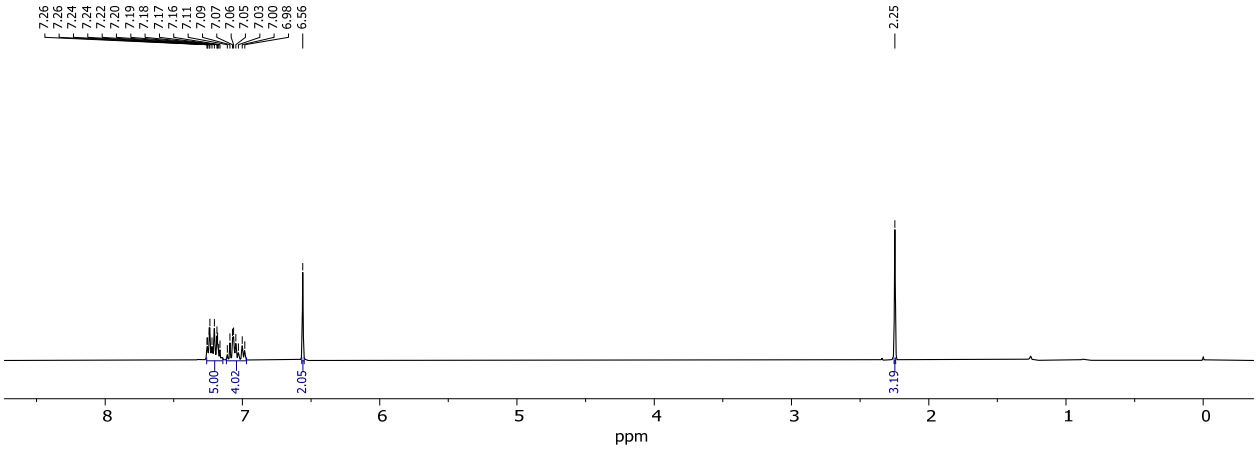

^{13}C{^{1}H} NMR (101 MHz, $CDCl_3$)

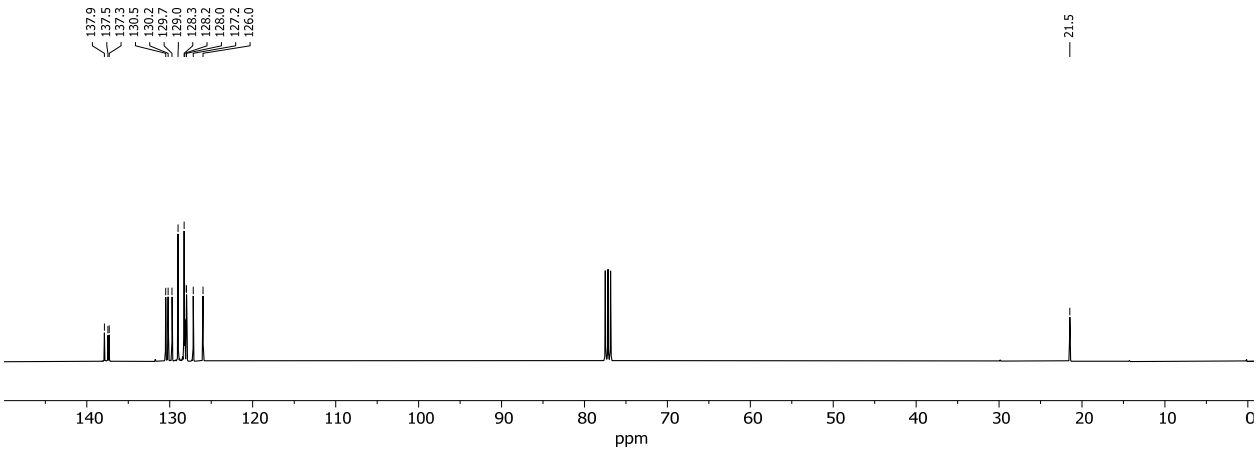

4d: (*Z*)-1-methyl-2-styrylbenzene

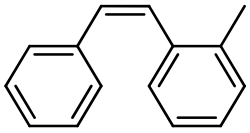

^{1}H NMR (400 MHz, $CDCl_3$)

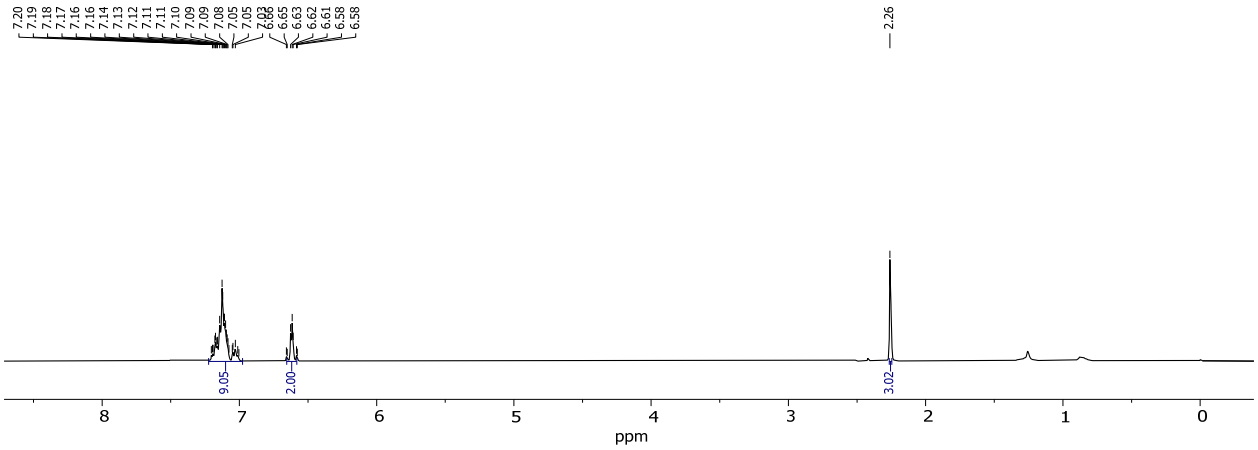

^{13}C{^{1}H} NMR (101 MHz, $CDCl_3$)

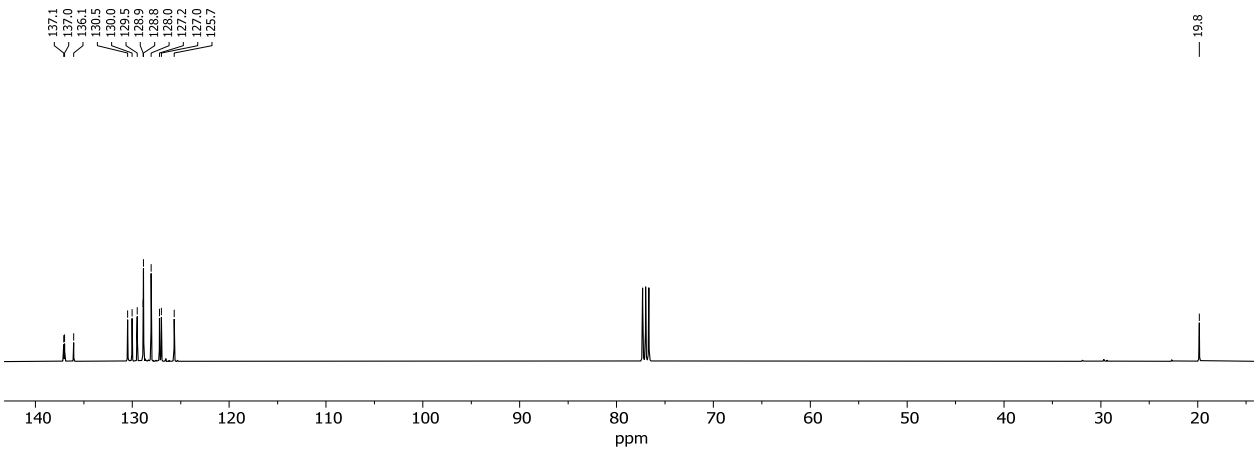

4e: (*Z*)-1-chloro-4-styrylbenzene

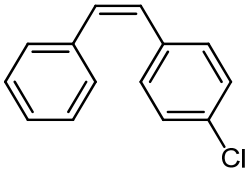

^{1}H NMR (400 MHz, $CDCl_3$)

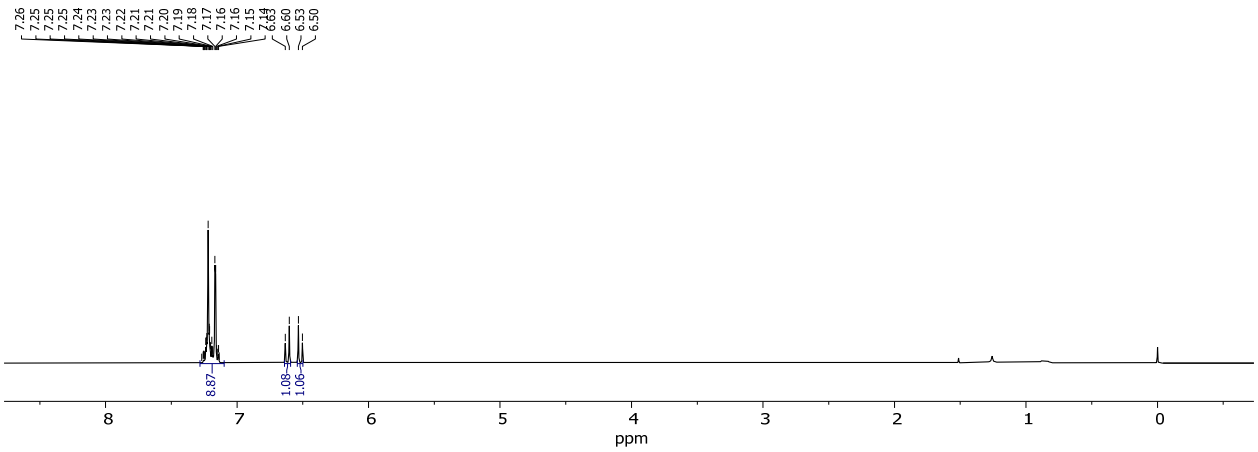

^{13}C{^{1}H} NMR (101 MHz, $CDCl_3$)

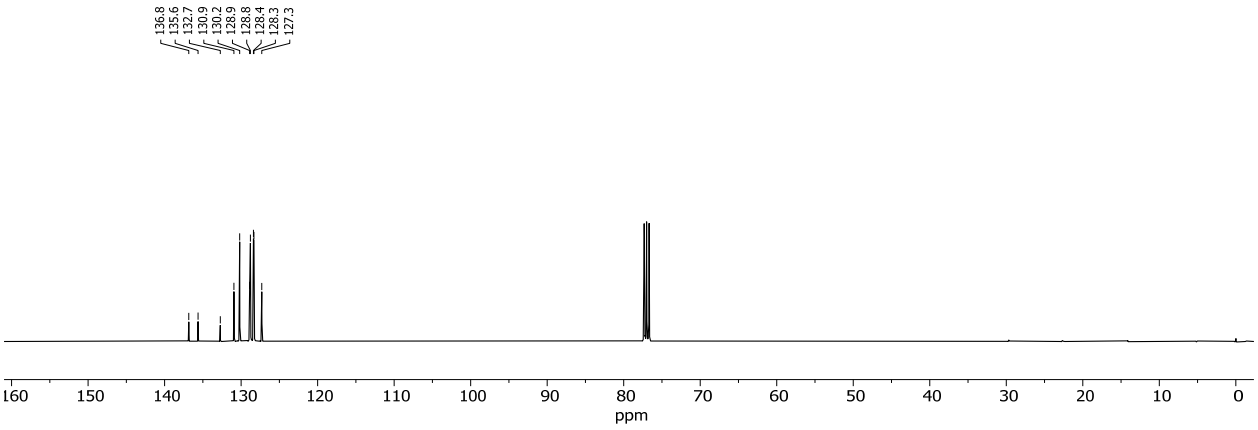

4f: (*Z*)-1-fluoro-4-styrylbenzene

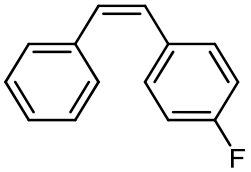

^{1}H NMR (400 MHz, $CDCl_3$)

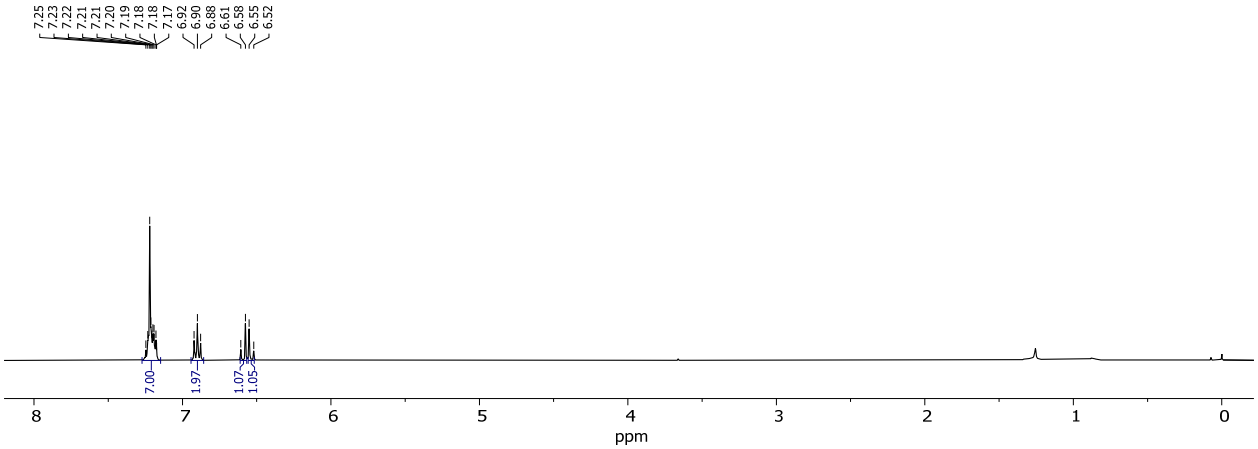

^{13}C{^{1}H} NMR (101 MHz, $CDCl_3$)

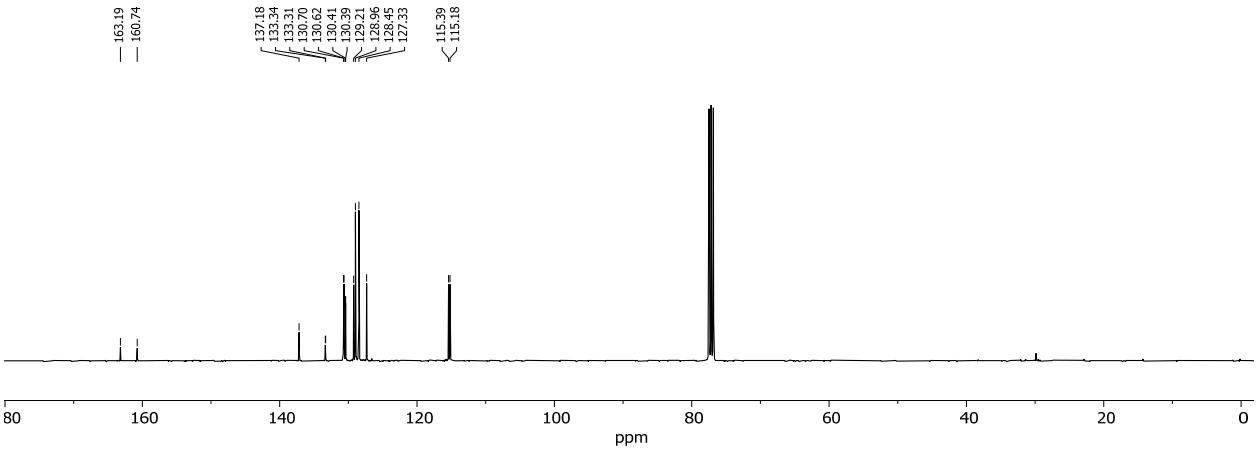

^{19}F NMR (377 MHz, $CDCl_3$)

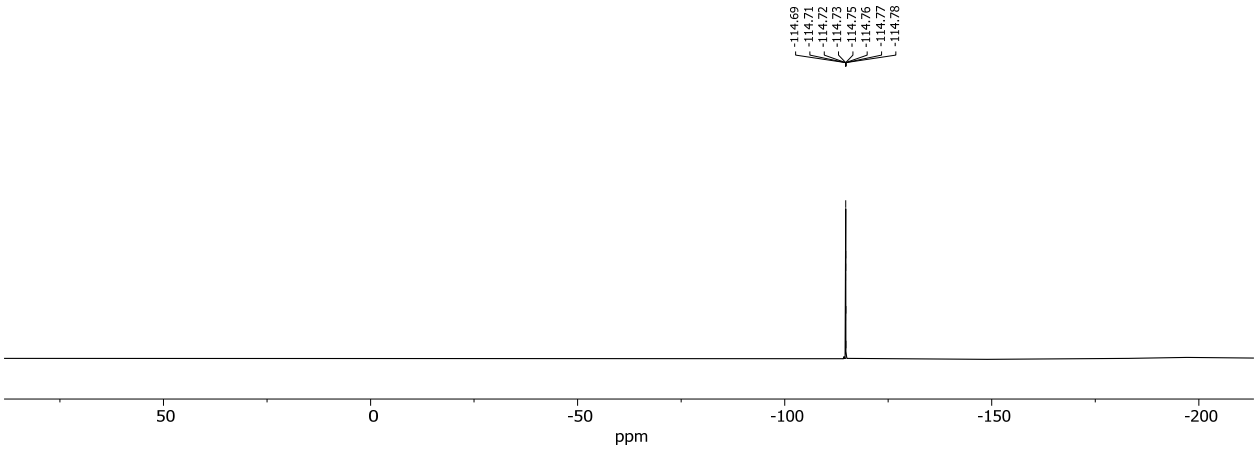

4g: (*Z*)-trimethyl(4-styrylphenyl)silane

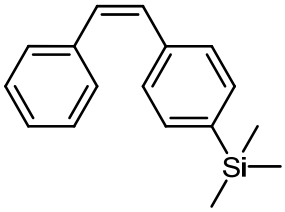

^{1}H NMR (400 Hz, $CDCl_3$)

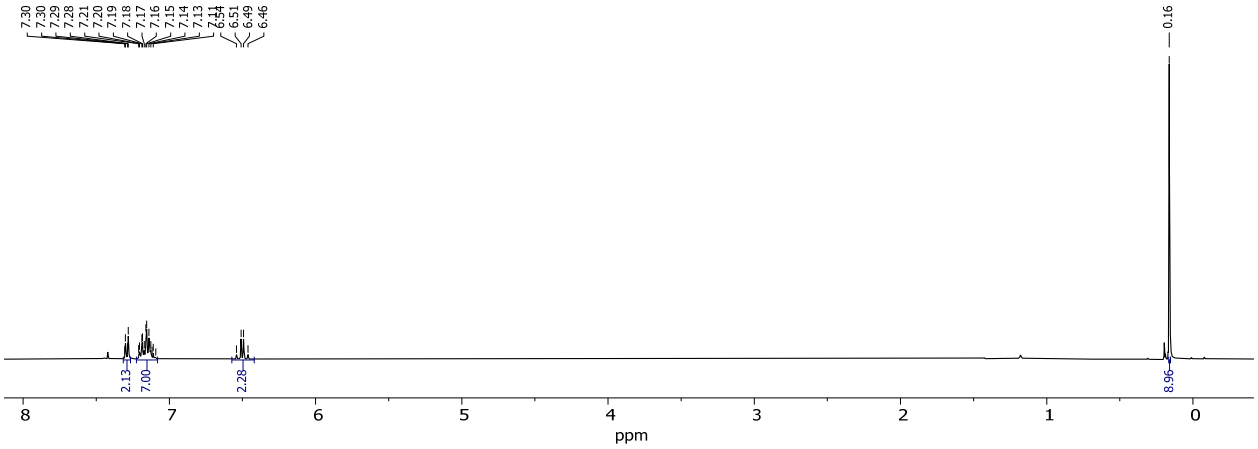

^{13}C{^{1}H} NMR (101 MHz, $CDCl_3$)

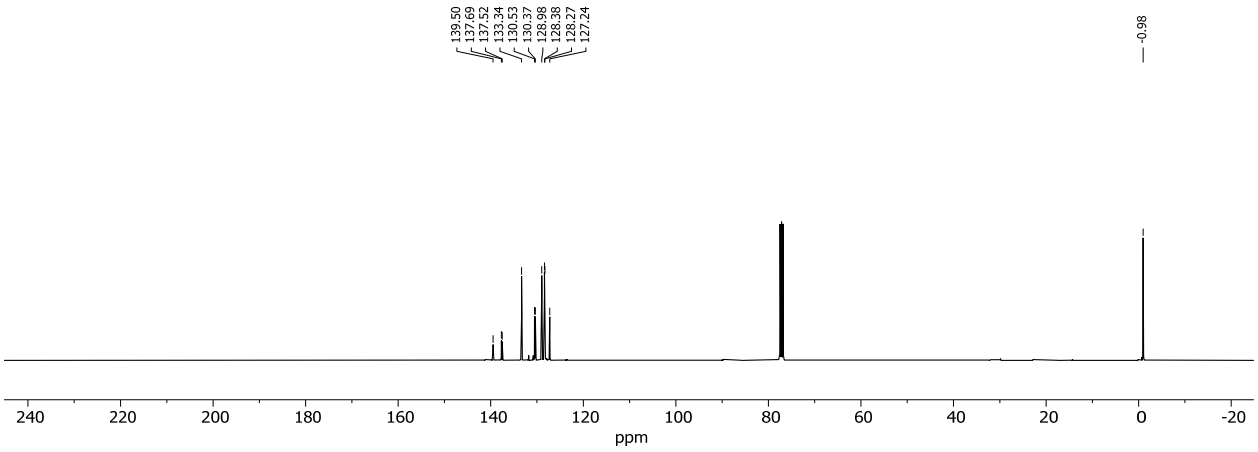

4h: (*Z*)-ethyl 4-styrylbenzoate

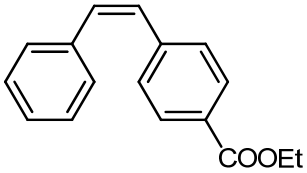

^{1}H NMR (400 MHz, $CDCl_3$)

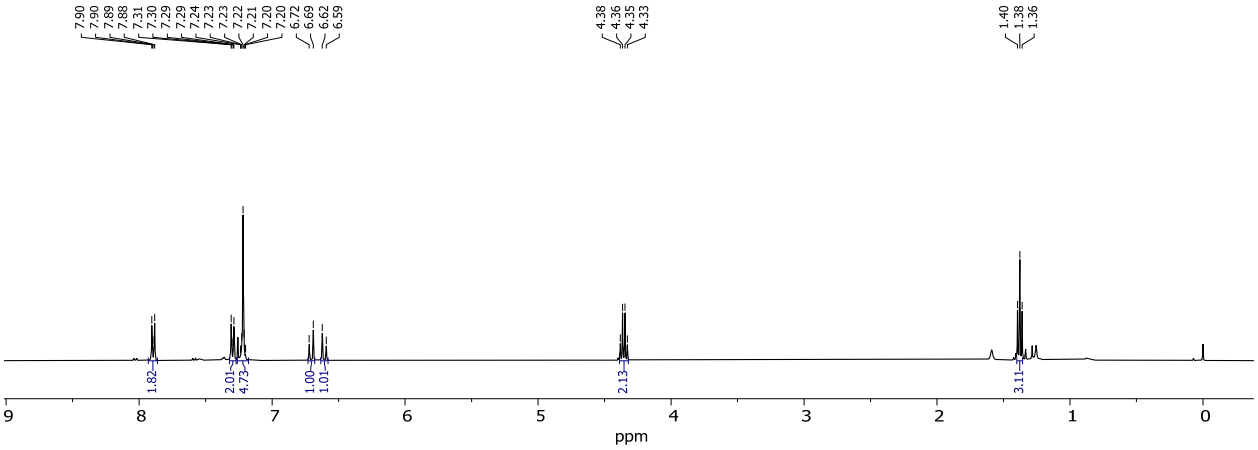

^{13}C{^{1}H} NMR (101 MHz, $CDCl_3$)

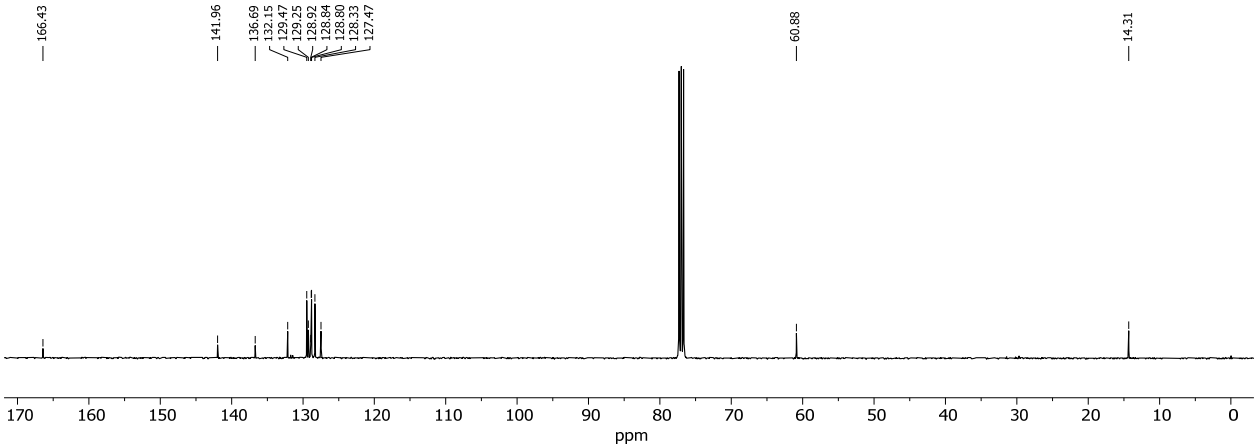

4i: (*Z*)-1-styrylnaphthalene

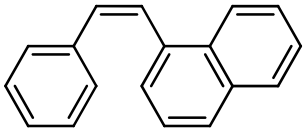

^{1}H NMR (400 MHz, $CDCl_3$)

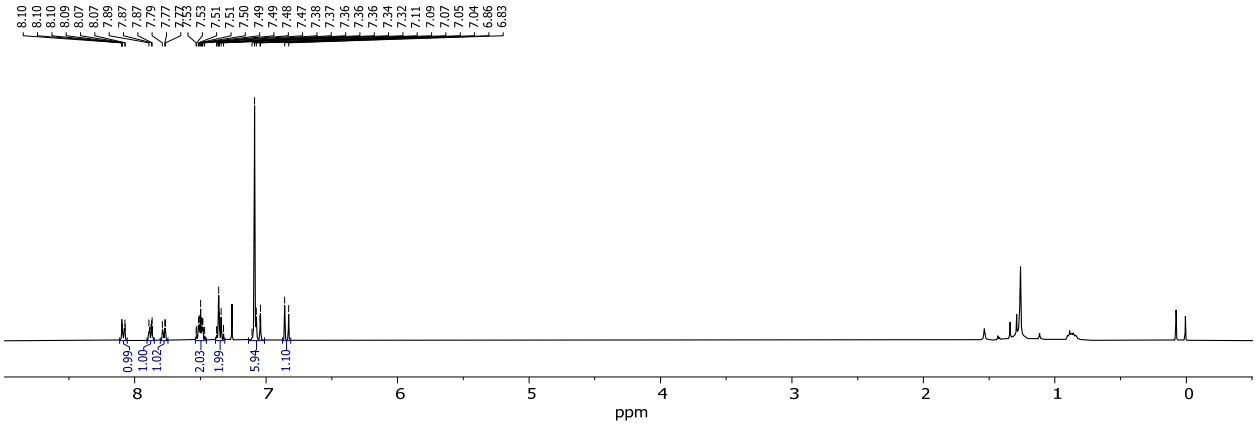

^{13}C{^{1}H} NMR (101 MHz, $CDCl_3$)

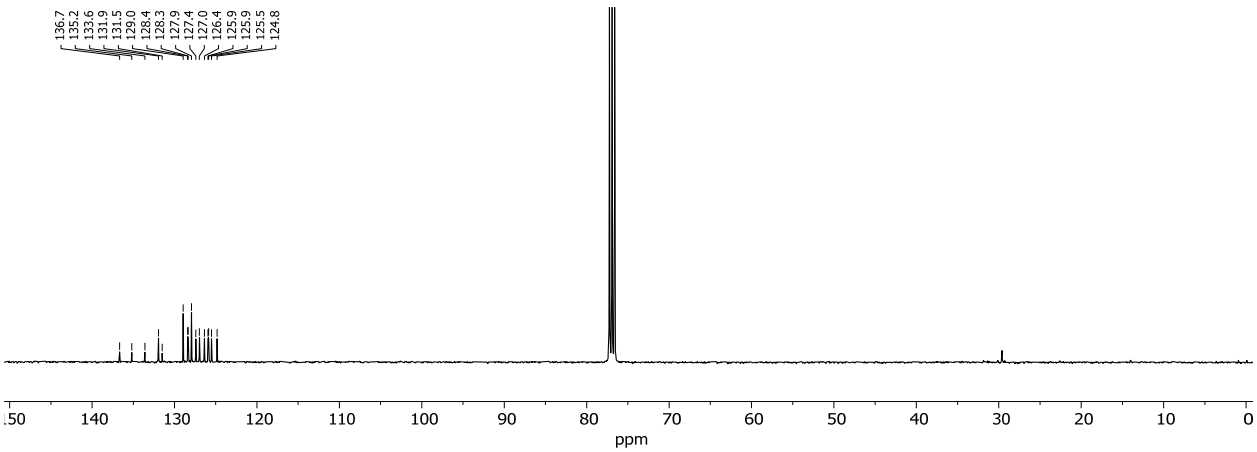

4j: (*Z*)-2-styrylthiophene

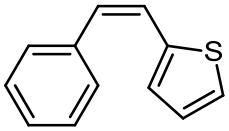

^{1}H NMR (400 MHz, $CDCl_3$)

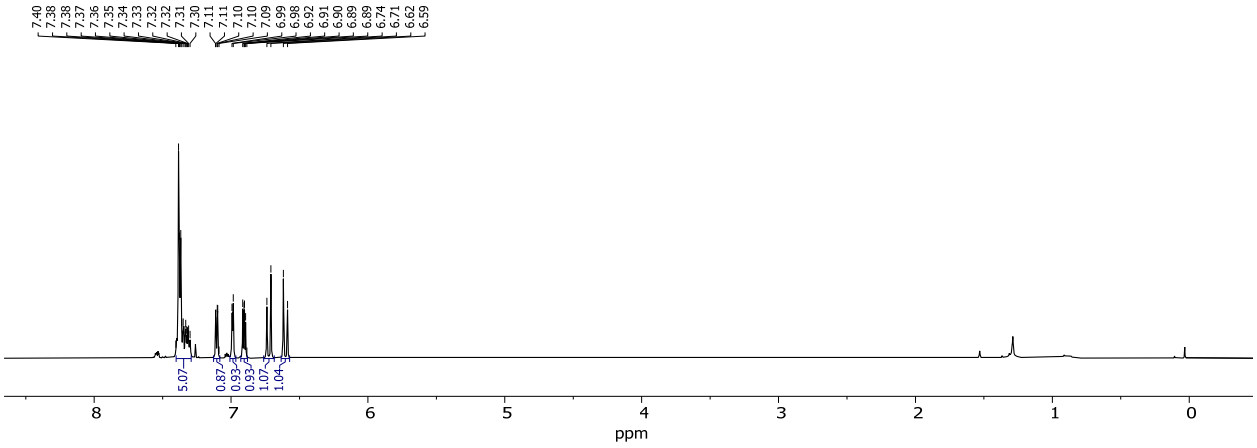

^{13}C{^{1}H} NMR (101 MHz, $CDCl_3$)

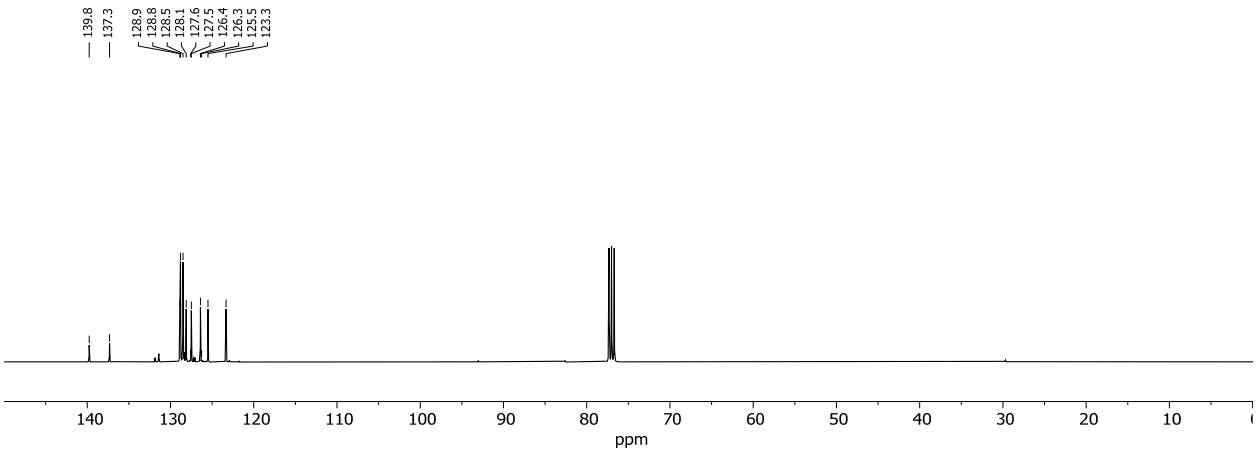

4k: (*Z*)-5-styrylpyrimidine

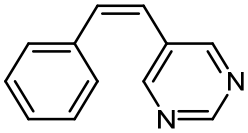

^{1}H NMR (400 MHz, $CDCl_3$)

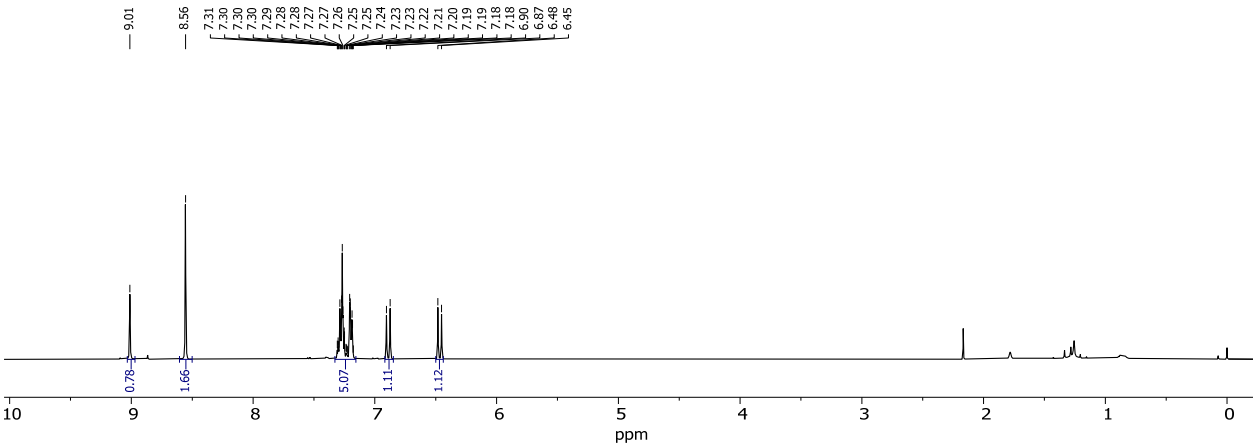

^{13}C{^{1}H} NMR (101 MHz, $CDCl_3$)

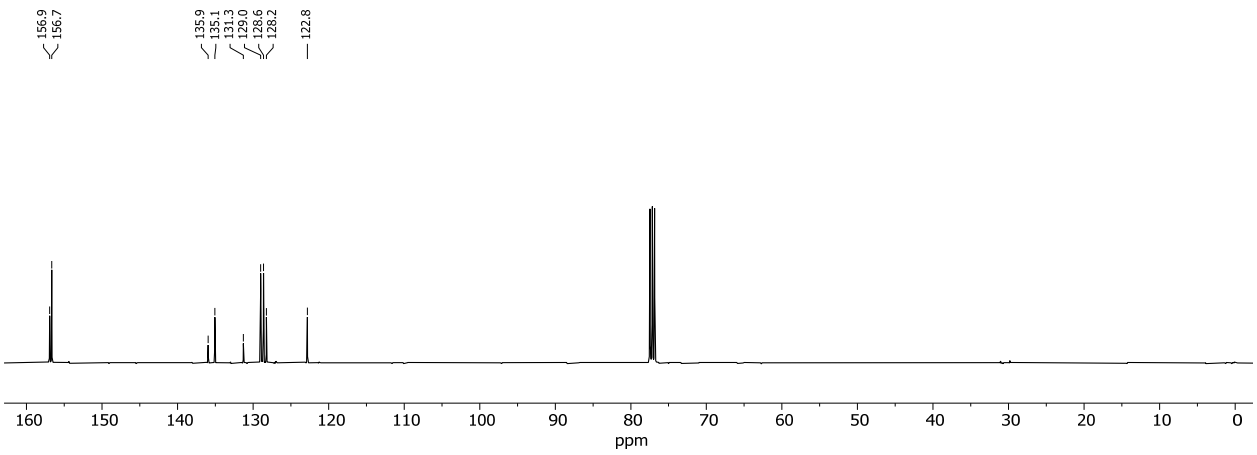

4l: (*Z*)-2-styrylpyridine

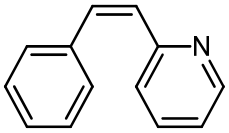

^{1}H NMR (400 MHz, $CDCl_3$)

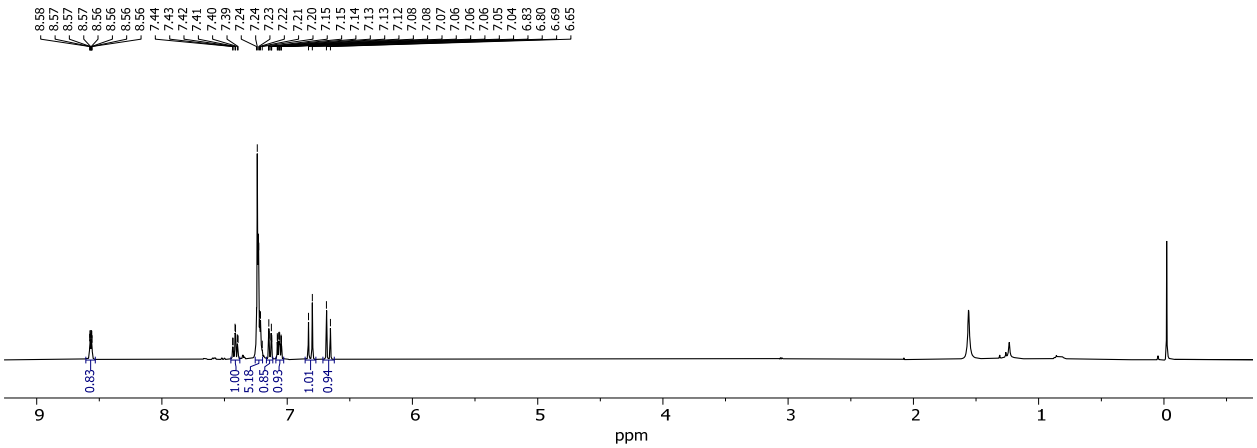

^{13}C{^{1}H} NMR (101 MHz, $CDCl_3$)

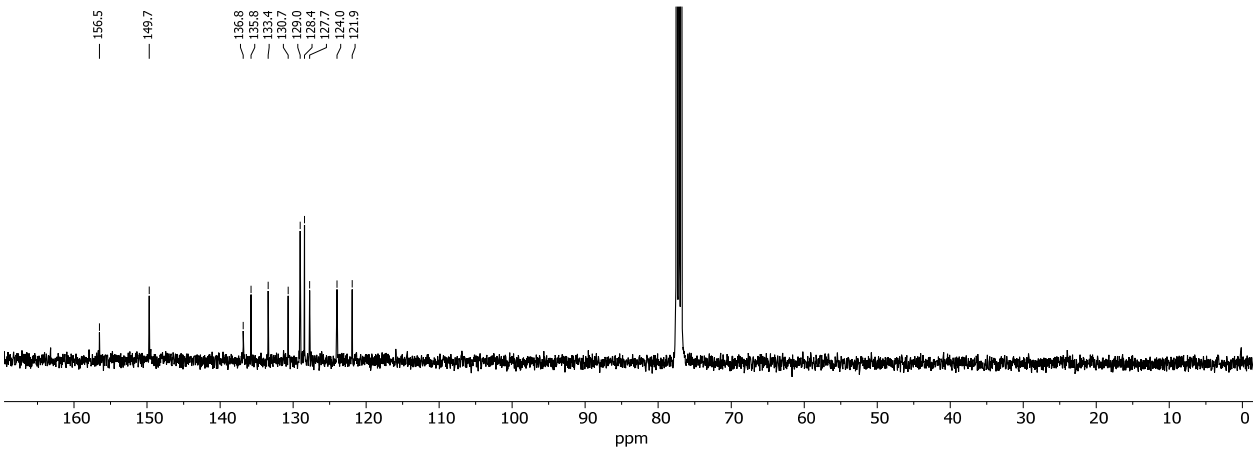

4m: (*E*)-4-styrylaniline

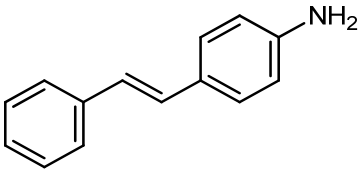

^{1}H NMR (400 MHz, $CDCl_3$)

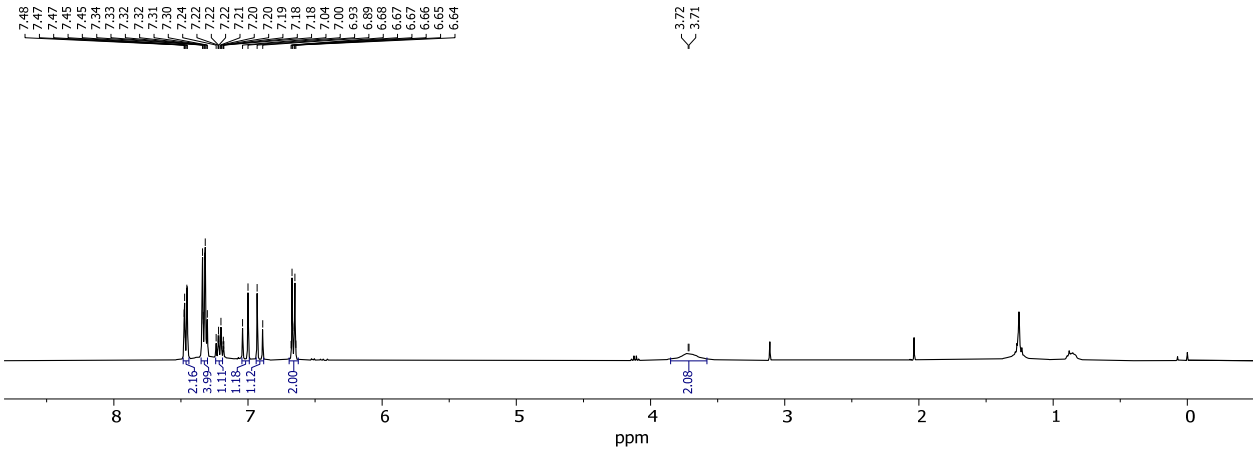

^{13}C{^{1}H} NMR (101 MHz, $CDCl_3$)

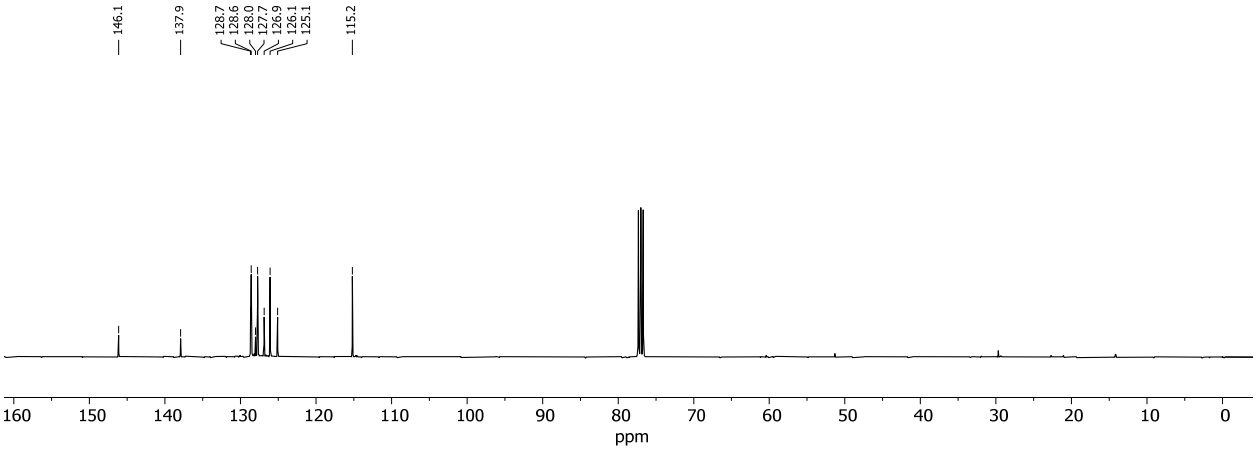

4n: (*Z*)-2-methoxy-5-(3,4,5-trimethoxystyryl)phenol - Combretastatin A4

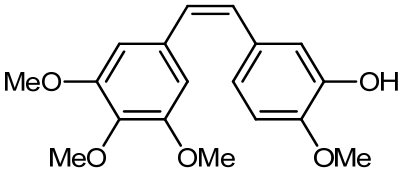

^{1}H NMR (400 MHz, $CDCl_3$)

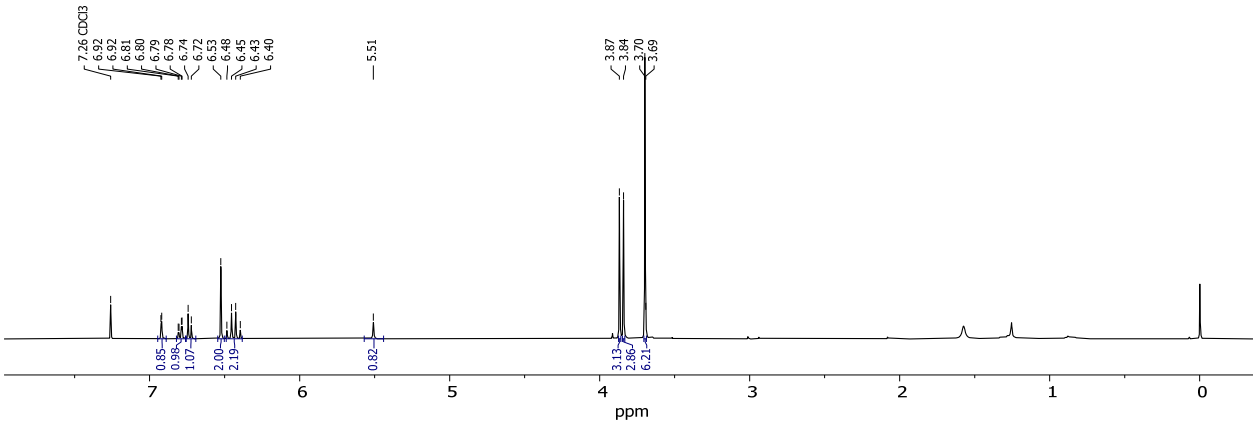

^{13}C{^{1}H} NMR (101 MHz, $CDCl_3$)

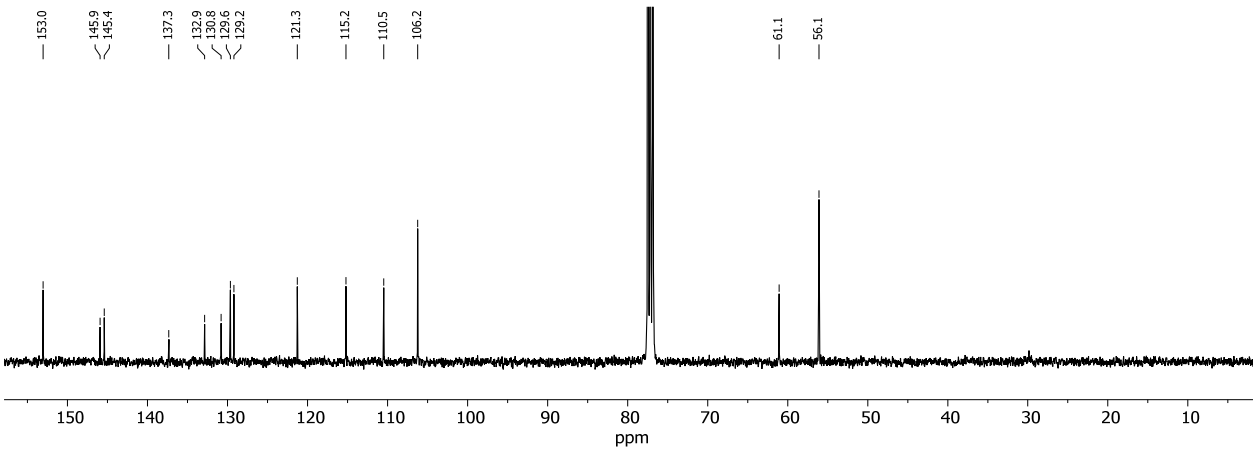

6. Electrochemistry

Table S4. Electrochemical potentials of compounds **L3**, **PdL3'**, **MnPdL3'** and **CoPdL3'** were determined by cyclic voltammetry (CV). **L3** was measured in THF/0.1 mol·L^{-1} [N(*n*Bu)$_4$]PF$_6$ and the complexes **PdL3'**, **MnPdL3'** and **CoPdL3'** were measured in CH_3CN/0.1 mol·L^{-1} [N(*n*Bu)$_4$]PF$_6$ with a scan rate of 100 mV·s^{-1} at room temperature under N_2 atmosphere. The scan range was from 1 V to –2 V. Ferrocene was used as internal standard at the end of the CV experiment to reference the reported potentials to the FcH/[FcH]$^+$ couple.

Compound	E_{PC} in V (I in µA)	E_{PA} in V (I in µA)	$E_{1/2}$ in V
L3	–1.60 (–5.2); –1.75 (–5.6)	0.71 (22.1); 0.81 (21.5)	
PdL3'		0.78 (24.0)	
MnPdL3'	–1.51 (–22.2);		
CoPdL3'	–1.41 (–16.6); –1.93 (–26.8)		
	–1.14 (–20.0)	–1.04 (5.6)	–1.09

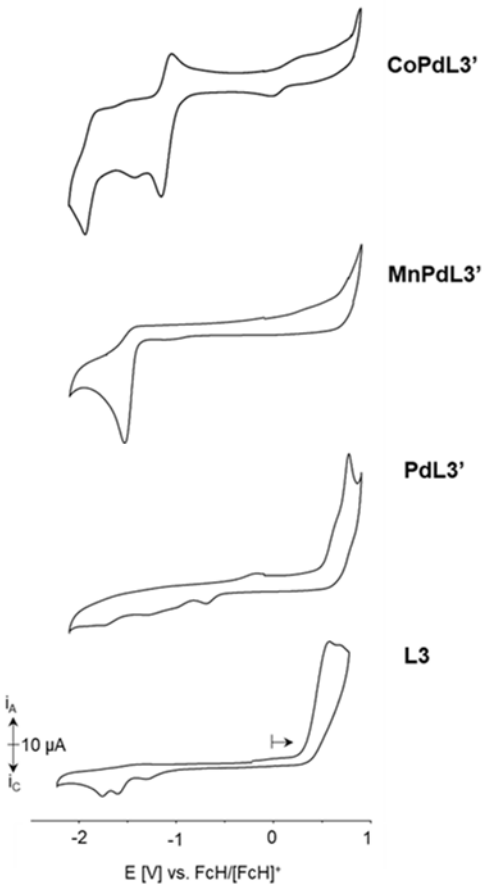

Figure S66. Cyclic voltammograms of the ligand **L3** in THF/0.1 mol·L^{-1} [N(nBu)$_4$]PF$_6$ and the complexes **PdL3'**, **MnPdL3'** and **CoPdL3'** in CH_3CN/0.1 mol·L^{-1} [N(nBu)$_4$]PF$_6$ with a scan rate of 100 mV·s^{-1}. The arrow represents the respective starting potential and scan direction.

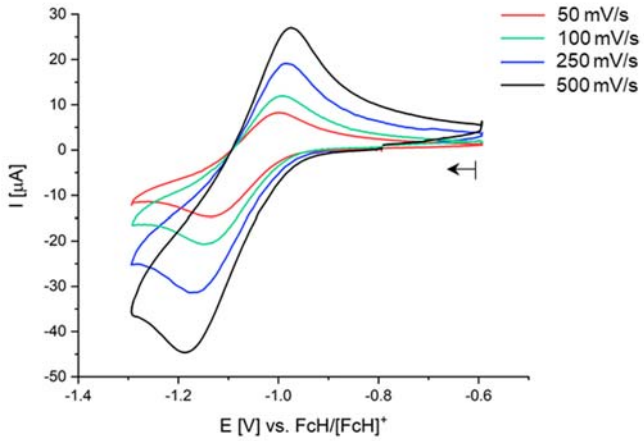

Figure S67. Cyclic voltammogram of **CoPdL3'** in $[N(nBu)_4]PF_6/CH_3CN$ showing the assumed Co^{II}/Co^{I} quasi-reversible process at different scan rates. The arrow represents the respective starting potential and scan direction.

7. References

1 a) R. H. Crabtree, *Chem. Rev.*, 2012, **112**, 1536–1554; b) J. A. Widegren and R. G. Finke, *J. Mol. Catal. A Chem.*, 2003, **198**, 317–341.

2 D. R. Anton and R. H. Crabtree, *Organometallics*, 1983, **2**, 855–859.

3 a) O. N. Gorunova, I. M. Novitskiy, Y. K. Grishin, I. P. Gloriozov, V. A. Roznyatovsky, V. N. Khrustalev, K. A. Kochetkov and V. V. Dunina, *Organometallics*, 2018, **37**, 2842–2858; b) V. M. Chernyshev, A. V. Astakhov, I. E. Chikunov, R. V. Tyurin, D. B. Eremin, G. S. Ranny, V. N. Khrustalev and V. P. Ananikov, *ACS Catal.*, 2019, **9**, 2984–2995.

4 S. Fu, N.-Y. Chen, X. Liu, Z. Shao, S.-P. Luo and Q. Liu, *J. Am. Chem. Soc.*, 2016, **138**, 8588–8594.

5 A. Moncomble, P. Le Floch, A. Lledos and C. Gosmini, *J. Org. Chem.*, 2012, **77**, 5056–5062.

6 K. Murugesan, C. B. Bheeter, P. R. Linnebank, A. Spannenberg, J. N. H. Reek, R. V. Jagadeesh and M. Beller, *ChemSusChem*, 2019, **12**, 3363–3369.

7 M. Das and D. F. O'Shea, *Org. Lett.*, 2016, **18**, 336–339.

8 J. Li, R. Hua and T. Liu, *J. Org. Chem.*, 2010, **75**, 2966–2970.

9 D.-J. Dong, H.-H. Li and S.-K. Tian, *J. Am. Chem. Soc.*, 2010, **132**, 5018–5020.

10 A. A. Camacho-Dávila, *Synth. Commun.*, 2008, **38**, 3823–3833.